

Cleared: October 2nd, 1974  
Clearing Authority: Aeronautical Systems Division

FOREWORD

This report was prepared by Fabric Research Laboratories, Inc., under USAF Contract No. AF 33(657)-10541. This contract was initiated under Project 7320, "Fibrous Materials for Decelerators and Structures," Task 732002, "Fibrous Structural Materials". This work was administered under the direction of the Nonmetallic Materials Division, Air Force Materials Laboratory, Research and Technology Division with Mr. J. H. Ross acting as project engineer.

This report covers work conducted from February 1963 to January 1964.

Mr. M. J. Coplan was the FRL® Director in charge of this study and Dr. W. D. Freeston, Jr. was the principal investigator. The authors wish to express their appreciation to Mr. J. W. Gardella and Mr. R. J. Coskren for their contributions on the textile processing phases of the program and the high speed impact testing respectively.

# Contracts

## ABSTRACT

The objective of this program is the development and evaluation of fibrous structural materials exhibiting good flexibility and high strength at temperatures from cryogenic to 2000°F.

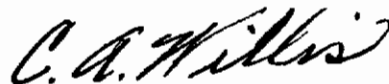
The weight, permeability, flexural rigidity, wrinkle recovery, tensile properties, tear strength, and fold endurance at 70°F of a fabric woven from a multifilament yarn composed of 0.0005 inch diameter nickel-chromium alloy wire are given. The high speed impact properties of a metal yarn, an HT-1 yarn and an HT-1 yarn wrapped with metal yarn are also given.

A preliminary investigation of the joining of panels of metal fabric by sewing is discussed. The properties of coreless cord braided from half-mil and one mil wire are given.

Metal yarns textured by the various textile texturing processes are evaluated. A preliminary investigation of metal filaments blended with other fibers is discussed.

The tensile properties at temperatures from 70°F to 850°F, and the fold endurances at 70°F of a series of graphite and carbon-based fabrics are given.

This technical documentary report has been reviewed and is approved.



C. A. WILLIS, Chief  
Fibrous Materials Branch  
Nonmetallic Materials Division

# Contrails

## TABLE OF CONTENTS

Section		Page
I	INTRODUCTION .....	1
II	METAL FABRIC .....	3
	A. Wire .....	3
	B. Yarn .....	5
	C. Fabric .....	6
	1. General .....	7
	2. Tensile Properties .....	7
	3. Flexural Rigidity .....	7
	4. Tear Strength .....	14
	5. Wrinkle Recovery .....	14
	6. Fold Endurance .....	17
	D. High Speed Impact Properties .....	17
	1. Yarn .....	17
	2. Fabric .....	28
III	SEAMING .....	32
IV	CORELESS CORD .....	38
V	TEXTURED YARN .....	43
VI	BLENDED YARN .....	62
VII	SILICA-CELLULOSE FIBER .....	66
VIII	GRAPHITE AND CARBON-BASED FIBROUS MATERIALS .....	67
	A. Tensile Properties .....	67
	B. Fold Endurance .....	75
IX	SPECIAL TEST FIXTURES .....	79
	A. High Temperature Test Equipment .....	79
	B. Low Temperature Test Equipment .....	93
X	BENDING RIGIDITY OF NONWOVEN FABRICS .....	105
XI	CONCLUSION .....	120
XII	FUTURE PLANS .....	121
XIII	RECOMMENDATIONS .....	122
XIV	LIST OF REFERENCES .....	124
APPENDIX	ANALYSIS OF IMPACT STRESSES AND STRAINS .....	126

# Contrails

## LIST OF ILLUSTRATIONS

Figure		Page
1	Stress-Strain Diagram of 0.5 mil Chromel R Wire .....	4
2	Metal Fabric .....	8
3	Load-Elongation Diagrams of 0.5 mil Chromel R Wire Fabric	10
4	Instron Tensile Tester .....	11
5	Cantilever Beam Flexural Rigidity Tester .....	13
6	Tongue Tear Test .....	15
7	Monsanto Wrinkle Recovery Tester .....	16
8	MIT Fold Endurance Tester .....	18
9	.22 Calibre Impact Tester .....	19
10	Bullet .....	20
11	Impact Test Set-Up .....	21
12	Impact Test Results .....	22
13	Velocity of Propagation of a Longitudinal Wave .....	27
14	Cold Gas Gun Impact Testing Machine .....	29
15	Seam Types .....	33
16	Slit Seam Sample .....	34
17	Braider .....	41
18	Coreless Metal Cords .....	42
19	Edge Crimped 0.5 mil Wire Yarn .....	44
20	Edge Crimped 1.0 mil Wire Yarn .....	45
21	Stuffer Box .....	48
22	Stuffer Box Textured 0.5 mil Wire Yarn .....	51
23	Stuffer Box Textured 1.0 mil Wire Yarn .....	52
24	FRL® Compactor .....	53
25	Compacted Wire Yarn .....	55

# Contrails

## LIST OF ILLUSTRATIONS (continued)

Figure		Page
26	Air-Jet Used in Production of Taslan® Textured Yarn .....	57
27	Fabric, 0.5 mil Wire Filling Yarn (30 x 80) .....	59
28	Fabric, 1.0 mil Wire Filling Yarn (30 x 80) .....	59
29	Fabric, 0.5 mil Compacted Wire Filling Yarn (31 x 80) ....	60
30	Fabric, 1.0 mil Compacted Wire Filling Yarn (31 x 80) ....	60
31	Fabric, 0.5 mil Taslan® Textured Filling Yarn (30 x 80) ..	61
32	Yarn Covering Machine .....	63
33	Fabric, Wire Wrapped HT-1 Filling Yarn (38 x 80) .....	65
34	FRL® Environmental Chamber .....	72
35	Environmental Chamber Design Modifications .....	73
36	High Temperature Tensile Test Jaws .....	80
37	Clam-Shell Oven Design .....	81,82
38	Clam-Shell Oven .....	83
39	Fabric Fold Endurance Tester .....	85,86,87
40	Yarn Abrasion Resistance Tester .....	89,90
41	Fabric Crease Recovery Tester .....	91,92
42	Fabric Permeability Tester .....	94,95
43	Fabric Flexibility Tester .....	96,97
44	Cryogenic Tensile Test Dewar .....	98
45	Cryogenic Tensile Test Set-Up .....	99
46	Cryogenic Test Set-Up .....	101
47	Cryogenic Fabric Fold Endurance Tester .....	102
48	Fabric Permeability (under biaxial stress) Tester .....	103,104
49	Nonwoven Fabric .....	106
50	Bending of the Unit Cell .....	108

# Contrails

## LIST OF ILLUSTRATIONS (continued)

Figure		Page
51	A Unit Cell .....	110a
52	Crossed-Rod Matrix .....	115
53	Oblique Impact .....	128
54	Oblique Impact Strain .....	131

# Contrails

## LIST OF TABLES

Table		Page
1	Filament Tensile Properties .....	3
2	Yarn Tensile Properties .....	6
3	Fabric Properties .....	9
4	Fabric Tensile Properties .....	9
5	Fabric Flexural Rigidity .....	12
6	Fabric Tear Strength, Wrinkle Recovery and Fold Endurance	14
7	Critical Velocities of Yarns .....	24
8	Oblique Impact Rupture Strains .....	26
9	Summary of Cold Gas Gun Impact Firings .....	30
10	Seam Trials .....	36
11	Coreless Metal Cord .....	39
12	Coreless Nylon Cord .....	39
13	Edge Crimped Wire Yarn .....	46
14	Stuffer Box Textured Wire Yarn .....	50
15	Compacted Wire Yarn .....	54
16	Taslan® Textured Wire Yarn .....	58
17	Covered Yarn .....	64
18	Construction of Graphite and Carbon-Based Fabrics .....	67
19	Tensile Properties of Graphite and Carbon-Based Fabrics .	68
20	Tensile Properties of Graphite and Carbon-Based Fabrics at 70°F after Exposure in Hot Air .....	74
21	Folding Endurance of Graphite and Carbon-Based Fabrics ..	75
22	Bending Rigidity of Nonwoven Fabrics .....	119



## I. INTRODUCTION

The success of many systems being developed for space exploration is contingent upon the availability of appropriate flexible fibrous structural materials. Retardation and recovery devices for re-entry vehicles are examples of such systems. The structures must be capable of being packaged into a small volume and successfully deployed at the proper time. Packaging must not damage the structure and when deployed, the material must withstand temperatures to 2000°F. Expandable rocket nozzles and expulsion bladders for cryogenic fluids in liquid propellant rockets are two additional examples of systems requiring flexible fibrous structural materials that must be packaged and, when deployed, perform successfully under extreme environmental conditions.

This report covers the past year's activity under a continuing program which has as its overall goal the development and evaluation of fibrous structural materials exhibiting good flexibility and high strength at temperatures from cryogenic to 2000°F.

Seven yards of eighteen inch wide fabric were woven from a twisted multifilament yarn containing 0.0005 inch diameter nickel-chromium alloy wire. The weight, permeability, flexural rigidity, wrinkle recovery, tensile properties, tear strength, and fold endurance of the fabric at 70°F are given in Section II. The fabric will be evaluated under liquid nitrogen (-320°F) and at elevated temperatures up to 2000°F during the next year's activity under the program.

The critical velocities of the metal yarn were measured under longitudinal impact, 45° impact, and transverse impact (Section II). The critical velocities of a nylon yarn, an HT-1 yarn and an HT-1 yarn wrapped with metal yarn were also measured. The test results are correlated with the analysis of impact stresses and strains given in the Appendix.

An attempt was made to determine the energy absorption of the metal fabric at various impact velocities with the ASD Cold Gas Gun. However, due to the fabric strength being considerably less than that for which the gun was designed, the degree of accuracy of the results rendered the data inconclusive.

The development and evaluation of fabrics woven from yarns composed of fine wires are only the first two steps toward the utilization of such structures in a deceleration or other space system. The fabric must be tailored into the required configuration, and the mechanical characteristics of the resulting configuration must be known. An investigation of the joining of panels of metal fabric by sewing was initiated, and the findings are discussed in Section III.

---

Manuscript released by the authors February 1964 for publication as a ML Technical Documentary Report.

# Contrails

The designs of some deceleration and other space systems require one component of the system to be attached to another component by a flexible line or cable with high temperature durability, for instance the payload and canopy of a Hyperflo Parachute. Therefore, the feasibility of braiding fine wire into coreless cord was investigated. The properties of the cords produced are given in Section IV.

Some systems requiring flexible fibrous structural materials may require a low porosity-thermally durable structure but not require the high strength of an all metal fabric. Therefore, metal yarns textured (crimped) by the various textile texturing processes are evaluated in Section V, metal filaments blended with other lower density fibers, organic, ceramic and carbonaceous, are evaluated in Section VI, and two nonmetallic fabrics are evaluated in Sections VII and VIII.

Texturing a yarn increases its bulk. Therefore when woven into a fabric high cover and good fabric shear stability are obtained with less weight per unit area than a non-textured fabric. Greater fabric flexibility and coating adhesion may also be obtained with textured yarn.

Blending is also a means of increasing yarn bulk for a given yarn weight per unit length. By blending the metal filaments with a fiber that does not volatilize but decomposes leaving a solid or viscous residue, high flexibility and low permeability can be maintained over a broad temperature range with the metal filaments providing the required structural strength.

The tensile properties at temperatures from 70° to 850°F, and fold endurances at 70°F of a series of graphite and carbon-based fabrics are given in Section VIII.

The designs of test fixtures which have been fabricated for the tensile testing of fibers, yarns and fabrics and fold endurance testing of fabrics under liquid nitrogen are given in Section IX. The designs of test fixtures which have been fabricated to enable the determination of fiber, yarn and fabric stress-strain response (i.e., tensile strength, rupture elongation, tensile modulus, repeated stress response, energy absorption and creep strength) and abrasion resistance, and fabric fold endurance, crease recovery, flexibility and porosity at temperatures to 2000°F are also given. This equipment will be used to evaluate several candidate flexible fibrous structural materials during the next year's activity.

Theoretical analyses of the effects of fiber diameter, fiber tensile and torsional stiffness, fiber distribution and fabric density on the bending rigidity of nonwoven fabrics are presented in Section X. The fibers are assumed to exhibit linear shear and tensile stress-strain behavior. The two extreme cases of complete freedom and no freedom of relative fiber motion are analyzed.

## II. METAL FABRIC

Approximately six pounds of 0.5 mil Chromel R\* wire (0.0005 inch diameter) were plied, cabled and woven. The fabric is seven yards long and eighteen inches wide. It is being used in the development of seaming techniques, the evaluation of mechanical properties at elevated temperatures, and in the investigation of the high speed impact behavior of metal fabric.

### A. Wire

The tensile properties of the 0.5 mil Chromel R wire were measured with an Instron tensile testing machine using a ten inch gage length and a jaw speed of 0.5 inch per minute. The wires were mounted in standard fiber jaws faced with masking tape to prevent jaw slippage. A typical, although not necessarily average, stress-strain curve is given in Figure 1.

Every fourth spool of wire supplied was tensile tested. Three tests were performed and the average yield load, yield elongation, rupture load and rupture elongation for each spool determined. The yield load and yield elongation were taken from the load-elongation curve at the point where the bisector of the angle formed by the extrapolations of the pre- and post-yield portions of the load-elongation curve intersects the load-elongation curve.

The among-spool averages of the average tensile properties of the wire on each tested spool are given in Table 1. The standard deviation,  $\sigma$ , and coefficient of variation, C.V., of the rupture elongation and rupture load are also given.

$$\sigma = \sqrt{\frac{\Sigma(\bar{x}^2) - \frac{1}{n} (\Sigma\bar{x})^2}{n - 1}}$$

and

$$C.V. = \frac{\sigma}{\bar{x}} \times 100$$

where  $n = 147$  is the number of spools tested.

TABLE 1

### FILAMENT TENSILE PROPERTIES

		<u>Yield Load</u>	<u>Yield Elongation</u>	<u>Rupture Elongation</u>	<u>Rupture Load</u>
0.5 mil Chromel R Wire	$\bar{x}$	11.4 gm	0.57%	6.97%	13.5 gm
	$\sigma$			1.65	1.27
	C.V.			23.7%	9.4%

\* Trademark, Hoskins Manufacturing Co., Detroit, Michigan; 73 Ni, 20 Cr, 3 Al, 3 Fe, 0.5 Si, <0.05 C.

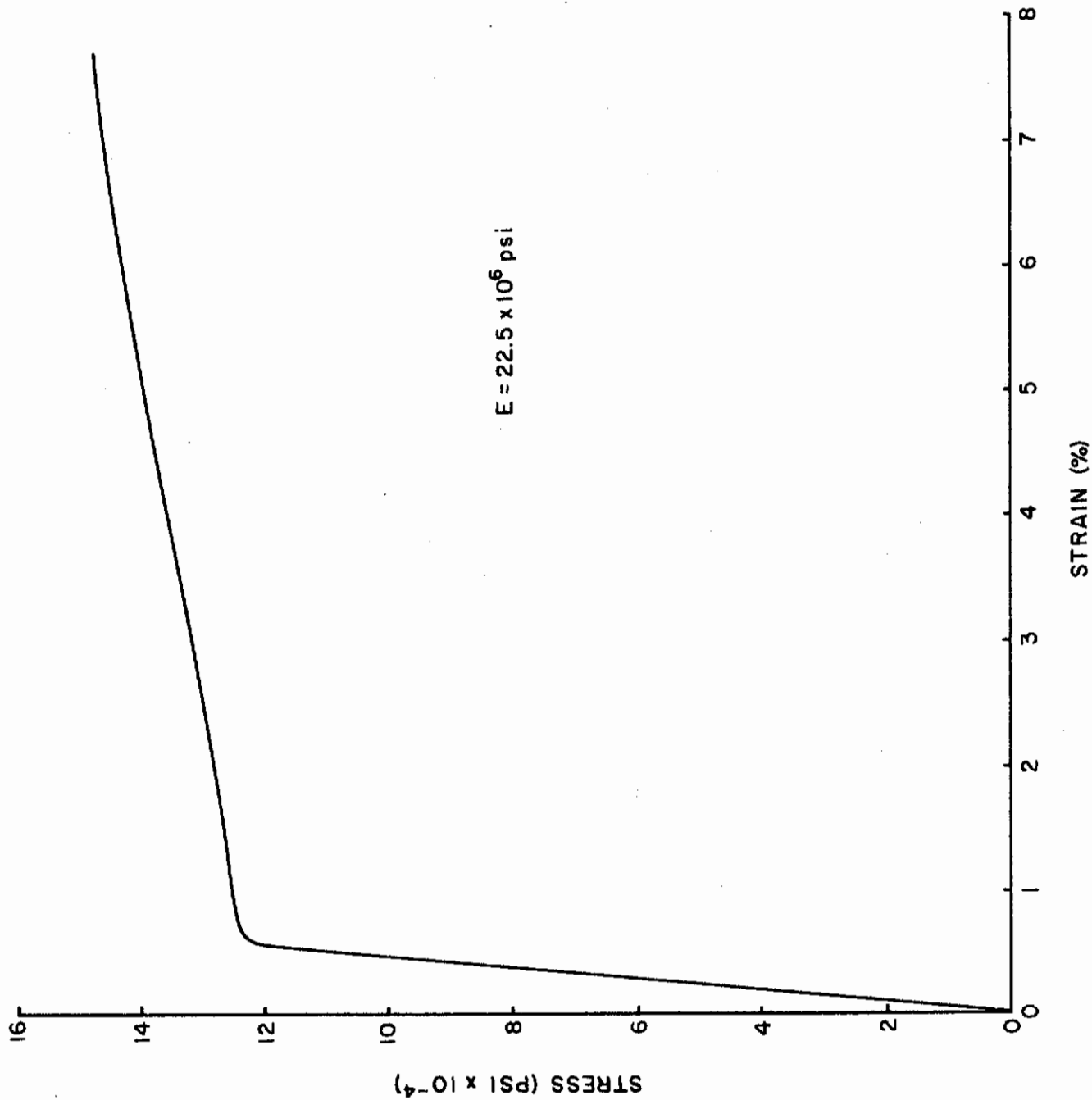


FIGURE 1 STRESS - STRAIN DIAGRAM OF 0.5 MIL CHROMEL R WIRE.

# Contrails

## B. Yarn

The 0.5 mil Chromel R wire was plied and cabled into a one hundred filament yarn (10/10/1, 3.0 S/3.0 Z tpi). Ten ends of the individual strands of wire were plied 3.0 Z turns per inch and ten ends of the plied yarn were then cabled 3.0 S turns per inch. The yarn is balanced, i.e., torque free.

The twisting was done on a textile ring-twister. The individual strands of wire were removed from their spools by pulling off over the end of the spool in conjunction with a "wisker disk"\*. A "wisker disk" consists of radially oriented nylon monofilaments glued between paper disks. It is held on the end of the spool over which the wire is pulled. The nylon monofilaments provide the correct amount of back tension on the wire, minimize wire contact with the spool flange and trap the wire (between filaments) upon rapid take-up decelerations, thereby preventing the wire from sluffing off the end of the spool. The back tension can be varied appropriately with wire diameter by taking a "wisker disk" with a large number of filaments and cutting out every third or fourth filament until a suitable tension is achieved. The tension can also be varied by using a disk made with different diameter monofilaments.

The wire was twisted at a spindle speed of 5400 rpm and a feed roll speed of 145 ft/min. Nylon travelers were used.

Considerable difficulty was encountered in twisting the first few pounds of the wire. Numerous individual wire breaks occurred during the plying operation. There appeared to be three major causes of these breaks: (1) The flanges of many of the plastic spools on which the first few pounds of wire were supplied were rough. This caused many breaks during the twisting since the wire is pulled off the spools over end. (2) Many breaks resulted from a trapped filament, principally at the ends of the traverse, i.e., at the spool flanges. (3) Broken filaments were encountered frequently on spools containing more than 0.025 pounds of 0.5 mil wire. This may result from lack of a tension gradient during the package buildup in the spooling of the wire.

Evidently as a result of Hoskins Manufacturing Co.'s tightening up their quality control and keeping the weight of wire wound on any one spool below 0.025 pounds, essentially no difficulties were experienced in twisting the last couple of pounds of wire.

The overall efficiency of the twisting operation would be improved considerably by supplying a greater quantity of wire on each spool. FRL® therefore suggests that the packaging of fine wire on a textile thread spool with a textile thread spool winder be considered. A spool with a flange on only one end, a tapered package, diamond wind, and tension gradient during the package buildup, all common to the winding of textile thread spools, might improve the ability of fine wire to be removed "over end" from the spools on which it is packaged.

---

\* Manufactured by Azonic Products, Inc., Palos Heights, Illinois

# Contrails

Before being woven, the wire yarn was coated with a synthetic wax\* by being run over a felt pad saturated with the wax in liquid form. The wax held the filaments in the yarn in a compact bundle and improved the yarn abrasion resistance. This facilitated weaving and improved the quality of the final fabric. The wax is water soluble and is, therefore, easily washed out of the fabric. The average tensile properties of the yarn before and after the wax was washed off are given in Table 2. The increased yield elongation over that of a single filament is due to twist. The decreased rupture elongation probably results from decreased elongation balance and work hardening during twisting.

The tensile strength of the yarn after washing off the wax is 90.7% of one hundred times the average filament tensile strength of 13.5 grams. It can be shown that a low twist yarn containing a normal distribution of filaments with a rupture elongation standard deviation of 1.65 (see Table 1) and a stress-strain diagram of the type shown in Figure 1 should have an efficiency of about 91% due to the variation in fiber properties alone<sup>(20)</sup>.

TABLE 2

## YARN TENSILE PROPERTIES

Construction	Yield		Rupture	
	Elongation (%)	Load (lbs)	Elongation (%)	Load (lbs)
10/10/0.5 mil/3.0 S/3.0 Z wax coated	0.60	2.31	3.9	2.55
10/10/0.5 mil/3.0 S/3.0 Z wax washed off	0.72	2.42	5.1	2.70

### C. Fabric

The metal yarn was woven into a two by two basket weave on a standard 40 inch wide silk loom<sup>(9)</sup>. A 40 dent oval wire reed with a 62 percent airspace was used. A 9.5 yard warp, made by winding the yarn on a reel with a circumference of 9.5 yards, each wrap of yarn alongside the next, 80 ends to the inch, for approximately 19 inches, was used. The yarns were clamped between metal strips at two immediately adjacent locations on the reel periphery. The yarn between the two sets of clamps was then taped and cut. One set of clamps was kept fastened to the reel, the other released and taped to a warp beam. The warp was then wound on the warp beam, a layer of paper between each wrap, and the beam placed in the loom. The warp was drawn through the heddles and reed, grouped in bunches of approximately 80 ends and tied to a cloth leader.

The filling yarn was wound on a conventional quill and the fabric woven at approximately 110 picks per minute with a standard shuttle.

\* S-52, Specialty Products Co., Jersey City, New Jersey. Polyethylene glycol 300 condensed with stearic acid, in solvent with freon as propellant.

# Contrails

The fabric was woven with a 3/4 inch wide cotton tape selvage. Selvage temples, which engaged only the tape, were used to prevent fabric contraction during weaving. The fabric width off the loom was approximately 1/4 inch less than the width at the reed.

Cotton yarn was used in the selvage to save wire. However, when the fabric was taken off the loom, the cotton contracted, puckering the metal fabric. The selvage was therefore cut inward for its full width every inch along its length after weaving. This enabled the fabric to lie flat.

## 1. General

A photograph of the fabric is given in Figure 2. The magnification is approximately 14.5X. Note the extent of yarn flattening that has occurred due to the low yarn twist.

The pick and end count, weight, thickness and permeability of the fabric are given in Table 3. The fabric air permeability was measured with a Frazier Permeometer, using 0.5 inch of water pressure drop across the fabric. The fabric was washed in hot water to remove the wax coating on the yarn before the permeability and other properties discussed below were measured.

## 2. Tensile Properties

The tensile properties of the fabric (after being washed) are given in Table 4. A typical load-elongation diagram for both the warp and filling directions is given in Figure 3. Three specimens in both the warp and filling directions were tested on an Instron tensile tester, Figure 4. A one inch fabric width, 3.5 inches gage length, and 0.5 inch per minute jaw speed were used. The tensile strength translation from filament to fabric is based on the average of the filament properties, Table 1. The strength translation of over one hundred percent exhibited by the fabric in the filling direction is due to either the wire being work hardened somewhat during twisting and weaving or the fact that the wire in the portion of the fabric tested had greater than average tensile strength. The moduli of elasticity are based on the linear portion of the fabric load-elongation curves.

## 3. Flexural Rigidity

The bending length and flexural rigidity of the fabric in both the warp and filling directions are given in Table 5. The data was obtained by the cantilever beam test. In this test one end of a fabric sample one inch wide is clamped in a horizontal position, Figure 5. Then the free length  $l$  of the sample is measured when the angle of the cord of the bent fabric sample with the horizontal is  $41.5^\circ$ . The bending length is  $l/2$  and the flexural rigidity (EI) is

$$(EI) = w \left( \frac{l}{2} \right)^3$$

where  $w$  is the fabric weight per unit area.

Two test specimens were taken, one in the warp direction and one in the filling direction. Four measurements were taken from each specimen, two at each end, one with each side of the fabric up. The fabric samples exhibited

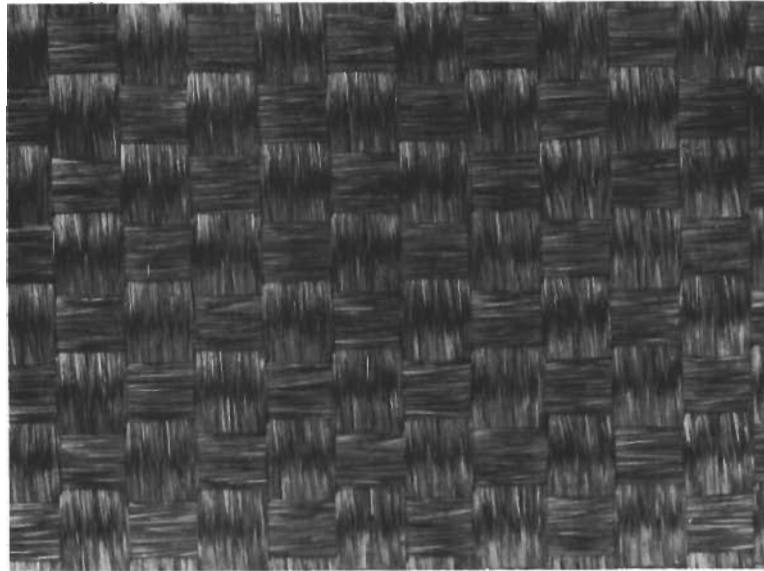


FIGURE 2 METAL FABRIC



TABLE 3

FABRIC PROPERTIES

Wire Diameter (mils)	Material	Yarn Construction	Weave Pattern	Ends per Inch	Picks per Inch	Weight (oz/yd <sup>2</sup> )	Thickness (inches)	Permeability (ft <sup>3</sup> /min ft <sup>2</sup> )
0.5	Chromel R	10/10/1, 3.0 S/3.0 Z tpi	Two by two basket	80-81	80-81	19.9	0.0077	2.1

TABLE 4

FABRIC TENSILE PROPERTIES

Yield Elongation (%)	Yield Load (lbs/inch)	Rupture Elongation (%)	Rupture Load (lbs/inch)	Tensile Strength Translation from Filament to Fabric (%)	Modulus of Elasticity (psi x 10 <sup>-8</sup> )
4.0	198	9.5	226	94.3	6.96
1.4	213	7.2	245	102.2	13.4

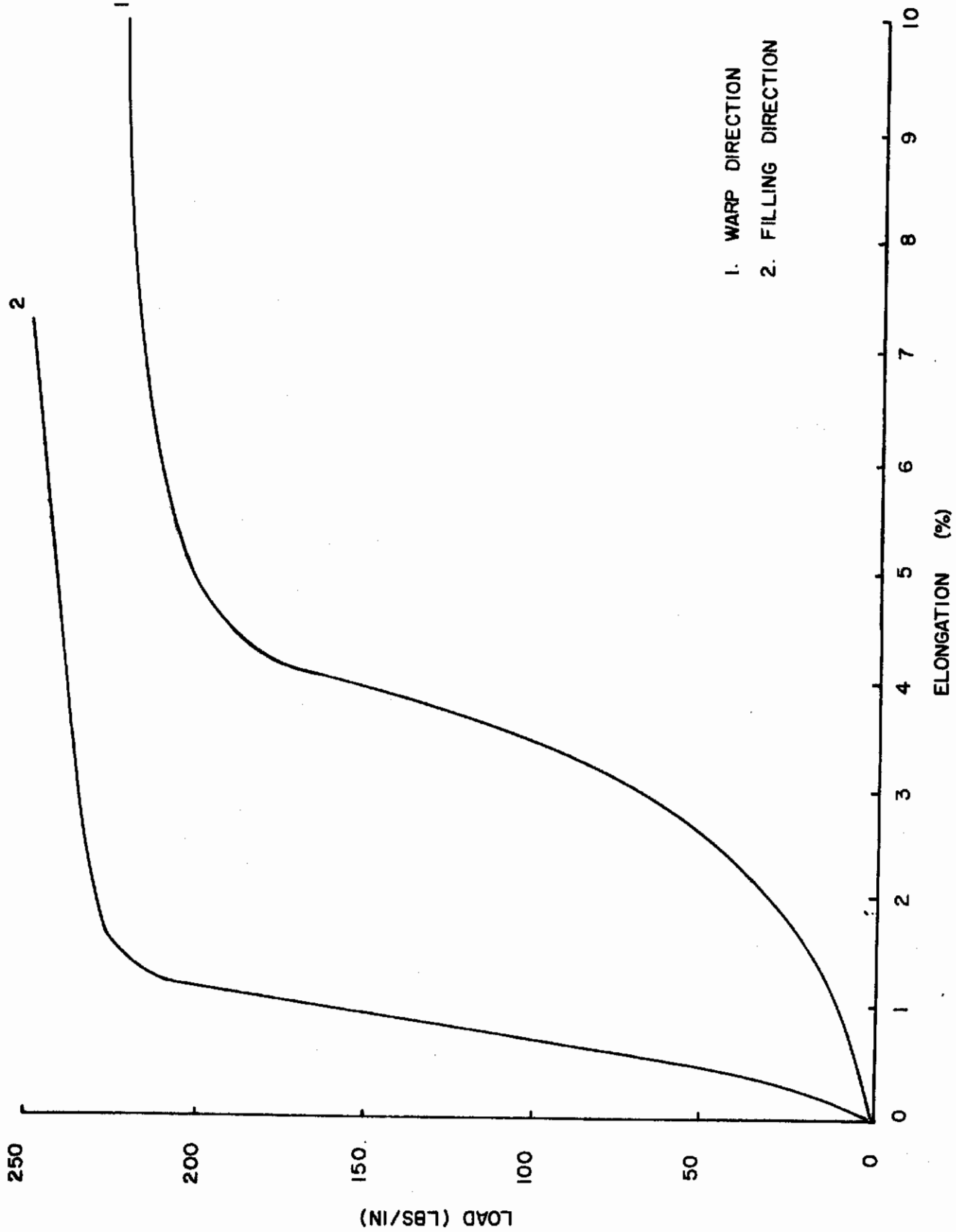


FIGURE 3 LOAD - ELONGATION DIAGRAMS OF 0.5 MIL CHROMEL R WIRE FABRIC



FIGURE 4 INSTRON TENSILE TESTER

TABLE 5  
FABRIC FLEXURAL RIGIDITY

Bending Length (cm)		Flexural Rigidity (gm cm <sup>2</sup> /cm)	Fabric Rigidity $\frac{n}{P}$ Filament Rigidity	
Warp	Filling		Warp	Filling
with curl	with curl	Warp	Warp	Warp
against curl	against curl	against curl	against curl	against curl
ave.	ave.	ave.	ave.	ave.
2.3	3.4	2.9	4.2	4.3
		1.8	5.3	5.3
		2.8	8.4	8.4
		2.1	6.3	6.3

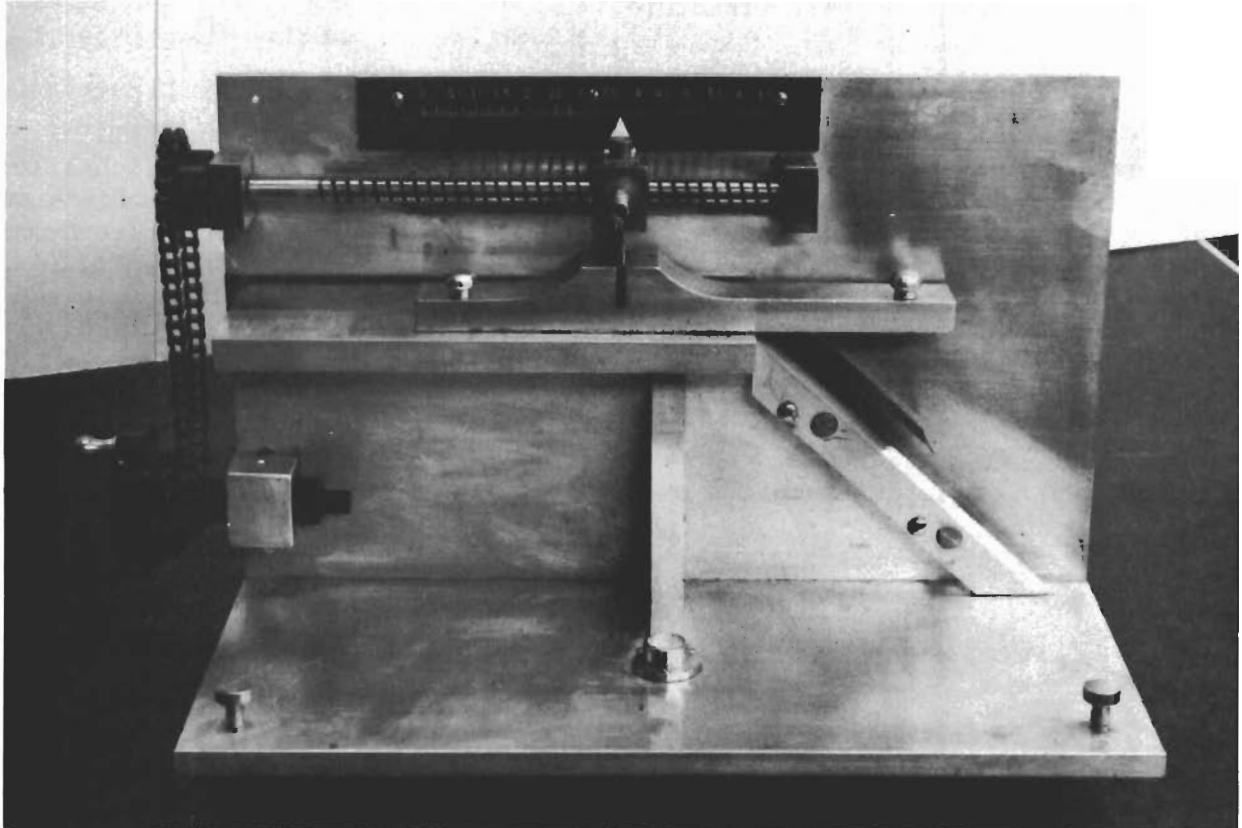


FIGURE 5 CANTILEVER BEAM FLEXURAL RIGIDITY TESTER

some tendency to curl. The bending length values given in Table 5 for bending with and against the curl each represent an average of two measurements. The measurements with and against the curl are also averaged. The average flexural rigidity in the warp and filling directions is given.

The ratio of the rigidity of the fabric per centimeter of width to the sum of the rigidities of the filaments in a centimeter of fabric width is also given in Table 5. If the restriction of freedom of individual filament motion in the yarn in the fabric is represented by clustering, this ratio is equal to the number of filaments per cluster  $n$  divided by the yarn packing factor  $P^{(9,18)}$ . The number  $n$  of filaments per cluster for the warp and filling yarns in the fabric is also given. These values are obtained from the  $n/P$  values by assuming a packing factor of 0.75, which is characteristic of an idealized yarn structure.

#### 4. Tear Strength

The tongue tear strength of the fabric in the warp and filling directions is given in Table 6. Specimens 3 inches wide and 4.5 inches long were used. They were cut lengthwise along their center-line for a distance of approximately 2 inches. The two portions of the cut end were placed one inch into Instron jaws, one in the upper jaw and one in the lower, Figure 6. The specimens were subjected to a constant rate of extension of two inches per minute for approximately 2 inches of tear, the load being recorded. Two specimens were used in both the warp and filling directions.

The load-elongation curve obtained in a tear test is sawtoothed with each peak representing one or several yarn breaks. The tear strength values given in Table 6 are the average peak values of the two tests.

TABLE 6

#### FABRIC TEAR STRENGTH, WRINKLE RECOVERY AND FOLD ENDURANCE

Tear Strength (lbs)		Monsanto Wrinkle Recovery (%)		MIT Fold Endurance (cycles)	
<u>Warp</u>	<u>Filling</u>	<u>Warp</u>	<u>Filling</u>	<u>Warp</u>	<u>Filling</u>
14.5	17.7	33.3	30.0	968	992

#### 5. Wrinkle Recovery

The wrinkle recovery of the fabric in the warp and filling directions is given in Table 6. It was measured with the Monsanto Wrinkle Recovery Tester (ASTM D1295-53T), Figure 7. In this test 1.5 by 4.0 centimeter test specimens are folded  $180^\circ$  with a 0.01 inch thick metal shim between the two fabric surfaces. A load of 1.5 pounds applied for five minutes is used to crease the specimens. The recovered angle is measured after a five minute free recovery time and its percentage of  $180^\circ$  is calculated, i.e., the percent wrinkle recovery equals  $\text{Recovered Angle}/180^\circ \times 100$ . Six specimens in both

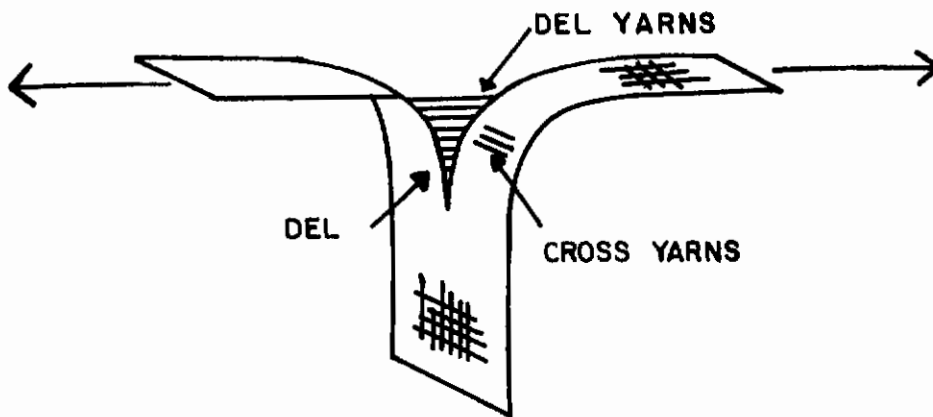


FIGURE 6 TONGUE TEAR TEST

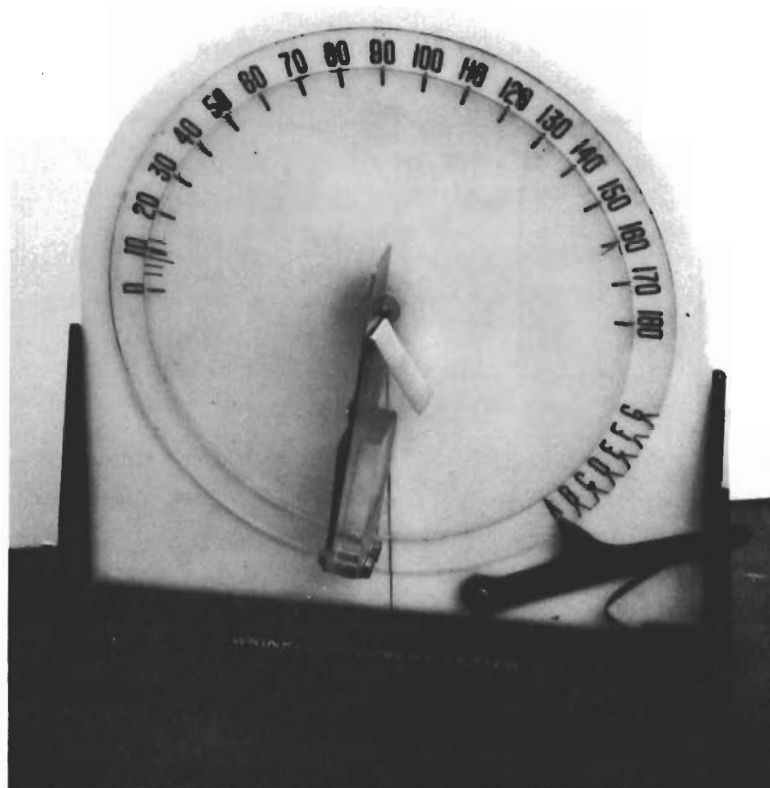


FIGURE 7 MONSANTO WRINKLE RECOVERY TESTER



the warp and filling directions, three bent against the direction of curl and three with the direction of curl, were tested and the results averaged.

## 6. Fold Endurance

The fold endurance of the fabric in both the warp and filling directions is also given in Table 6. It was measured with the MIT Folding Endurance Tester (ASTM D643-43, Method B), Figure 8. In this test both ends of the fabric are clamped in jaws. The lower jaw is subjected to a rotary oscillating movement such that the fabric is folded through an angle of  $135 \pm 5$  degrees to both the right and left of the center-line position. The folding surfaces of the jaw have a radius of curvature of approximately 0.015 inch. A tension of 1.5 kg was applied to the test specimen at the upper jaw.

Test specimens 0.59 inch wide and 4.5 inches long were used. Two specimens were tested in both the warp and filling directions. The results given in Table 6 are the averages of the two tests. The opening width of the jaw used was 0.01 inch.

## D. High Speed Impact Properties

The flexible fibrous structural materials required in some deceleration and other space systems will experience high rates of loading. An investigation of the high speed impact properties of the metal fabric was therefore undertaken. Before investigating the fabric, one of the impact properties, the critical velocity, of the yarn from which the fabric is woven was measured. Critical velocity is defined theoretically as the lowest impact velocity at which the filament breaks immediately upon impact at the point of impact. It is the lowest striking velocity at which there is no strain propagation away from the point of impact. The filament therefore breaks without absorbing any of the kinetic energy of the impacting missile, i.e., the velocity of the missile is not decreased by the impact. However, for experimental purposes critical velocity is defined herein as that missile impact velocity at which rupture of the yarn occurs at the point of impact within 40-50 microseconds after impact. This means the velocity at which the yarn ruptures with essentially no elongation.

### 1. Yarn

The yarn critical velocities were determined with a 0.22 calibre smooth bore rifle, Figure 9. A notched bullet, Figure 10, is fired which engages and ruptures the yarn sample. The manner in which the sample is mounted is shown in Figures 9 and 11. The supporting cord is used to position the sample accurately in the path of the bullet.

Before striking the yarn sample, the bullet breaks a tinfoil strip, electrically triggering an EG&G Multi-Microflash which emits fifteen separate high intensity light flashes. The time between flashes is of the order of 40-50 microseconds.

Prior to each test the room lights are extinguished and the shutter of a Polaroid camera focused on the yarn sample opened. The only light is that emitted by the Multiflash. The position of the bullet before, during and after impact is recorded as a multiple exposure, as shown in Figure 12.

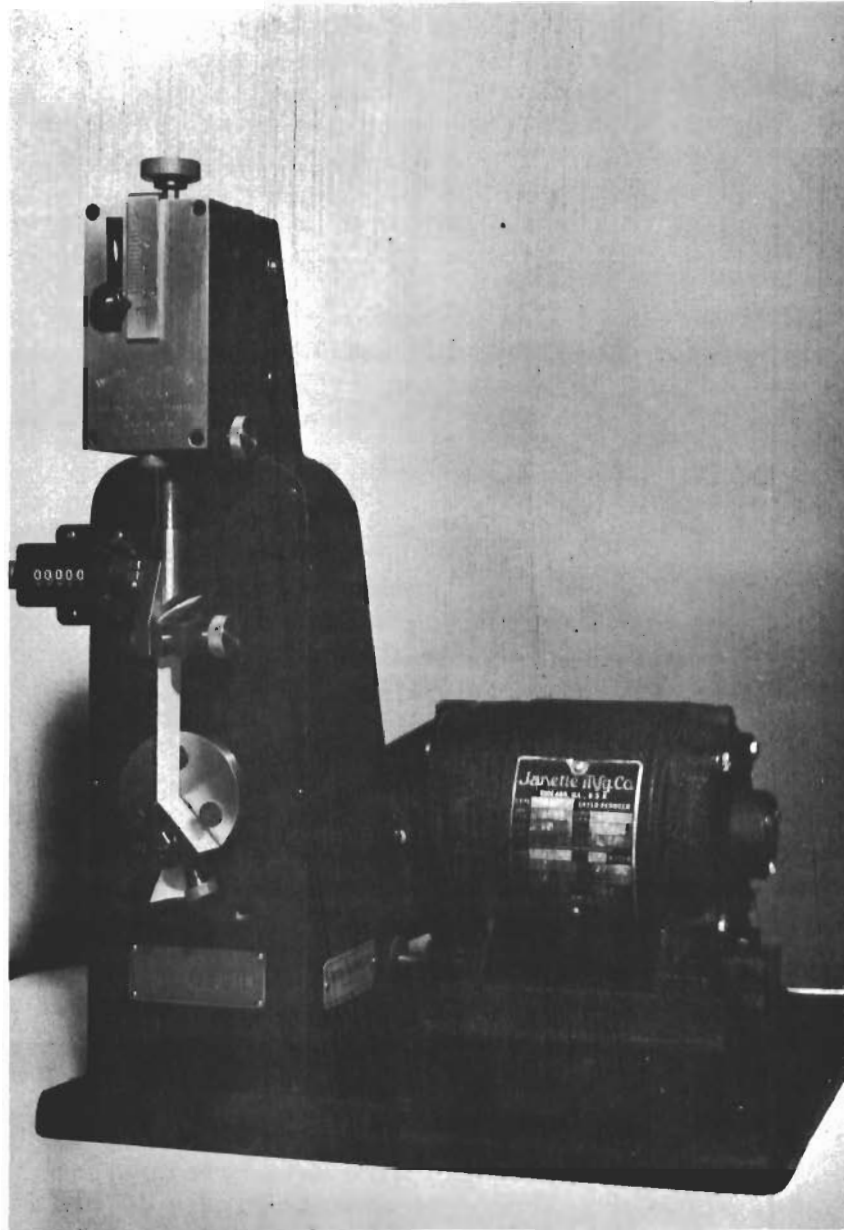


FIGURE 8 MIT FOLD ENDURANCE TESTER

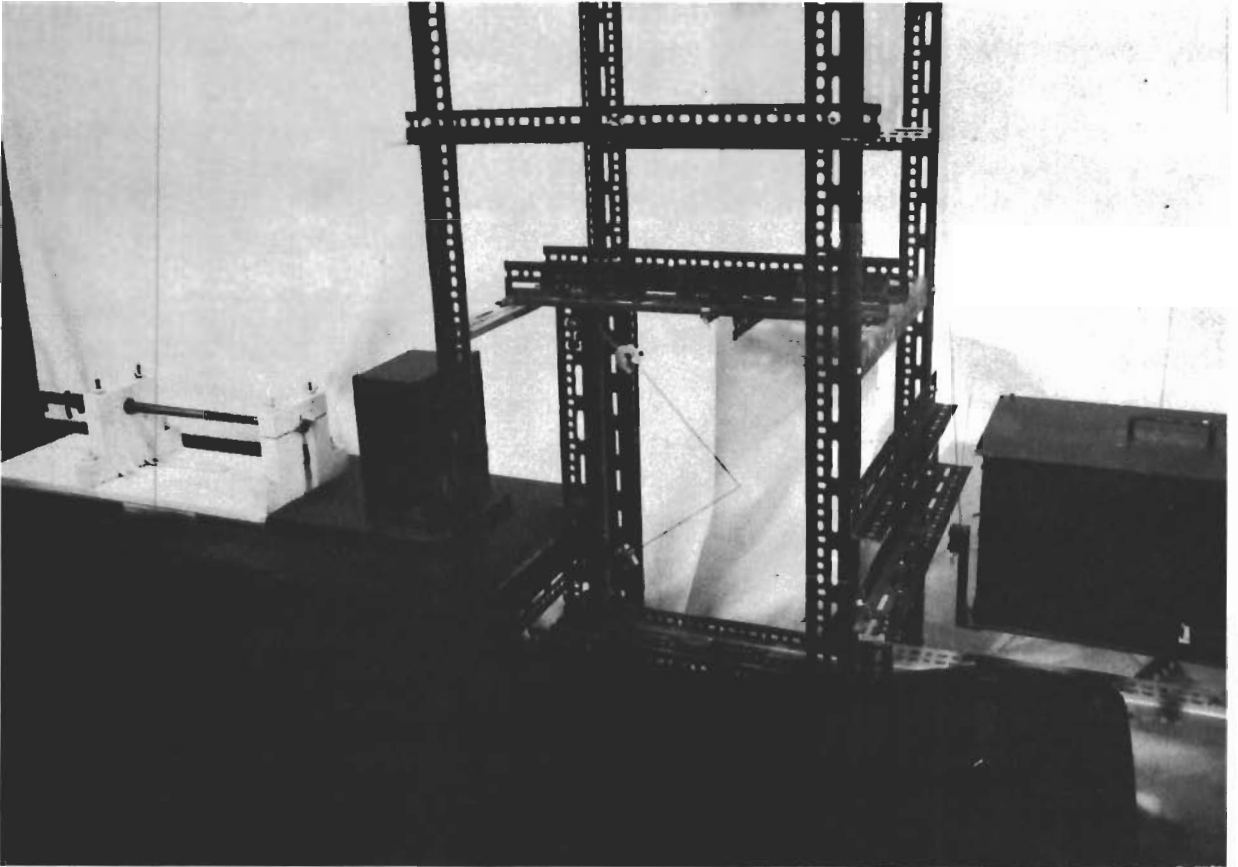


FIGURE 9 .22 CALIBRE IMPACT TESTER

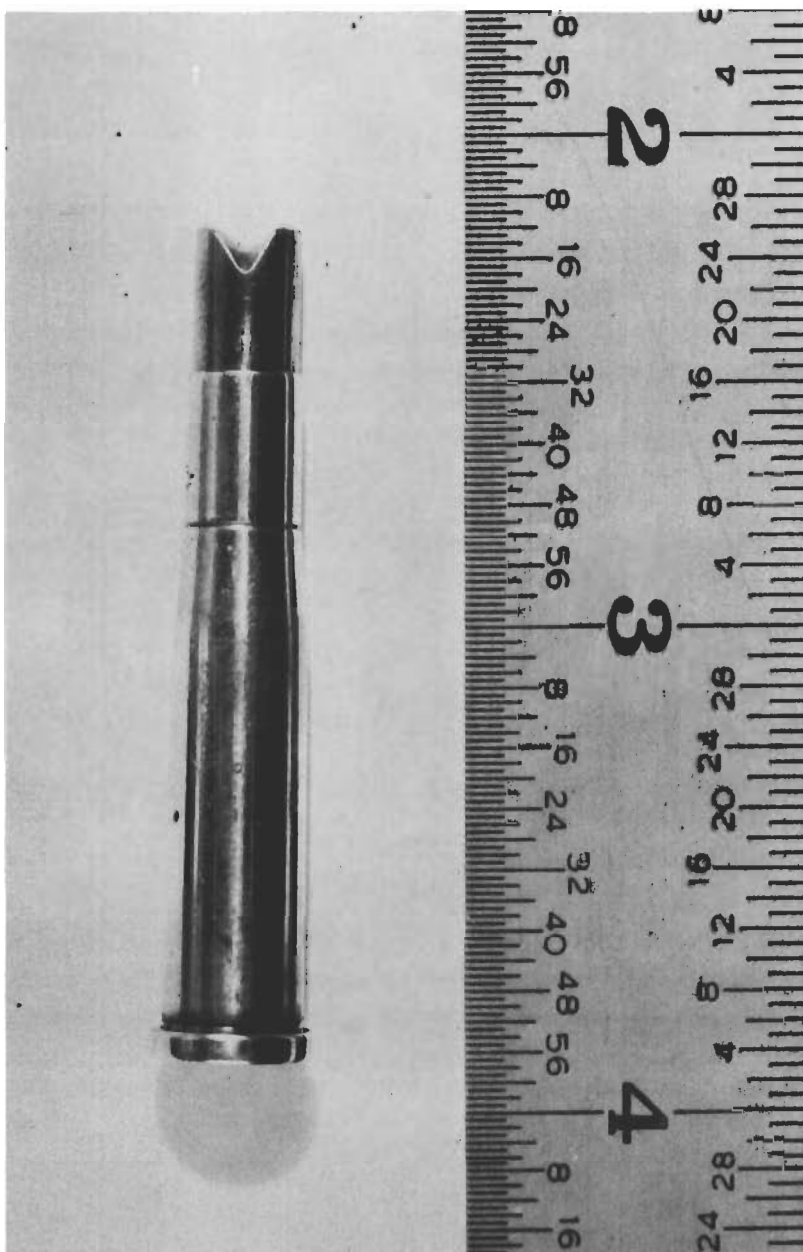


FIGURE 10 BULLET

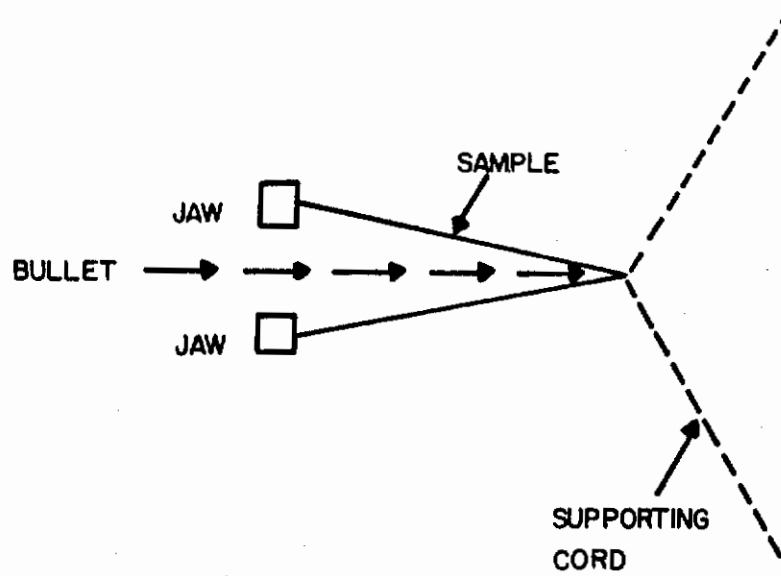
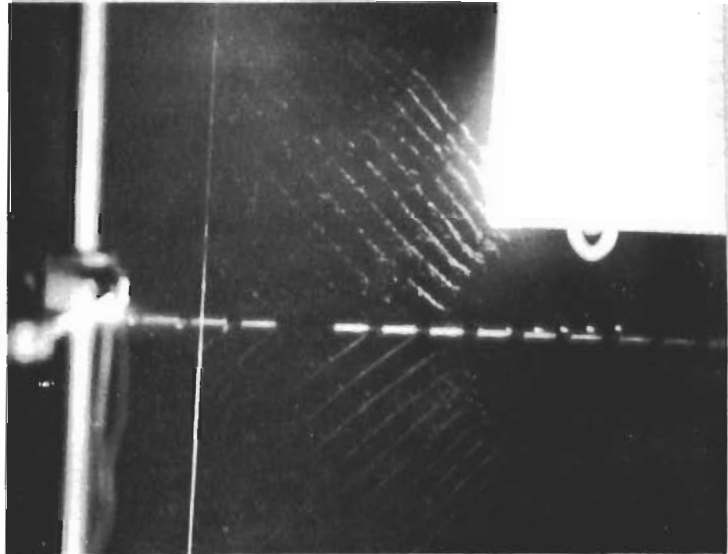
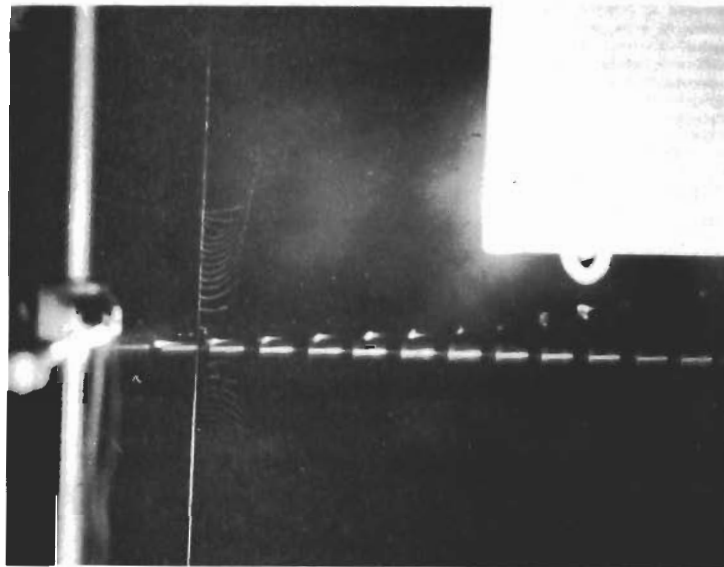


FIGURE 11 IMPACT TEST SET-UP



(a)



(b)

FIGURE 12 IMPACT TEST RESULTS

# Contrails

After breaking the yarn, the bullet is caught in a ballistic pendulum. The velocity of the bullet is calculated from the deflection of the pendulum, knowing the mass and period of the pendulum and the mass of the bullet. The kinetic energy of the bullet absorbed in breaking the yarn sample is insignificant.

The length of one leg of the yarn sample being tested is approximately one foot. The velocity of sound in typical materials of interest is of the order of 10,000 ft/sec. Therefore, the length of time it would take a stress wave to travel from the point of impact, be reflected at the jaw and return to the point of impact is of the order of  $2 \times 10^{-4}$  seconds. As previously noted, critical velocity is defined herein as the velocity at which rupture occurs within  $4$  to  $5 \times 10^{-5}$  seconds after impact at the point of impact. This is, therefore, roughly one-twentieth of the time it takes a stress wave to travel to the jaw and back. Sample rupture due to a stress buildup resulting from stress wave reflections can therefore be neglected.

The manner in which the critical velocity is determined can be seen by examining Figures 12(a) and 12(b). The photograph in Figure 12(a) shows a test in which the impact velocity is below critical. As shown the yarn is still around the nose of the bullet several exposures after impacting the sample. Considerable yarn elongation is taking place demonstrating that this particular impact velocity is below critical. This is further confirmed by the presence of the traveling transverse wave.

In Figure 12(b) the yarn sample has broken before the second exposure after impact, i.e., the sample has ruptured within 40-50 microseconds, the time between light flashes, after impact. This impact velocity is therefore the critical velocity for this sample, as per the definition.

By making a large number of tests over a range of impact velocities, it is possible to determine the critical velocity for a particular sample quite accurately.

The impact test results for the one hundred filament Chromel R wire yarn are given in Table 7. The critical velocity is given for lateral impact ( $\beta = 90^\circ$ ),  $45^\circ$  impact ( $\beta = 45^\circ$ ), and longitudinal impact ( $\beta \approx 0$ ). The critical velocities are given within plus or minus 25-50 feet per second. This is the anticipated range due to variation in yarn properties, an insufficient number of tests, and the lack of precision of the test method.

In testing the samples longitudinally the jaws are positioned one above the other with sufficient room between them to allow the bullet to pass. The angle  $\beta$  is therefore not  $0^\circ$  but approximately  $10^\circ$ . Theoretically critical velocity should increase only slightly with increasing angle for small angles (see the Appendix).

As noted in Table 7, the critical velocities of the wire yarn are low. Therefore, a brief investigation of the feasibility of improving upon the impact performance of the metal yarn by putting in greater geometric elongation was carried out. The structure examined was a wire covered HF-1 yarn (see Section VI). The critical velocities of the HF-1 yarn and the covered yarn are also given in Table 7. As shown the critical velocities of the HF-1 yarn are considerably greater than those of the metal yarn and the critical velocities of the composite yarn are between those of the metal and

TABLE 7

CRITICAL VELOCITIES OF YARNS  
(ft./sec)

Yarn Sample	Longitudinal ( $\beta = 10^\circ$ )		$\beta = 45^\circ$		Lateral ( $\beta = 90^\circ$ )	
	Vel. (ft./sec)	Condition	Vel. (ft./sec)	Condition	Vel. (ft./sec)	Condition
10/10/0.5 mil/3.0 S/3.0 Z	157	Below Critical	162	Below Critical	193	Well Below Critical
	164	Below Critical	167	Below Critical	315	Well Below Critical
	182	Just Below Critical	172	Below Critical	677	Just Below Critical
	199	Just Critical	180	Below Critical	701	Just Below Critical
	209	Just Critical	183	Below Critical	747	Just Above Critical
	210	Just Critical	191	Just Below Critical		
	214	Just Critical	209	Just Critical		
	290	Above Critical				
		Critical vel. = 200 ± 25		Critical vel. = 200 ± 25		Critical vel. = 710 ± 40
200-100 HT-1 (1/2 Z)	438	Well Below Critical	648	Below Critical	1220	Below Critical
	445	Well Below Critical	719	Just Below Critical	1326	Below Critical
	485	Well Below Critical	724	Just Below Critical	1373	Below Critical
	488	Well Below Critical	736	Just Above Critical	1413	Just Below Critical
	508	Below Critical	759	Just Above Critical	1437	Just Below Critical
	608	Below Critical	794	Above Critical	1454	Just Critical
	625	Just Below Critical			1454	Just Critical
	648	Very Close to Critical			1472	Just Above Critical
	683	Just Below Critical			1478	Just Above Critical
	730	Just Above Critical			1513	Above Critical
	811	Above Critical				
		Critical vel. = 700 ± 25		Critical vel. = 725 ± 25		Critical vel. = 1450 ± 50
Covered yarn 200-100 HT-1 Core, 10/10/0.5 mil/3.0 S/3.0 Z Chromel R Covering Yarn	187	Well Below Critical	163	Well Below Critical	269	Well Below Critical
	233	Well Below Critical	234	Well Below Critical	531	Below Critical
	245	Well Below Critical	239	Well Below Critical	578	Below Critical
	286	Well Below Critical	250	Well Below Critical	636	Just Below Critical
	309	Just Below Critical	327	Below Critical	654	Just Below Critical



TABLE 7 (continued)

CRITICAL VELOCITIES OF YARNS

(ft./sec)

Yarn Sample	Longitudinal ( $\beta = 10^\circ$ )		$\beta = 45^\circ$		Lateral ( $\beta = 90^\circ$ )	
	ft./sec	Remarks	ft./sec	Remarks	ft./sec	Remarks
Covered Yarn 200-100 HT-1 Core, 10/10/0.5 ml/3.0 S/3.0 Z Chromel R Covering Yarn (continued)	327	Very Close to Critical	329	Below Critical	735	Just Below Critical
	327	Just Critical	361	Very Close to Critical	765	Just Critical
	327	Just Below Critical	380	Just Below Critical	776	Just Above Critical
	345	Just Below Critical	426	Just Above Critical	800	Above Critical
	350	Close to Critical - Below				
	368	Close to Critical - Below				
	371	Just Critical				
	378	Just Critical				
	384	Just Critical				
		Critical vel. = 350 $\pm$ 25		Critical vel. = 400 $\pm$ 25		Critical vel. = 750 $\pm$ 25
840-140 Nylon Type 700, Bright (1/2 Z)	701	Below Critical	689	Below Critical	1431	Below Critical
	736	Below Critical	975	Below Critical	1629	Below Critical
	765	Below Critical	1080	Below Critical	1859	Below Critical
	788	Just Below Critical	1080	Below Critical	1879	Below Critical
	829	Just Below Critical	1080	Below Critical	1981	Just Below Critical
	836	Just Above Critical	1119	Below Critical	2072	Just Above Critical
	841	Just Above Critical	1180	Just Below Critical		
	858	Just Above Critical	1256	Above Critical		
	881	Just Above Critical				
	969	Just Above Critical				
989	Just Above Critical					
	Critical vel. = 800 $\pm$ 50		Critical vel. = 1200 $\pm$ 50		Critical vel. = 2025 $\pm$ 50	

# Contrails

HT-1 yarns. This appears to indicate that the impact performance of metal yarns can be improved by wrapping them around other yarns.

For comparison, the critical velocities of a nylon yarn are also given in Table 7.

An analysis of oblique impact stresses and strains is given in the Appendix. The results of the analysis, Figure 53, enable the impact rupture strain to be calculated from the critical velocity for any angle of impact if the velocity of propagation of a longitudinal wave in the sample being investigated is known.

The velocities of propagation of a longitudinal wave in the wire yarn, HT-1 yarn and nylon yarn over a range of strains are given in Figure 13. The data was obtained with the Pulse Propagation Meter.\* By means of oscillating crystals this instrument sends discrete strain pulses along the yarn length. The time taken for the pulses to travel along the yarn from a transducer to a receiver a known distance away is measured, thereby giving the velocity of propagation of a longitudinal stress wave. The velocity is obtained as a function of strain by performing the test with the sample mounted in an Instron. The position of the crystals is fixed in space and the pulse travel time is recorded as a function of cross head position.

As shown in Figure 13, the propagation velocities of the nylon and HT-1 yarns increase with increasing strain while that of the metal yarn remains constant.

The impact rupture strains of the metal, HT-1 and nylon yarns are given in Table 8 for longitudinal, 45°, and transverse impact. This data was obtained by successive iterations from the critical velocities given in Table 7, the longitudinal wave velocities in Figure 13, and the analysis in the Appendix (Figure 53). As shown the impact rupture strains for each yarn are approximately the same for the three different impact angles. Note also that the rupture strains of the nylon and HT-1 yarns are considerably greater than that of the metal yarn.

A range of strain values rather than a single value is given in each case in Table 8 because the critical velocities given in Table 7 are plus or minus 25-50 ft/sec.

TABLE 8  
OBLIQUE IMPACT RUPTURE STRAINS  
(percent)

Yarn Sample	Longitudinal ( $\beta = 10^\circ$ )	$\beta = 45^\circ$	Lateral ( $\beta = 90^\circ$ )
10/10/0.5 mil/3.0 S/3.0 Z Chromel R	1.3 - 1.6	0.9 - 1.2	1.2 - 1.4
200-100 HT-1 (1/2 Z)	5.9 - 6.3	4.7 - 5.1	4.1 - 4.5
840-140 Nylon Type 700, Bright (1/2 Z)	6.5 - 7.2	7.5 - 8.0	6.6 - 6.9

\* Manufactured by KLI Research and Development Corp., Boston, Mass.

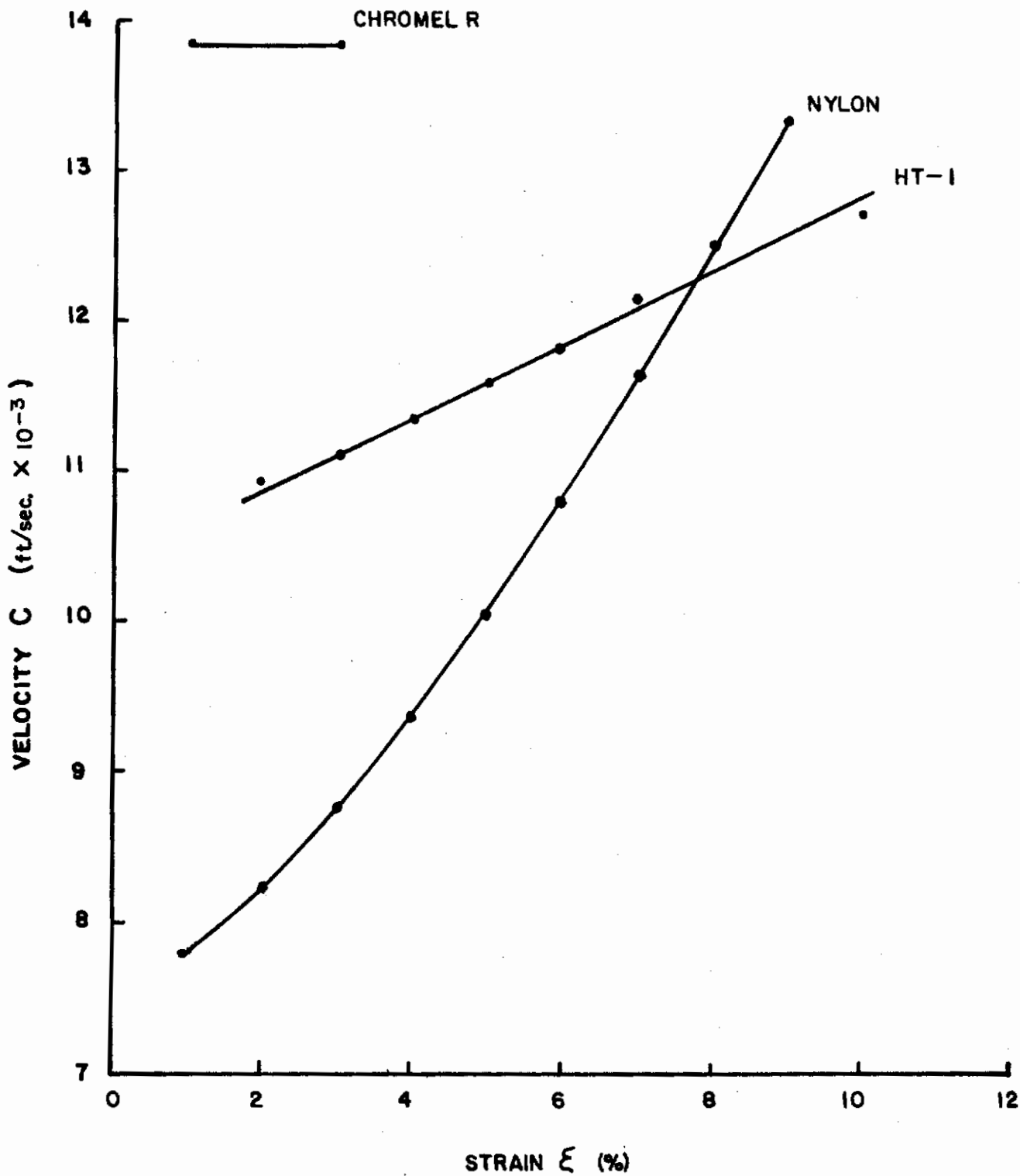


FIGURE 13 VELOCITY OF PROPAGATION OF A LONGITUDINAL WAVE

## 2. Fabric

The ASD Cold Gas gun impact testing machine (2,5,6), Figure 14, was used in the investigation of the high speed impact energy absorption of the metal fabric. Briefly, in this test the fabric specimen is folded in the shape of a "V" and fastened to a pendulum. A missile whose mass can be from 2 ounces to 10 pounds is propelled from a helium (or nitrogen) operated gun at velocities from 200 to 750 ft/sec, and ruptures the specimen. The deflection of the pendulum resulting from the impact is recorded. After rupturing the specimen, the missile is caught by a second pendulum. The deflection of this pendulum is also recorded.

Knowing the period and displacement of the first pendulum, the loss in missile velocity as a result of rupturing the specimen can be determined. Similarly, knowing the period and displacement of the second pendulum, the residual velocity of the missile can be determined. The missile impact velocity is the sum of the residual velocity and velocity loss, and the impact energy absorption E of the specimen is given by

$$E = \frac{1}{2} m (V_1^2 - V_2^2)$$

where  
m = missile mass  
V<sub>1</sub> = missile impact velocity  
V<sub>2</sub> = missile residual velocity

The weight of the lightest linen-inserted phenolic plastic missile is approximately 8 ounces and the lowest velocity that this missile can be propelled at is approximately 200 ft/sec. The kinetic energy KE of an 8 ounce missile traveling at 200 ft/sec is

$$KE = \frac{8 \text{ oz} \times (200 \text{ ft/sec})^2}{2 \times 16 \text{ oz/lb} \times 32.2 \text{ ft/sec}^2} = 310 \text{ ft lbs} .$$

The rupture of a specimen must not absorb more than approximately 10 percent of the kinetic energy of the missile in order to be able to assume that the missile velocity is constant during the impact. The width of the nose of the missile is 2 inches and the maximum specimen width that is practical is 1.5 inches.

The tensile strength of the metal fabric being impacted is approximately 200 lbs/inch and its rupture elongation in the warp direction approximately 7 percent. The energy U that a 1.5 inch strip of the fabric of length GL can absorb is conservatively given by

$$U = \frac{1.5 \text{ in} \times 200 \text{ lbs/in} \times 0.07 \text{ in/in} \times GL}{2} = 10.5 \text{ GL(ft)} .$$

Equating this expression to 31 ft lbs shows that approximately 3 feet of a 1.5 inch wide strip of the metal fabric is required to absorb 10 percent of the kinetic energy of the 8 ounce missile impacting the fabric at 200 ft/sec. This means that the legs of the "V" must be 18 inches long, which is the standard test length. Two inch diameter capstan jaws are used, therefore a total specimen length of 5.5 feet is required.

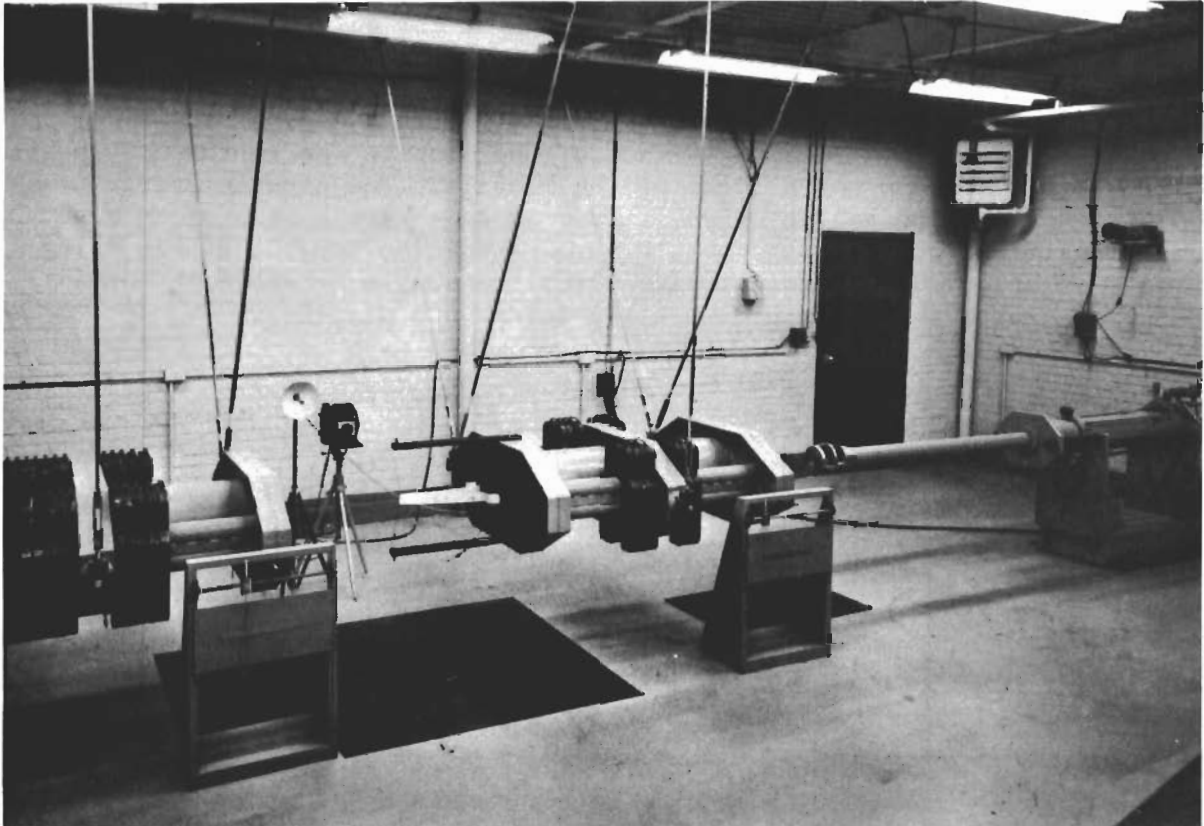


FIGURE 14 COLD GAS GUN IMPACT TESTING MACHINE

# Contrails

The cold gas gun impact firings are summarized in Table 9. The multifilament yarn wire fabric and a monofilament wire cloth were tested. The wire cloth is a 90x90 mesh, type #316 stainless steel, 0.00525 inch wire diameter cloth. It exhibits a tensile strength of 152 lbs/inch and an elongation of 19.8% as measured on an Instron tensile tester. A one inch fabric width, 3.5 inches gage length, and 0.5 inch/minute jaw speed were used.

The multifilament wire yarn fabric impact data indicates approximately the same energy absorption over a wide impact velocity range. Several of the impact velocities are considerably in excess of the longitudinal critical velocity of the yarn, the velocity above which the material should rupture with no energy absorption, as determined with the 0.22 calibre impact tester. These results are at variance with similar data on nonmetallic cloth, and may reflect experimental inaccuracies as described below.

A balsa wood missile with a weight of two ounces was used in some of the firings. The impact resistance of the missile was improved by putting a thick epoxy coating on the nose of the missile. The kinetic energy of a two ounce missile traveling at 200 ft/sec is one-quarter that of an eight ounce missile. Therefore the metal fabric should be capable of absorbing 40 percent of the balsa wood missile kinetic energy. As shown, essentially the same results were obtained with the balsa wood missiles.

TABLE 9

## SUMMARY OF COLD GAS GUN IMPACT FIRINGS

<u>Fabric Sample</u>	<u>Missile Weight (lbs)</u>	<u>Missile Velocity (ft/sec)</u>	<u>Energy Absorbed (ft lbs)</u>	<u>Remarks</u>
Monofilament wire cloth	0.096	160	18	
	0.096	225	24	
	0.096	230	27	
Monofilament wire cloth - two thicknesses	0.104	199	64	Sample did not break
	0.104	208	70	Sample did not break
	0.104	258	24	
Multifilament wire yarn fabric	0.44	173	40	
	0.106	195	25	
	0.096	198	59	Sample did not break
	0.44	228	36	
	0.104	250	37	
	0.105	278	33	
	0.44	284	49	
0.106	383	48		

# Contrails

The apparent discrepancy between the yarn and fabric data appears to be due to the low tensile strength of the metal fabric. The cold gas gun impact testing machine was designed for 10,000 pound strength webbings. When impacting fabric with a strength of only a few hundred pounds, the correction applied to the deflection of the first pendulum for the gas blast effect becomes one-half of the total pendulum deflection. Also, in the case of the low strength samples, the total pendulum deflection is only a couple tenths of an inch.

The current pendulums used with the cold gas gun impact testing machine weigh 300 pounds. A quick design study indicated that the pendulum weight could be reduced to 100 pounds. When testing the metal fabric, this would result in a pendulum deflection of approximately 0.5 inch, of which 0.1 inch would be gas effect. This would not give a sufficient improvement in the accuracy of the data obtained to warrant the expense of the modification. The investigation of the high speed impact performance of metal fabrics has therefore been discontinued.

### III. SEAMING

The results of a preliminary metal fabric seaming investigation are given below.

The following expression may be used as a rough guide in calculating the minimum sewing thread strength, stitches per inch and number of rows of stitches required for a given fabric strength<sup>(3)</sup>.

$$\frac{[2 \times \text{thread strength (lbs)} \times \text{loop efficiency}][\text{no. of rows of stitches}]}{[\text{stitches per inch}] = \text{fabric strength (lbs/inch)} .$$

Previous work on nylon cloth seams indicates that approximately ten stitches per inch of the 301 type is optimum<sup>(3)</sup>. The above expression therefore indicates that a metal sewing thread to be used in sewing a two row seam in a metal fabric with a 200 lbs/inch tensile strength must have a tensile strength equal to or greater than (assuming a loop efficiency of 0.60<sup>(3)</sup>)

$$\begin{aligned} \text{thread strength} &= \frac{200 \text{ lbs/inch}}{2 \times 0.60 \times 2 \times 10 \text{ stitches/inch}} \\ &= 8.3 \text{ lbs} . \end{aligned}$$

To insure that good seam efficiency would be obtained a sewing thread with approximately 50 percent greater strength than that given by the above calculation was designed and twisted. Ten ends of 0.5 mil Chromel A\* wire were plied 3.1 Z tpi, ten ends of the plied yarn cabled 9.0 S tpi and five ends of the cabled yarn recabled 6.1 Z tpi. The thread is approximately balanced and has a tensile strength of 13.4 lbs and an elongation of 1.8%. One-half of a pound of the thread was twisted.

The thread was given a Teflon coating to improve its abrasion resistance. It was passed through a water dispersion of Teflon at 30 percent solids, the coating being cured at approximately 800°F for 45 seconds.

The knot strength of the thread was measured in the Instron by testing a length of yarn with a simple overhand knot at its midpoint. The knot efficiency was found to be 61%. The knot efficiency of the 100 filament yarn (10/10/1, 3.1 S/3.1 Z, 0.5 mil Chromel A) is 73%.

Two three-inch square panels of the multifilament yarn metal fabric were sewn together using an integral IS-2 seam (Figure 15, seam type A) at 10 stitches, of the 301 type, per inch and with a 1/4 inch gage (distance between rows of stitches). A standard type 400W1 industrial Singer sewing machine and a number 18 needle were used.

The seam was tested by the slit seam method<sup>(3)</sup>, Figure 16. As shown, the sewn fabric was slit laterally inward from each edge above and below the sewn seam for 1/2 inch. This left a two inch wide central section of intact transverse yarns. The sewn sample was then clamped in three inch wide Instron jaws just above the slits and tested at a jaw speed of one inch

\* Trademark, Hoskins Manufacturing Co., Detroit, Michigan; 80 Ni, 20 Cr.



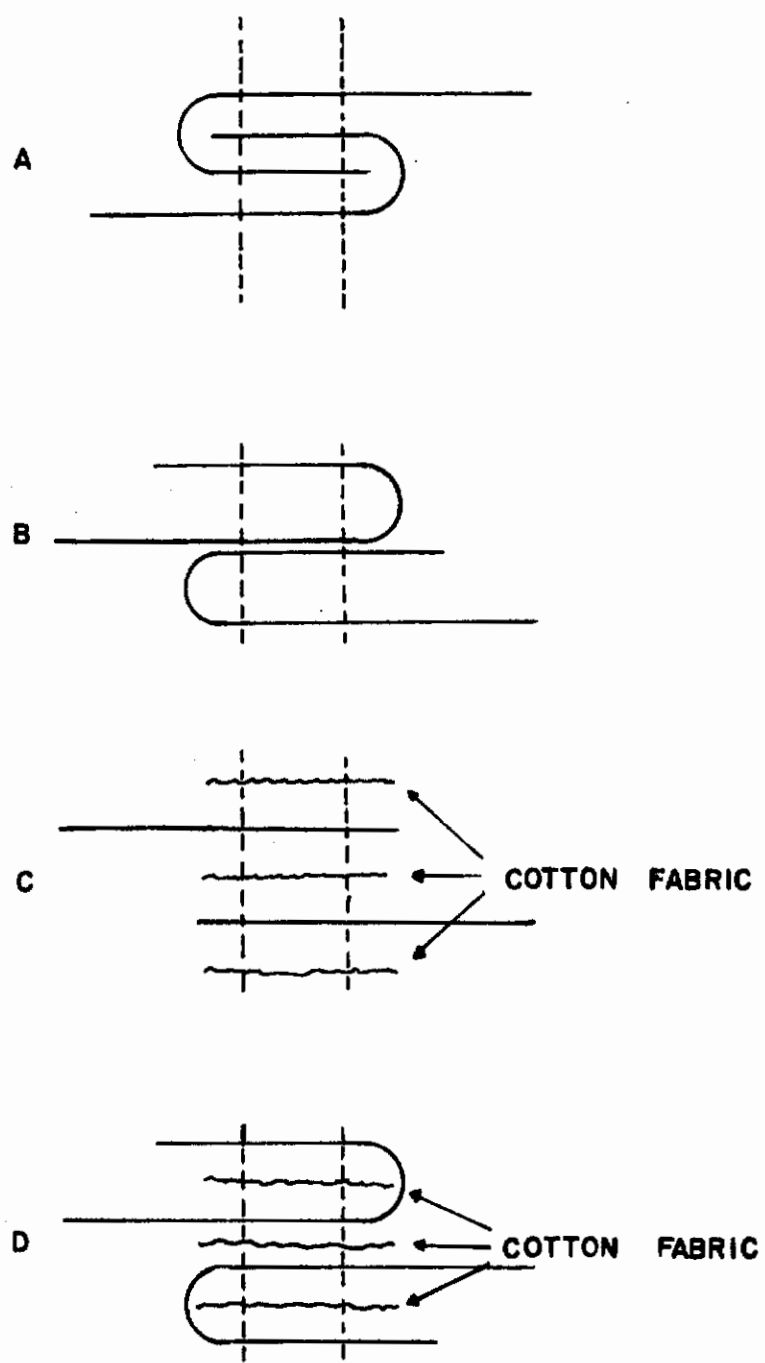


**FIGURE 15 SEAM TYPES**

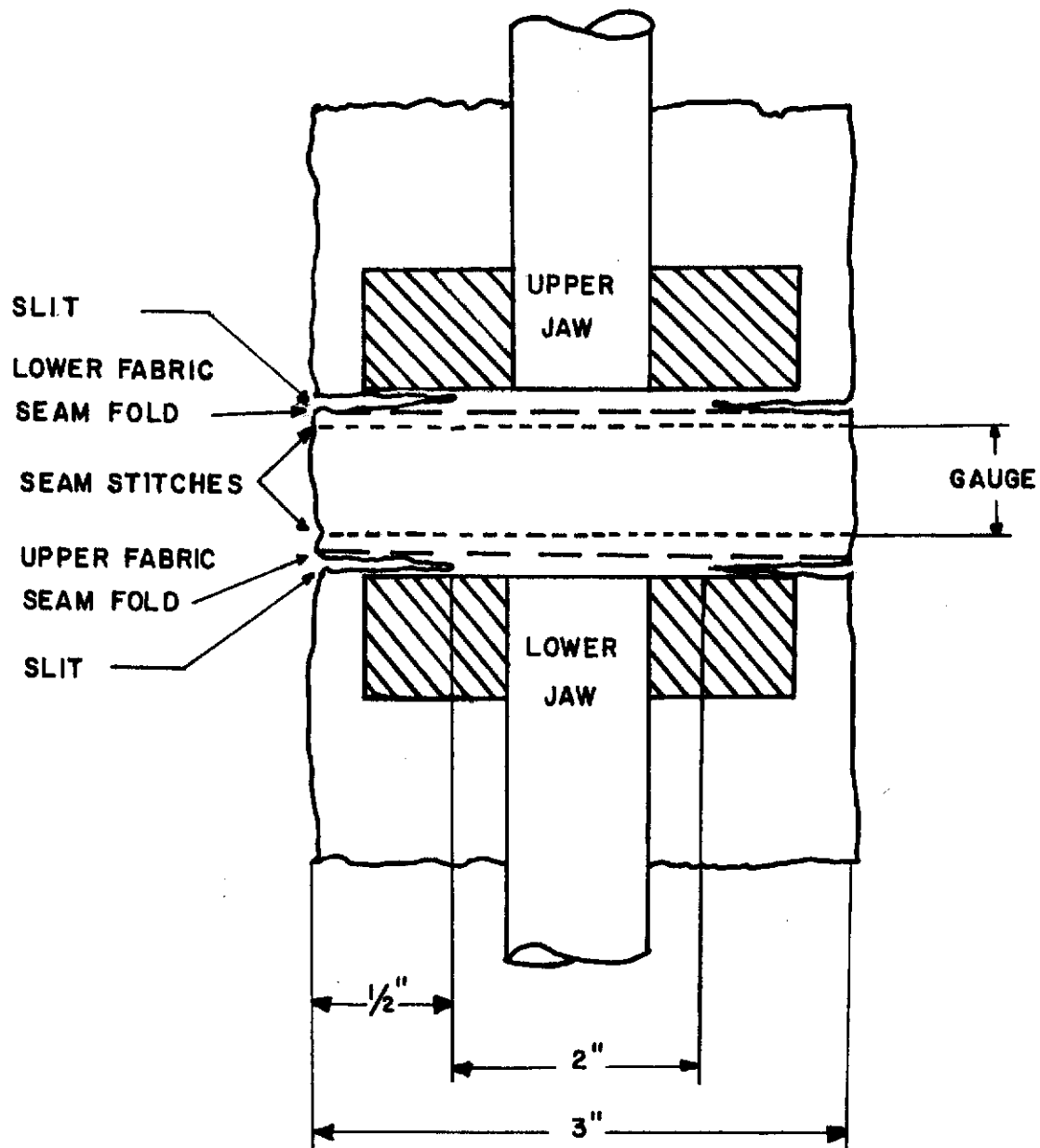


FIGURE 16 SLIT SEAM SAMPLE

# Contrails

per minute. As shown in Table 10, the seam efficiency was 52 percent. The yarns appeared to break where they passed under the sewing thread. A second sample was made using less sewing thread tension. The increase in seam efficiency was not significant. These disappointing test results indicated that an extensive sewing study would be required. In an effort to conserve fabric, one inch strips were used in further sewing and testing.

The study was begun by going to the B type seam shown in Figure 15, and varying the number of stitches per inch. It was hoped that the B type seam and fewer stitches per inch might prevent the early rupture of the fabric yarns. As shown (test nos. 3-9) in Table 10, a 47 percent efficiency was the highest obtained. It should be pointed out that these results are very approximate since few tests and only one inch wide fabric strips were used. It was hoped that these test results would indicate a direction to go for improvement. Numerous tests would then be made with larger samples in order to get accurate data.

Following analysis of the above results, some detective work was carried out. Two strips of fabric were sewn together and then the sewing thread pulled out. The fabric strip exhibited one hundred percent of its original strength (test no. 10). This shows that the sewing operation itself does not damage yarns. Next two rows of stitches were run across a strip of fabric (test no. 11). The strip exhibited an 85 percent strength efficiency. This indicates that the yarn angulation caused by the presence of the sewing thread results in approximately a 15 percent decrease in fabric strength. This is a significant loss but does not explain the 50 percent efficiencies observed.

Four rows of stitches and a few stitches per inch were tried (test no. 12) with no improvement in efficiency. A low sewing thread tension during sewing was also tried (test nos. 13 and 14) with no improvement. A seam was made with a softer sewing thread (HT-1) of comparable diameter (test no. 15) with no improvement.

To decrease metal-to-metal contact, seams were sewn with strips of cotton fabric between fabric layers, Figure 15, seam types C and D. As shown by the results in Table 10 (test nos. 16-24), no significant increase in seam efficiency was obtained.

Further tests were then made using the B type seam. Various combinations of stitches per inch and rows of stitches were tried. As shown (test nos. 25-31) a 58 percent efficiency was the largest obtained. Most of the seam breaks were of a progressive type. The fabric yarns in a narrow area of the fabric broke first, with adjacent yarns breaking progressively thereafter. This indicates poor yarn-to-yarn elongation balance. Since the metal yarns from which the fabric is woven have a very low elongation, about 5 percent, poor elongation balance is to be expected. In an effort to overcome this shortcoming of fine wire metal yarns, the distance between rows of stitches, gage, was increased from 1/4-1/2 inch to 1 and 2 inches on two samples (test nos. 25 and 28). However, no significant improvement in efficiency was observed.

Two tests were made using a large diameter HT-1 sewing thread (test nos. 32 and 33). These samples exhibited efficiencies of 59.5 and 65

# Contrails

TABLE 10

SEAM TRIALS

Test Number	Stitches per Inch	Rows of Stitches	Seam Type	Sewing Thread Tension	Gage (inches)	Efficiency (%)	Comments
1	10	2	A	high	1/4	52	Yarns broke
2	10	2	A	medium	1/4	54	Yarns broke
3	6	2	B	medium	1/4	33	Sewing thread broke
4	6	2	B	medium	1/4	19	Sewing thread broke
5	7-1/2	2	B	medium	1/4	45	Yarns broke
6	8	2	B	medium	1/4	41	Yarns broke
7	10	2	B	medium	1/8	47	Yarns broke
8	10	2	B	medium	1/4	39	Yarns broke
9	15	2	B	medium	1/4	34	Yarns broke
10	10	2	B	medium	1/4	100	Sewing thread removed and strip tested
11	10	2	-	medium	1/4	85	Single fabric strip stitched and tested
12	6	4	B	medium	1/4	45	Sewing thread broke
13	8	2	B	low	1/4	40	--
14	8	2	B	low	1/4	51	--
15	10	2	B	medium	1/4	29	HT-1 sewing thread
16	10	2	C	medium	1/4	23	Yarns pulled out
17	6	4	C	medium	1/8	36	Yarns pulled out
18	10	4	C	medium	1/8	35	Yarns pulled out
19	10	2	D	medium	1/4	29	--
20	10	2	D	medium	1/4	33	--
21	10	4	D	medium	1/4	55	--
22	6	4	D	medium	1/4	48	--
23	10	4	D	medium	1/8	49	Cotton sewing thread used
24	10	4	D	medium	1/8	51	Cotton sewing thread used
25	10	2	B	medium	2	55.7	
26	6	3	B	medium	1/4	28	Sewing thread broke
27	10	4	B	medium	1/4	51	
28	7	4	B	medium	1	58	
29	6	4	B	medium	1/2	57.7	
30	6	4	B	medium	1/2	55	
31	6	4	B	medium	1/4	56	
32	6-1/4	4	B	medium	1/4	59.5	#24 HT-1 thread
33	6	4	B	medium	1/2	65	#24 HT-1 thread

# Contrails

percent. The latter efficiency is the best obtained in any of the metal fabric seam tests.

Examination of the seam trials made to date indicates that the seam efficiency of the metal fabric might be improved by using a larger diameter sewing thread and fewer stitches per inch. A larger diameter sewing thread should result in the fabric yarns being less severely bent where they pass under the sewing thread and, thereby, improve the seam efficiency. It is also recognized that a larger sewing thread diameter will increase fabric yarn angulation due to the presence of the sewing thread, thereby decreasing the seam efficiency. However, it is anticipated that the first effect of a larger thread will exceed that of the second effect.

Six stitches per inch is the smallest number a standard type 400W1 industrial Singer sewing machine can sew. A 111W115 Singer sewing machine has therefore been rented. It is a high speed, heavy duty industrial machine capable of as few as three and a half stitches per inch. Excessive sewing thread abrasion was experienced during initial trials with this machine due to its high speed. The machine is currently being modified so that it can be run at slower speeds.

Three ends of the 500 filament metal sewing thread used in the seam trials discussed above have been plied together, and, as soon as the sewing machine is operational, the seaming investigation will be resumed.

IV. CORELESS CORD

Two coreless cords were braided from a metal yarn composed of three hundred 0.5 mil wires. The construction of the yarn is as follows. Ten ends of fully annealed 0.5 mil Chromel A wire were plied 4.0 Z tpi, ten ends of the plied yarn cabled 8.0 S tpi and three ends of the cabled yarn recabled 4.0 Z tpi. The yarn is balanced and has a diameter of approximately<sup>(10)</sup>

$$20.5 \text{ (rings)} \times 0.0005 \text{ inch (wire diameter)} = 0.01025 \text{ inch}$$

to

$$2 \text{ (ply diameters in a yarn diameter)} \times 11.25 \text{ (rings in a ply)}$$

$$\times 0.0005 \text{ inch (wire diameter)} = 0.01125 \text{ inch .}$$

The geometric and physical properties of the cords are given in Table 11.

Approximately 1.8 yards of the regular stitch cord were braided and 2.2 yards of the basket stitch cord. These lengths were too small to allow the use of capstan jaws in determining the breaking strengths of the cords. Therefore, one inch of each end of five inch lengths of the cords were heavily coated with an epoxy resin. After the resin dried, the coated ends were clamped in flat serrated Instron jaws, leaving a three inch gage length. A jaw speed of two inches per minute was used. All breaks occurred at the jaws.

The sum of the tensile strengths of all the filaments in the regular stitch metal cord is given by

$$\frac{16 \text{ carriers} \times 6 \text{ ends/carrier} \times 300 \text{ filaments/end} \times 13.1 \text{ gm}^{(9)}}{454 \text{ gm/lb}} = 831 \text{ lbs .}$$

The regular stitch cord, therefore, exhibits a strength translation from filament to cord of 56.0 percent. The sum of the tensile strengths of the filaments in the basket stitch metal cord is 415.5 lbs, giving a strength translation of 76.5 percent.

The difference in tensile strength translation between the two cords is, at least in part, due to the difference in angle of the yarns to the axis of the cord, as reflected in the factor of two in picks per inch between the two cords.

The strength of both cords was not as large as it might have been because of considerable filament breakage during braiding. This was caused by yarn abrasion on the small metal yarn guides on each carrier.

A 630 denier three ply nylon yarn has a diameter of approximately<sup>(11)</sup>

$$0.0383 \sqrt{\frac{630}{5315}} = 0.0132 \text{ inch}$$

$$2 \times 0.0383 \sqrt{\frac{210}{5315}} = 0.0152 \text{ inch .}$$

The geometric structure and physical properties of a typical coreless cord<sup>(13)</sup> braided from a 630 denier nylon yarn (MIL-C-7515B (USAF), Amendment 1, Type III) are given in Table 12.

TABLE 11

CORELESS METAL CORD

No. of Carriers	Type of Stitch	Wire Diameter (mils)	Picks per Inch	Ends per Carrier	Total Ends	Weight (yds/lb)	Breaking Strength (lbs)	Yarn
16	regular (two over and two under)	0.5	7.0	6	96	13.0	465	3/10/10/0.5 mil wire/ 4.0 Z/8.0 S/4.0 Z
16*	basket (one over and one under)	0.5	3.5	6	48	27.4	318	3/10/10/0.5 mil wire/ 4.0 Z/8.0 S/4.0 Z
16	regular (two over and two under)	1.0	10.0	6	96	13.5	677	3/5/5/1.0 mil wire/ 4.0 Z/8.0 S/6.0 Z-2.0 S

\* The bobbin on every other carrier contained no yarn

TABLE 12

CORELESS NYLON CORD

Type Cord	No. of Carriers	Picks per Inch	Ends per Carrier	Total Ends	Weight (yds/lb)	Breaking Strength (lbs)	Elongation (%)	Yarn Denier	Yarn Ply
III	16	8.5 - 10	6	96	50	750	20	210	3

# Contrails

As a comparison of the properties of this nylon cord, Table 12, and the larger of the two 0.5 mil wire cords, Table 11, shows, the nylon cord has a considerably larger breaking strength. This is due to the greater diameter of the nylon yarn braided than that of the metal yarn braided, numerous broken filaments in the metal yarn, and the larger characteristic rupture elongation of nylon ( $\approx 8.5\%$ ). The greater elongation increases the opportunity for elongation balance and allows greater decrease in the angle of the yarns to the axis of the cord during tensile testing.

The flexibility of the two 0.5 mil wire cords was so great that it appeared that 1.0 mil wire might be safely used in such structures. To insure that the cord would be of a high quality, a 16 carrier #1 New England Butt Braider with Mossberg carriers, Figure 17, was purchased. The carriers were equipped with center sheave wheel take-offs, braider stops with sheave wheels and Alsimag\* top thread guides. These modifications minimize wire abrasion during braiding.

Five ends of 1.0 mil Chromel A wire were plied 4.0 Z tpi, five ends of the plied yarn cabled 8.0 S tpi and three ends of the cabled yarn re-cabled 6.0 Z and then 2.0 S tpi. The 75 filament yarn was balanced. This yarn has approximately the same diameter as the yarn composed of three hundred 0.5 mil wires. One pound of the 1.0 mil wire was braided. The construction and properties of the coreless cord are given in Table 11.

Two inch diameter capstan jaws and a jaw speed of two inches per minute were used in determining the breaking strength of the cord. The gage length was approximately five inches.

The sum of the tensile strengths of all the filaments in the cord is given by

$$\frac{16 \text{ carriers} \times 6 \text{ ends/carrier} \times 75 \text{ filaments/end} \times 50.8 \text{ gms}^{(9)}}{454 \text{ gms/lb}} = 806 \text{ lbs.}$$

The cord, therefore, exhibits a strength translation from filament to cord of 84 percent. As anticipated, this is considerably greater than was obtained with 0.5 mil wire. As previously noted the strength translation is not 100 percent because of the angle of the yarns to the axis of the cord.

The cord braided from 1.0 mil wire is very flexible, indicating that 0.5 mil wire does not have to be used in such structures. Photographs of all three of the metal cords are shown in Figure 18.

---

\* Manufactured by American Lava Corporation, Chattanooga, Tennessee



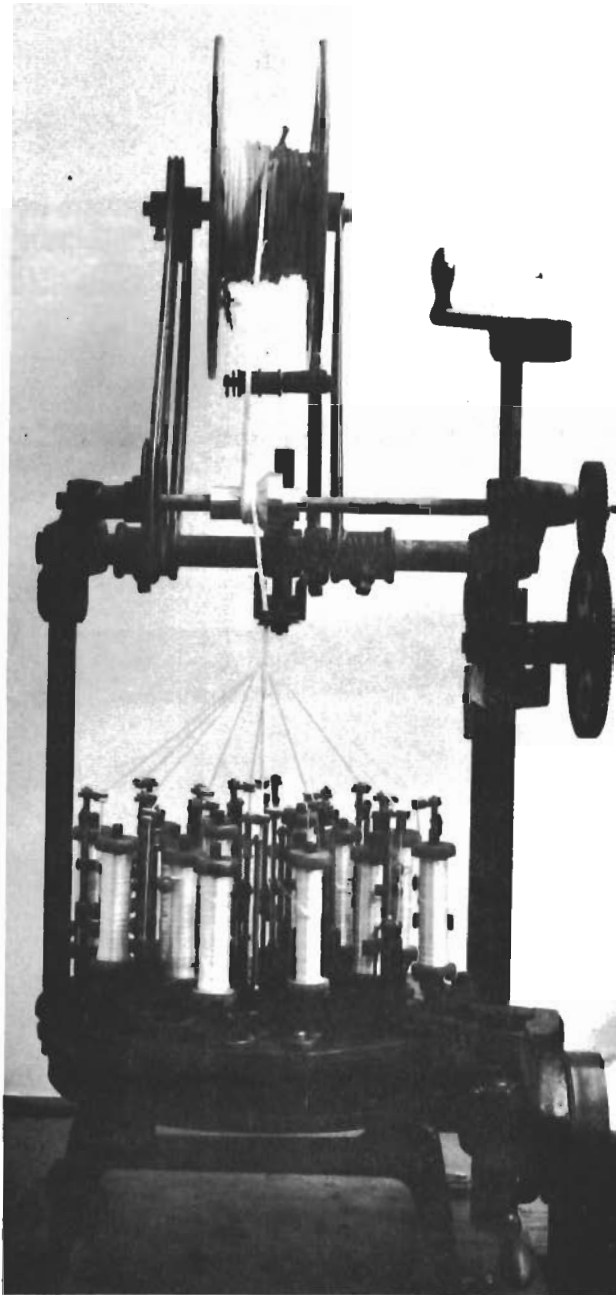


FIGURE 17 BRAIDER



0.5 mil wire  
regular stitch



0.5 mil wire  
basket stitch



1.0 mil wire  
regular stitch

FIGURE 18 CORELESS METAL CORDS

## V. TEXTURED YARN

Texturing a yarn increases the yarn bulk. When woven into a fabric this may result in increased fabric flexibility and bending recovery, and greater cover.

Approximately one-half pound of 0.5 mil diameter Chromel A wire was plied and cabled (10/10/1, 3.1 S/3.1 Z tpi). One-half of a pound of 1.0 mil Chromel A wire was also plied and cabled (5/5/1, 2.0 S/3.0 Z tpi). Both yarns were essentially balanced, torque-free. The results of an investigation of the various possible methods of bulking multifilament metal yarns using these yarns are discussed below.

The yarn configurations shown in Figures 19 and 20 were obtained by pulling yarn 90 degrees around mandrels of various diameters, using different yarn back tensions. The smaller size mandrels were supported by taping them to a 1/4 inch rod.

The yarns were tensioned by winding a cord around the empty portion of the barrel of the spool from which the yarn was taken-off and attaching one end of this cord to a weight and the other to a fixed eye. The actual yarn tension (see Table 13) resulting from this brake assembly was determined with an Instron tensile tester by fastening the system to the cross-head.

As shown in Figures 19 and 20, this method of imparting crimp to a yarn can give a high bulk; the smaller the mandrel diameter and the larger the yarn tension (see Table 13), the greater the yarn bulk.

In an effort to quantitatively characterize the bulk of each of the crimped yarn samples, the percent take-ups of the yarns were measured. The percent take-up of a crimped yarn is defined as

$$\text{Percent take-up} = \frac{L_2 - L_1}{L_2} \times 100$$

where  $L_1$  is the initial length of the crimped yarn sample and  $L_2$  is the length of the sample when extended out straight.

The percent take-ups of the 0.5 mil and 1.0 mil edge crimped multifilament wire yarns are given in Table 13. The initial yarn length  $L_1$  was measured under a tension of 0.2 gram and the extended length  $L_2$  was determined by pulling the sample out straight by hand and measuring the sample length. As shown, a very high percent take-up can be obtained using this crimping procedure.

The crimped yarns were tensile tested in an Instron tensile tester at a jaw speed of 0.5 inch/minute. The strength translation from the uncrimped yarn to the crimped yarn was noted. Initially, low strength translations were observed due to poor elongation balance resulting from clamping some of the crimped portion of the yarn in the jaws. This difficulty was avoided by taping the yarn every twelve inches prior to pulling it over the mandrels. The taped portions of the crimped yarn were then inserted in the Instron jaws. As shown in Table 13, the strength translation is excellent, particularly in the case of mandrel diameters of 14.5 mils and greater.

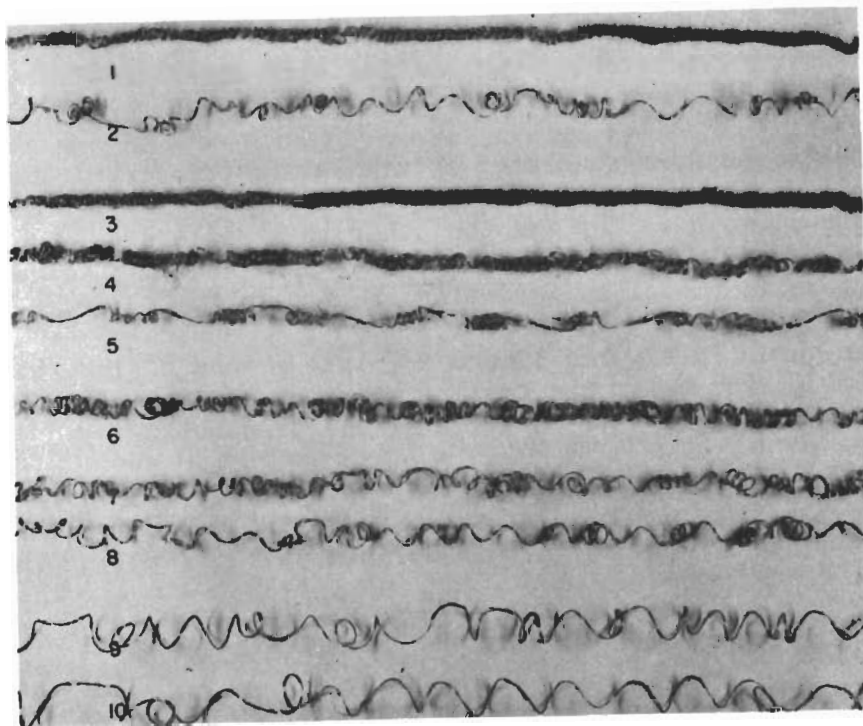


FIGURE 19    EDGE CRIMPED 0.5 MIL WIRE YARN

# Contrails

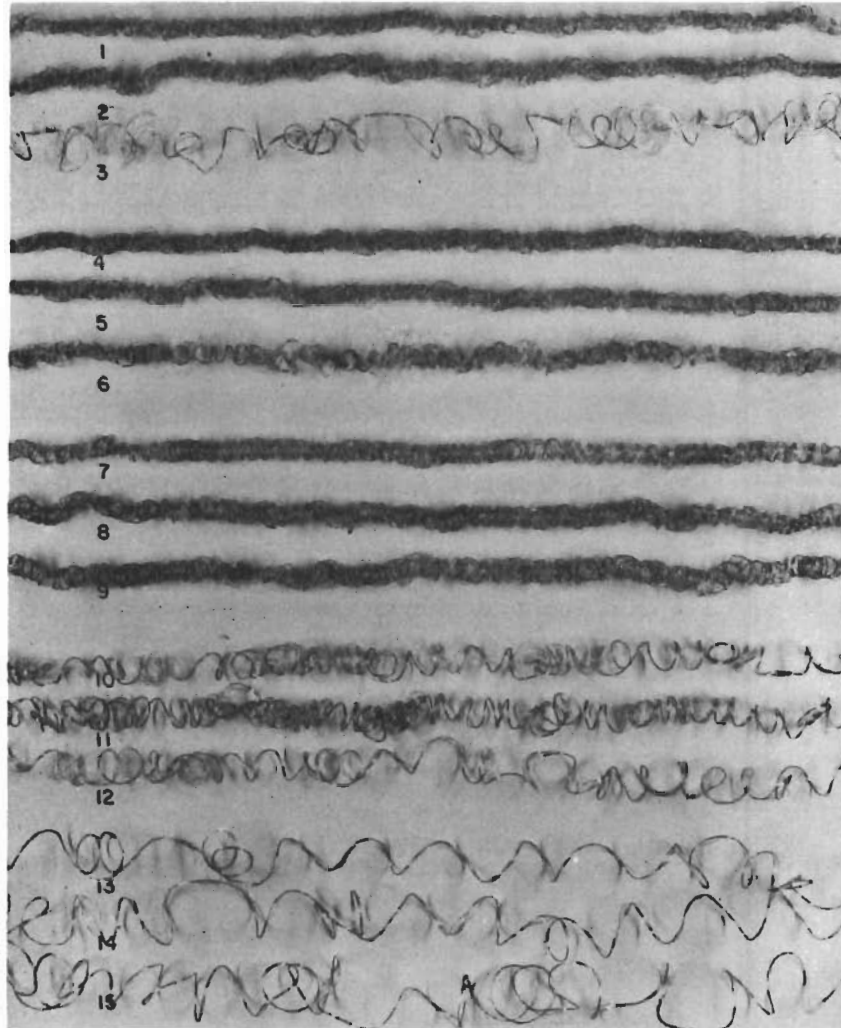


FIGURE 20 EDGE CRIMPED 1.0 MIL WIRE YARN

TABLE 13  
EDGE CRIMPED WIRE YARN

Wire Diameter (mils)	Material	Yarn Construction	Sample	Wire (gauge)	Mandrel Diameter (mils)	Yarn Tension (grams)	Yarn Take-up (percent)	Yarn Tensile Strength (grams)	Strength Translation from Uncrimped to Crimped Yarn (percent)	Uncrimping Force (grams)
0.5	Chromel A	10/10/1, 3.1 S/3.1 Z tpi	1	—	4.4	80	83	1021	81*	67
			2	—	4.4	15	52	1168	93	68
			3	79	14.5	200	84	1197	95	64
			4	79	14.5	120	78	1193	95	54
			5	79	14.5	80	65	1234	98	50
			6	69	29.2	200	69	1225	97	59
			7	69	29.2	120	56	1211	96	60
			8	69	29.2	80	49	1225	97	50
			9	55	52.0	200	17	--	--	--
			10	55	52.0	120	11	--	--	--
			11	55	52.0	80	9	--	--	--
1.0	Chromel A	5/5/1, 2.0 S/3.1 Z tpi	1	—	4.4	260	81	--	--	--
			2	—	4.4	90	84	1134	91**	51
			3	—	4.4	15	50	1227	99	80
			4	79	14.5	260	85	1204	97	24
			5	79	14.5	150	83	1243	100	30
			6	79	14.5	90	81	1250	100	31
			7	69	29.2	260	84	1228	99	20
			8	69	29.2	150	85	1218	98	22
			9	69	29.2	90	86	1160	93	33
			10	55	52.0	260	74	--	--	--
			11	55	52.0	150	72	--	--	--
			12	55	52.0	90	65	--	--	--
			13	46	81.0	260	59	--	--	--
			14	46	81.0	150	32	--	--	--
			15	46	81.0	90	15	--	--	--

\* based on an uncrimped yarn tensile strength of 1256 grams

\*\* based on an uncrimped yarn tensile strength of 1244 grams

-- not measured

# Contrails

The uncrimping force of the crimped yarns is also given in Table 13. This force is essentially the tensile force required to remove the crimp in the yarn. It is defined as the force at the point where the vertical projection of the intersection of the extrapolation of the linear portion of the load-elongation curve to the zero load axis intersects the load-elongation curve. As shown in Table 13, the yarn uncrimping force is 0.5% to 6.5% of the yarn tensile strength.

As shown in Figures 19 and 20, crimping metal yarns by the above procedure results in a helical yarn configuration; all filaments are approximately in phase. It would be desirable to have a bulked yarn in which the helical paths of the filaments are not in phase. One would anticipate that this could be accomplished by pulling the individual filaments over a small diameter mandrel before plying and cabling them into a yarn, or by pulling the individual plied yarns over small diameter mandrels before cabling. However, approximately the same final configurations were obtained by using these procedures as pulling the cabled yarn itself around a small diameter mandrel. Most of the helices were still in phase.

An investigation of the twist-untwist process as a means of bulking multifilament metal yarns was carried out. It was anticipated that this process would result in a bulked yarn since the vector sum of all filament bending moment vector components perpendicular to the axis of a twisted yarn is zero. However, considering each filament as a structural element, if the bending moment components perpendicular to the yarn axis are not externally resisted, each unrestrained filament end will move outward radially from the yarn center. Similarly, the vector sum of all components of the filament torsion vectors in a twisted yarn cross-section which are perpendicular to the yarn axis is zero. Nevertheless, considering each filament as a structural element, the filament torque components perpendicular to the yarn axis, if not externally resisted, would cause each unrestrained filament end to move radially inward. This tendency would be resisted by the corresponding bending components. It can be shown that the bending component for any filament acts in an opposite sense to the torsional component for that filament, and the ratio is independent of the filament helix angle, the ratio depending only on the ratio of the filament torsional rigidity to the filament bending rigidity. This ratio of rigidities for metal filaments is less than unity. Thus, cut filaments in a yarn will broom out rather than move inward<sup>(18,19)</sup>.

However, attempts to bulk the 0.5 mil and 1.0 mil multifilament metal yarns by the twist-untwist process were unsuccessful. Various combinations of inserted and removed twists per inch were tried but no appreciable increase in yarn bulk was obtained.

One of the numerous methods used to texture nylon yarn is the stuffer box process<sup>(22)</sup>. As shown in Figure 21, a weighted tube in the top of the unit compresses the column of yarn accumulated in the stuffer chamber. The incoming yarn is forced into the chamber by the feed rolls and as it bears against the previously processed material its filaments buckle and crimp. The amplitude and frequency of the crimp are varied by regulating the ratio of the yarn input to output, the weight of the tube and the feed roll pressure. The crimp amplitude can also be varied by reducing the diameter of the stuffer chamber for a short distance just above the feed rolls. The collar inserted in the stuffer chamber to accomplish this is referred to as a choke.

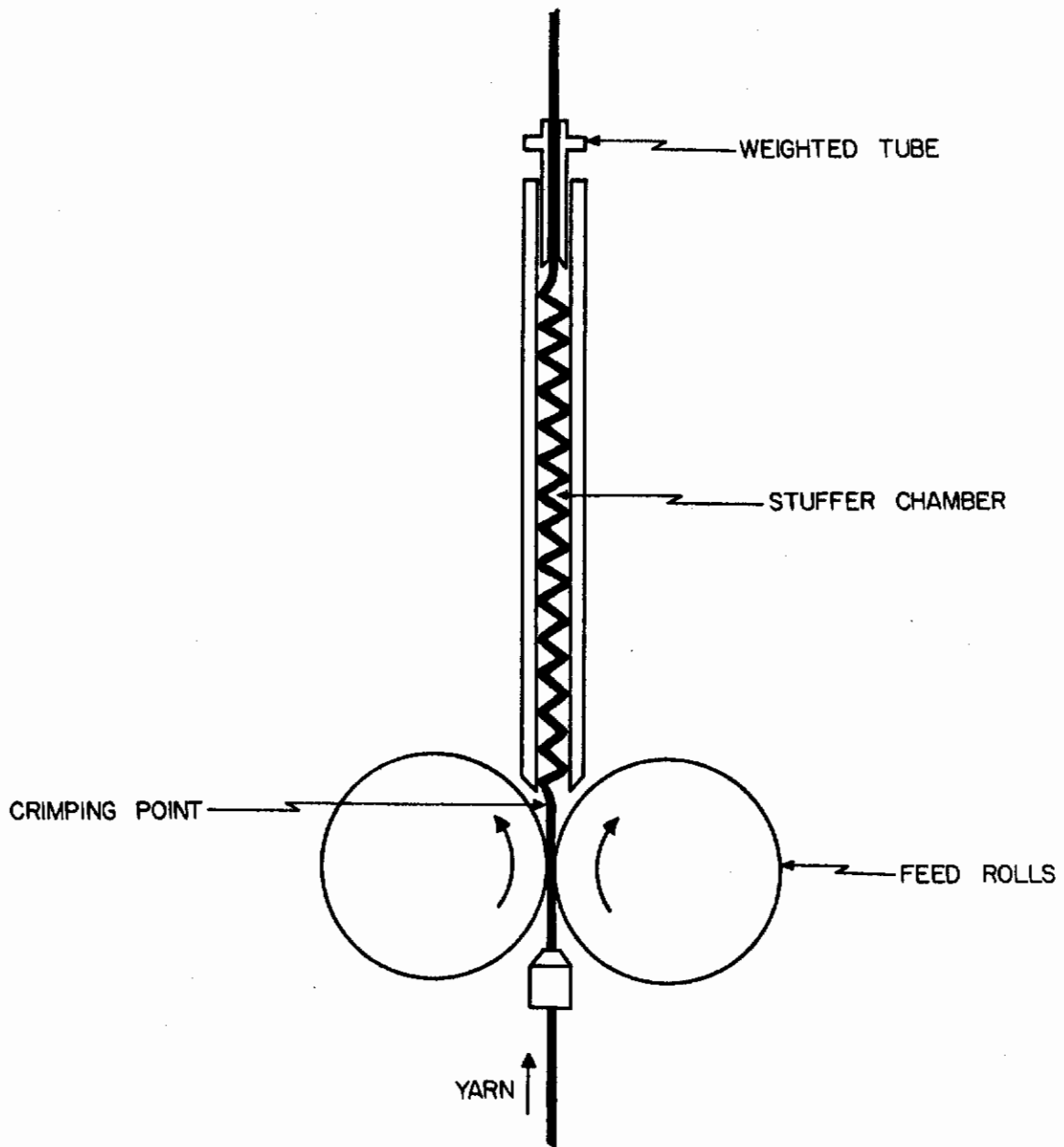


FIGURE 21 STUFFER BOX



# Contrails

Several hundred yards of the 0.5 mil Chromel A wire yarn (10/10/1, 3.1 S/3.1 Z tpi) were nylon coated and forwarded to the Joseph Bancroft and Sons Company to be textured by the stuffer box crimping process. The various running conditions at which the yarn was processed are given in Table 14, and a photograph of each sample in Figure 22. The yarn was given the nylon coating to increase its abrasion resistance. Previous trials had shown that this was necessary<sup>(4)</sup>.

The percent take-ups of the stuffer box textured 0.5 mil wire yarns are given in Table 14. The initial yarn length  $L_1$  was measured under a tension of 0.2 gram and the extended length  $L_2$  was taken as the yarn length at the point of intersection of the extrapolation of the linear portion of the load-elongation curve with the zero load axis on the Instron chart. As shown, high percent take-ups can be obtained with the stuffer box process.

The yarn breaking load (jaw speed of 0.5 inch per minute) and strength translation from the uncrimped yarn to the crimped yarn are also given in Table 14. As shown, it is possible to obtain stuffer box textured 0.5 mil wire yarns with take-ups of 68 percent and strength translations of 75 percent.

Several hundred yards of nylon coated 1.0 mil Chromel A wire yarn (5/5/1, 2.0 S/3.1 Z tpi) were also textured with the stuffer box crimping process by Joseph Bancroft and Sons Company. The various running conditions at which the yarn was processed are given in Table 14, and a photograph of each sample in Figure 23.

The percent take-ups of the yarn samples are given in Table 14. The yarn breaking loads (jaw speed of 0.5 inch per minute) and strength translations from the uncrimped yarn to the crimped yarn are also given. As shown a strength translation of 59 percent at a take-up of 72.4 percent was obtained. This is not as good as was achieved with the nylon coated 0.5 mil Chromel A wire yarn textured at the same conditions with the stuffer box process.

The uncrimping force of the stuffer box textured wire yarn is also given in Table 14. As shown, it is 1 to 13 percent of the straight yarn tensile strength.

Some of both the 0.5 mil wire yarn and the 1.0 mil wire yarn were textured by the FRL<sup>®</sup> Compactor process<sup>(23,24)</sup>. As shown in Figure 24, in this process yarn is forced between two rolls moving at different speeds by feeding the yarn between a blade and the top roll. The differential speed between the two rolls crimps the yarn. The crimp amplitude and frequency can be regulated by varying the ratio of the speed of the top roll to that of the bottom roll, the roll clearance, and the horizontal position of the blade.

The running conditions at which the two wire yarns were processed are given in Table 15 and a photograph of each sample in Figure 25. All samples were run with a roll clearance of 0.003 inch. A 0.004 inch clearance resulted in no crimp and a 0.002 inch clearance resulted in numerous broken filaments. The horizontal blade setting of 0.300 inch used with the 0.5 mil wire yarn resulted in fewer broken filaments than a 0.210 inch setting. Broken filaments did not appear to be a problem with the 1.0 mil wire yarn, and the 0.210 inch horizontal blade setting gave higher 1.0 mil wire yarn bulk than the 0.300 inch setting.

TABLE 14  
STUFFER BOX TEXTURED WIRE YARN

Wire Diameter (mils)	Yarn Construction	Sample	Choke Diameter (inches)	Feed Roll Pressure (lbs)	Yarn Take-Up (%)	Rupture Load (gms)	Rupture Strength Translation (%)	Uncrimping Force (gms)
0.5 Chromel A	10/10/1, 3.1 S/3.1 Z tpi	1	0.240	5-1/2	61	23	2*	1.9
		2	0.245	7-1/2	75	652	52	100
		3	0.245	6-1/2	76	780	62	112
		4	0.245	5-1/2	68	937	75	137
		5	0.250	7-1/2	60	793	63	94
		6	0.250	6-1/2	69	837	67	130
		7	0.250	5-1/2	68	880	70	95
		8	0.255	7-1/2	60	853	68	99
		9	0.255	6-1/2	57	835	66	113
		10	0.255	5-1/2	34	874	70	77
1.0 Chromel A	5/5/1, 2.0 S/3.1 Z tpi	1	0.240	5-1/2	85.5	597	47**	158
		2	0.245	7-1/2	86.0	535	42	161
		3	0.245	5-1/2	72.4	745	59	144
		4	0.250	7-1/2	82.5	605	48	142
		5	0.250	5-1/2	85.2	703	55	159
		6	0.255	7-1/2	81.8	517	41	143
		7	0.255	5-1/2	80.2	644	51	126

\* based on an uncrimped yarn tensile strength of 1256 grams

\*\* based on an uncrimped yarn tensile strength of 1244 grams

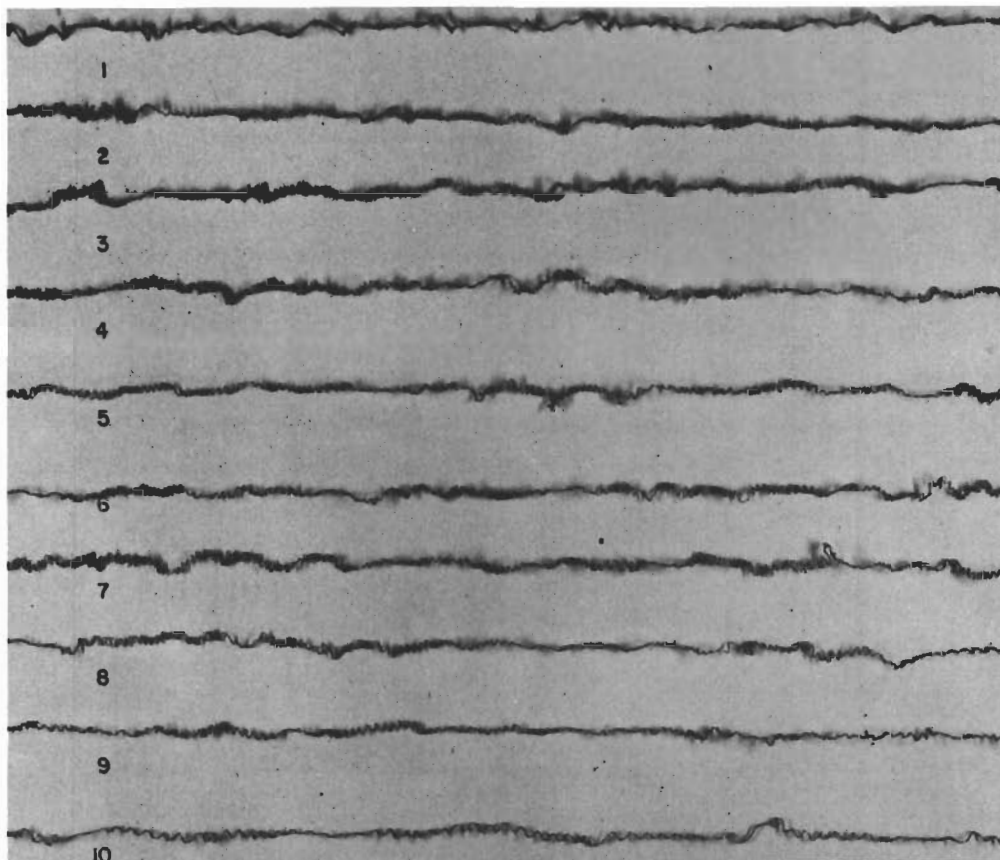


FIGURE 22 STUFFER BOX TEXTURED 0.5 MIL WIRE YARN

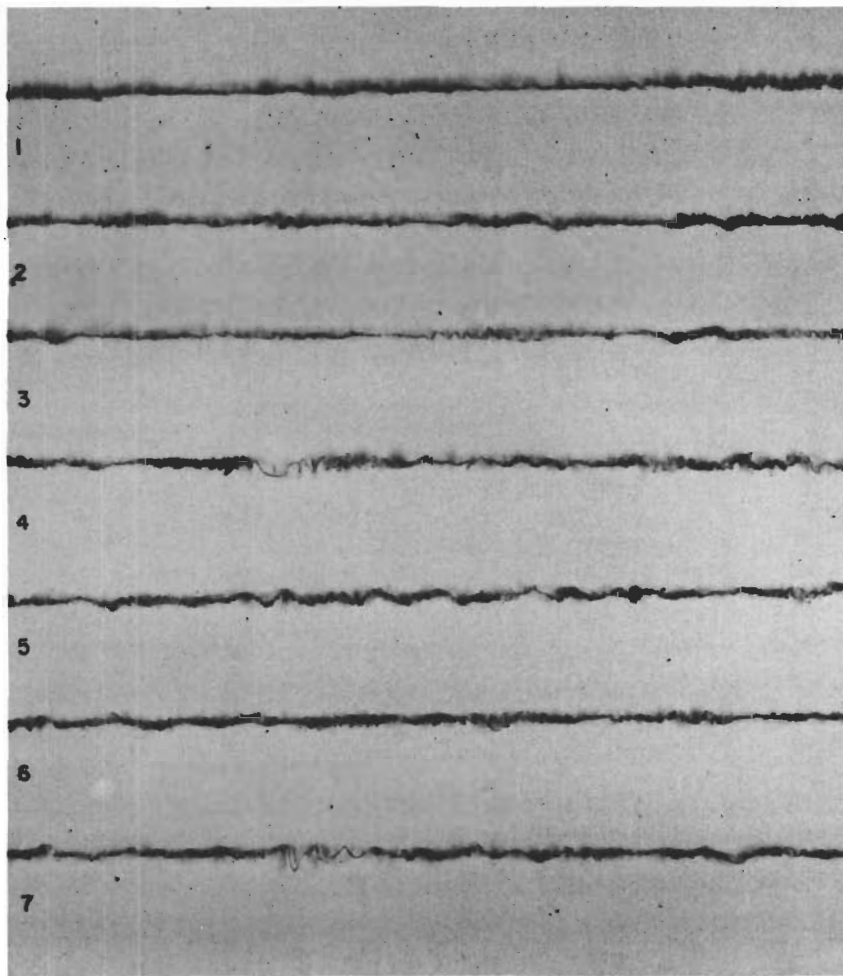


FIGURE 23 STUFFER BOX TEXTURED 1.0 MIL WIRE YARN

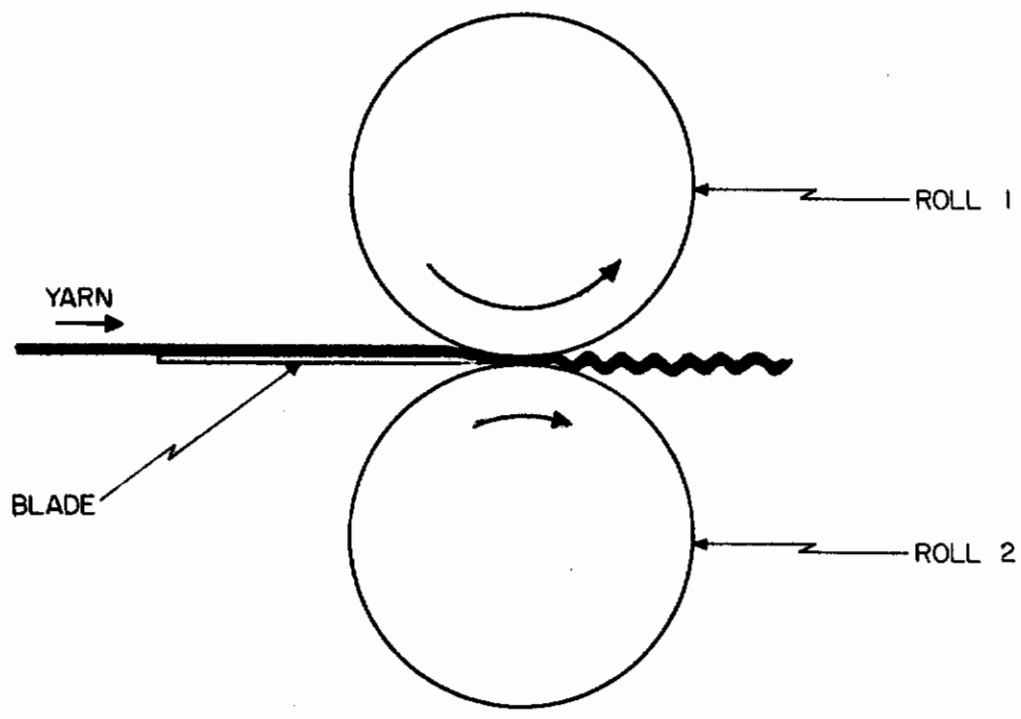


FIGURE 24 FRL<sup>®</sup> COMPACTOR

**TABLE 15**  
**COMPACTED WIRE YARN**

Wire Diameter (mils)	Yarn Construction	Sample	Ratio of		Horizontal Setting (inches)	Yarn Take-Up (%)	Rupture Load (gms)	Rupture Strength Translation (%)	Uncrimping Force (gms)	
			Bottom Roll Speed to Top Roll Speed	Speed to						
0.5 Chromel A	10/10/1, 3.1 S/3.1 Z tpi	1	0	---	---	0	1256			
		2	0.22	0.306	0.306	30	564	45	133	
		3	0.42	0.306	0.306	28	764	61	125	
		4	0.22	0.306	0.306	yarn straightened and then relaxed				
		5	0.42	0.306	0.306	yarn straightened and then relaxed				
1.0 Chromel A	5/5/1, 2.0 S/3.1 Z tpi	6	0	---	---	0	1244			
		7	0.22	0.210	0.210	54	634	51	113	
		8	0.42	0.210	0.210	39	910	73	143	
		9	0.22	0.210	0.210	yarn straightened and then relaxed				
		10	0.42	0.210	0.210	yarn straightened and then relaxed				

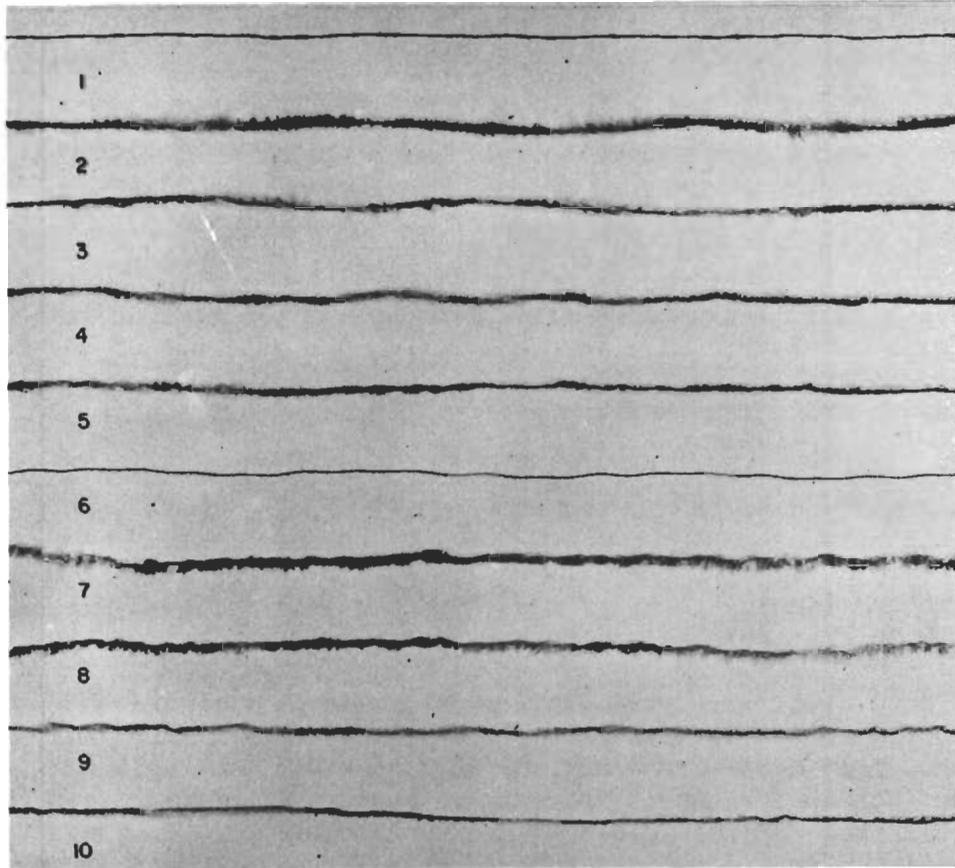


FIGURE 25 COMPACTED WIRE YARN

# Contrails

Wetting the yarn with water prior to compacting appeared to increase the yarn bulk and decrease the number of broken filaments. The water evidently acts as a mild lubricant. All the compactor textured yarn samples were, therefore, pulled over a wet felt placed in front of the blade. The rolls were also kept wet.

A slight back tension on the yarn appeared to improve yarn bulk and was therefore utilized in making the above samples.

Metal yarn was also run through the compactor with both rolls at the same rpm. The yarn exhibited no crimp, appearing to indicate that the crimp obtained when a differential roll speed is used is not due solely to the yarn passing over the front edge of the blade.

Compacted metal yarns of higher quality than the above samples might be produced by using a smoother top roll and a bottom roll with finer surface roughness.

The take-up, breaking load and strength translation (from straight yarn to textured yarn) of the compacted wire yarns are given in Table 15. As shown, the strength translations are approximately the same as those found with stuffer box textured wire yarn. However, the take-ups of the compacted yarns are considerably lower. The compacted 1.0 mil wire yarn samples exhibit higher take-ups and strength translations than the 0.5 mil wire yarn samples.

As noted in Table 15, the compacted yarn samples were pulled out straight and allowed to relax. As shown in Figure 25, these yarn samples still exhibit bulk.

The uncrimping force of the compacted yarns is also given in Table 15. It is 9 to 11.5 percent of the straight yarn tensile strength.

The 0.5 mil wire yarn was also textured by the Taslan® process (22). As shown in Figure 26, in this process yarn is overfed through a zone of compressed air. This causes random loops to form along each filament and the yarn to contract in length and increase in bulk. On emerging from the air-jet the yarn collapses and the looped filaments become locked in place by inter-filament friction and mechanical interference. The yarn bulk (size and frequency of the loops) is determined by processing speed, rate of overfeed, air pressure, jet size, needle setting, yarn diameter, number of filaments per yarn and yarn twist.

The running conditions at which the 0.5 mil wire yarn was processed are given in Table 16 along with the textured yarn properties. The yarn has a very low strength translation (from straight yarn to textured yarn). However, the yarn exhibits a very high bulk that cannot be easily removed by pulling the yarn. The diameter of the textured yarn is approximately 0.015 inch, which is about three times the diameter of the straight filament yarn.

---

\* Process developed and licensed by Du Pont.



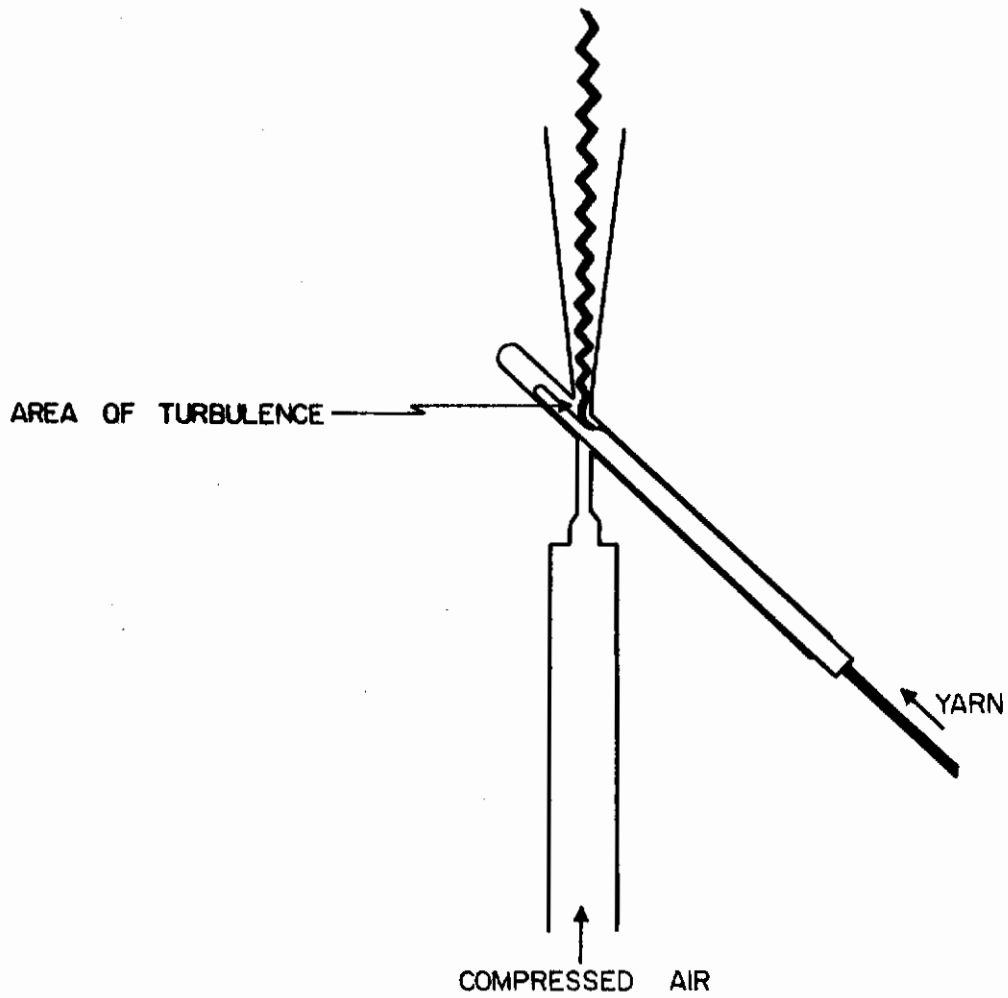


FIGURE 26 AIR-JET USED IN PRODUCTION OF TASLAN TEXTURED YARN

TABLE 16

TASLAN® TEXTURED WIRE YARN

Wire Diameter (mils)	Yarn Construction	Jet	Air Pressure (lbs/in <sup>2</sup> )	Yarn Overfeed (%)	Rupture		Rupture Strength Translation (%)
					Elongation (%)	Load (gms)	
0.5 Chromel A	10/10/1, 3.1 S/3.1 Z tpi	42 BS	≈65	15 - 20	14	448	36*

\* based on an uncrimped yarn  
tensile strength of 1256 grams

An attempt was made to texture the 1.0 mil wire yarn by the Taslan® process without success. A higher twist 25 filament 1.0 mil wire yarn was also tried without success. It appears that a greater number of filaments per yarn is required.

Due to the shape of the stress-strain curve of the Taslan® textured wire yarn it is not possible to define an uncrimping force. In tensile testing the yarn it still exhibited some crimp as filaments were breaking.

In conclusion, the preceding data on textured metal yarns shows the Taslan® and FRL® Compactor textured yarn to be the most interesting. The Taslan® textured wire yarn exhibits poor strength translation but very high bulk while the compacted yarn exhibits greater strength translation and somewhat less bulk.

A 4-1/4 inch wide 200 denier nylon yarn warp was drawn into a small hand loom at 80 ends per inch. Six inch long samples of fabric were woven with the uncrimped, compacted and Taslan® textured 0.5 mil and 1.0 mil wire yarn as filling. The fabrics are a warp rib weave<sup>(9)</sup>. Photographs of the fabric samples are shown in Figures 27 through 31. The magnification is approximately 13X.

By comparing Figures 29 through 31 with Figures 27 and 28, it is clear that a textured metal yarn does not exhibit much bulk in fabric form. This results from two properties that are characteristic of metal. Firstly, as previously noted in this section, small straightening forces on textured metal yarns tend to remove the crimp with the possible exception of Taslan® textured yarn, which exhibits poor strength translation. The forces imposed on the yarn in respooling and weaving tend to exceed the minimum straightening force. Therefore, the metal yarns in the woven fabrics shown in Figures 29 through 31 do not exhibit much bulk. Secondly, metal does not possess a memory like that of polymeric materials. A polymeric yarn can be textured, the yarn pulled out straight, wound on a spool and woven. Off the loom the filaments in the yarn in the fabric may still appear straight. However, when the yarn is placed in an elevated temperature environment, the filament crimp reappears, due to the memory effect, and bulked yarn fabrics are obtained.

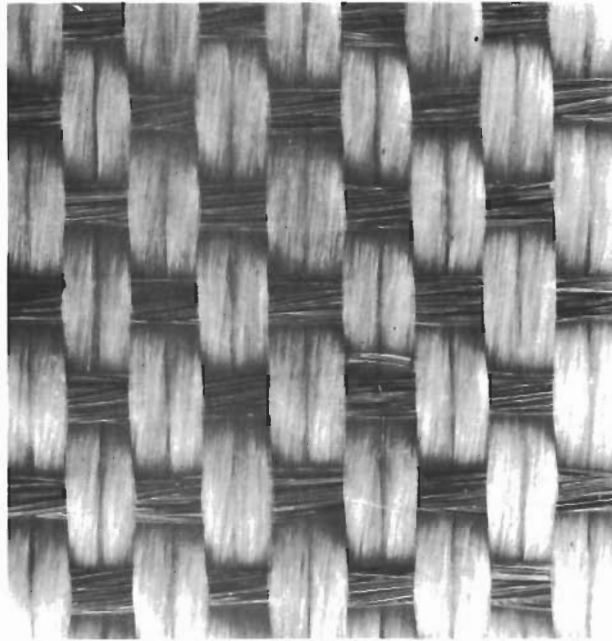


FIGURE 27 FABRIC, 0.5 MIL WIRE FILLING YARN ( 30 x 80 )

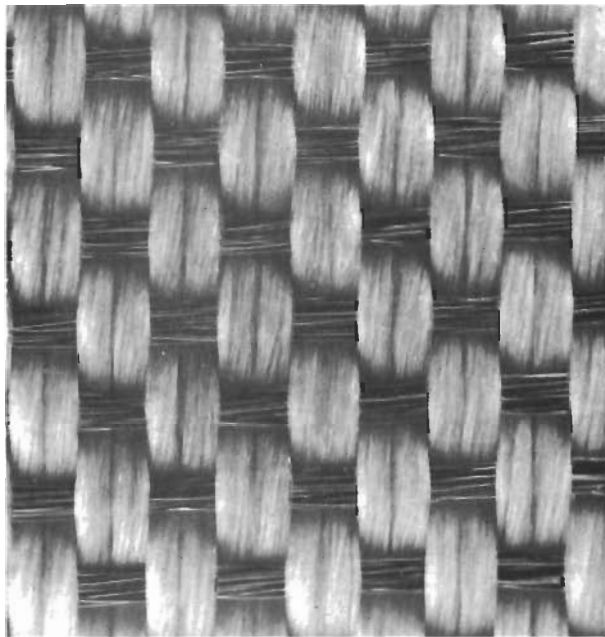


FIGURE 28 FABRIC, 1.0 MIL WIRE FILLING YARN ( 30 x 80 )

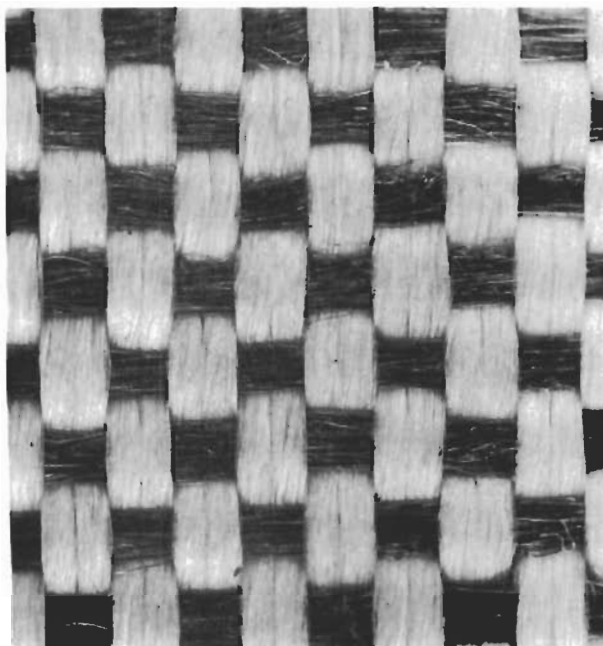


FIGURE 29 FABRIC, 0.5 MIL COMPACTED WIRE FILLING YARN (31 x 80)

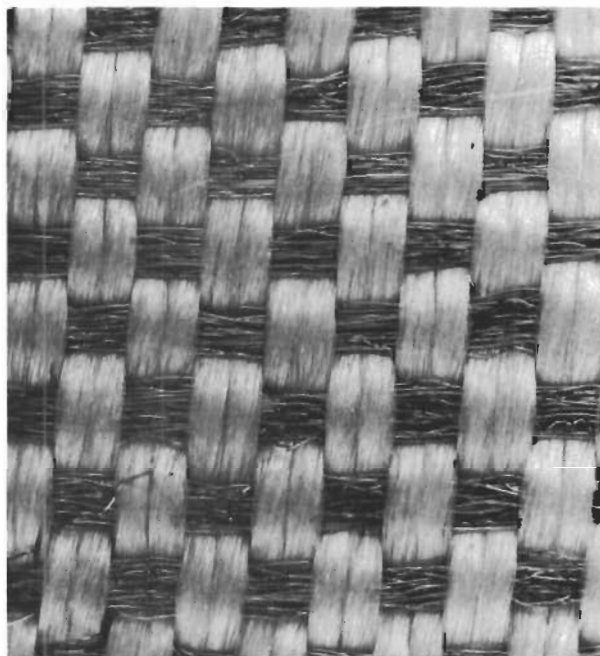


FIGURE 30 FABRIC, 1.0 MIL COMPACTED WIRE FILLING YARN (31 x 80)

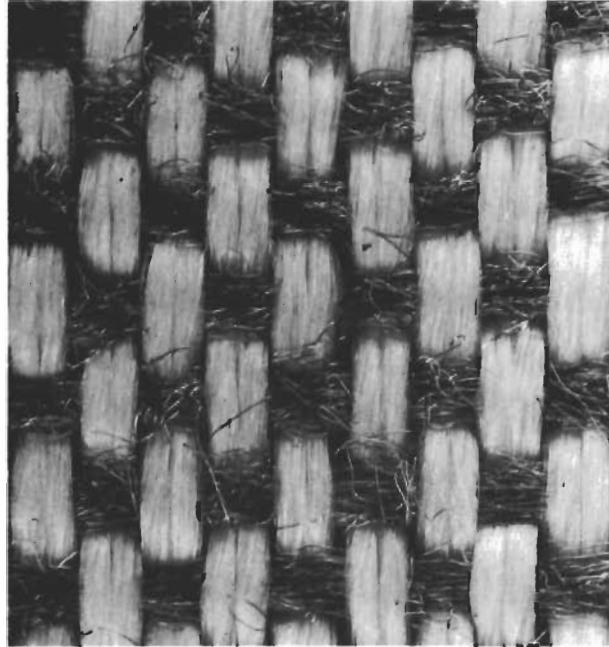


FIGURE 31 FABRIC, 0.5 MIL TASLAN TEXTURED  
FILLING YARN ( 30 x 80 )

## VI. BLENDED YARN

The various methods of blending metal filaments with other fibers such as flameproofed organic fibers (wool), HT-1, oxide fibers (leached glass, quartz) and carbonaceous fibers (graphite, carbon) are being investigated. An important consideration in this investigation is the tensile moduli of the various fibers. The moduli of fibers may differ by as much as two orders of magnitude (wire and wool).

Blending can be done on a ring-twister by plying together the different yarns. However, if the component yarns have considerably different moduli and elongation the blended yarn will exhibit low tensile strength efficiency due to poor elongation balance.

An efficient blended yarn can be made by wrapping the high modulus yarn around the low modulus yarn. By appropriately adjusting the helix angle of the covering yarn, good elongation balance can be achieved. Since high modulus fibers, as a class, exhibit greater thermal durability than low modulus fibers, covering the low modulus yarn might also give it some measure of protection.

The design of a machine for covering yarn is shown in Figure 32. FRL® has assembled a unit of this type. The covered yarn samples made to date on the unit have been HT-1 yarns covered with metal yarn. The construction of two such covered yarns and the tensile properties at 70°F of the component yarns and the covered yarn are given in Table 17. As shown, the covered yarns exhibit considerably greater elongation than the straight metal yarns.

Both the core yarn and the covering yarn were observed to break at the same time in the tensile tests of the covered yarn. However, it was difficult to ascertain whether the clean breaks were due to good elongation balance or the metal yarn cutting the HT-1 yarn due to the lateral pressure of the covering yarn on the core yarn.

The HT-1 yarn in the covered yarn is almost completely covered by the metal yarn. The covered 200 denier HT-1 yarn was woven as filling in the 4-1/4 inch wide 200 denier nylon yarn warp drawn in the small hand loom at 80 ends per inch. A photograph of the fabric is shown in Figure 33. The magnification is approximately 13X.

Leached glass, quartz and graphite yarns could be covered with metal filaments in the same manner as the HT-1 yarn was. A fabric is going to be woven from a blended yarn of this type and evaluated over a wide temperature range. One would anticipate that it would have greater flexibility, crease recovery, fold endurance, and tear strength than an all metal fabric, yet still exhibit moderate strength and low porosity at elevated temperatures. The adhesion of a fabric coating to this type of a fabric might be better than in the case of an all metal fabric.

FRL® has had preliminary conversations with Rohr Products Company, a potential supplier of inexpensive short length bundles of fine wire. The potential of this type of material for blending and weaving is being considered.

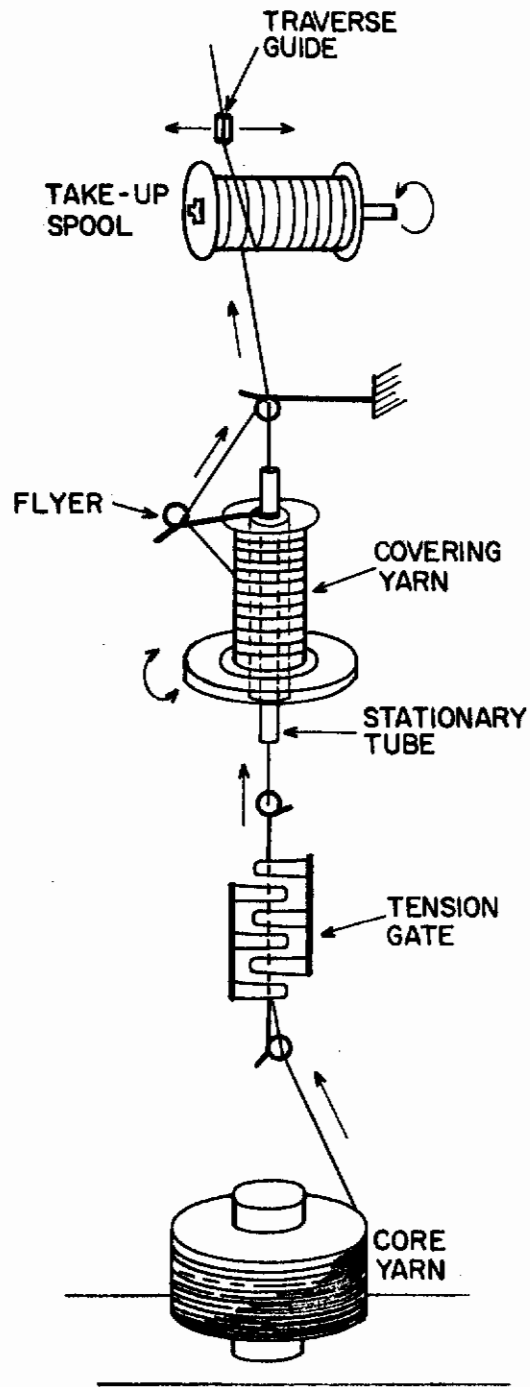


FIGURE 32 YARN COVERING MACHINE

TABLE 17  
COVERED YARN

Core Yarn		Covering Yarn			Covered Yarn				Tensile Strength	
Type	Elongation (%)	Strength (grams)	Type	Elongation (%)	Strength (grams)	Wraps per Inch	Diameter (mils)	Elongation (%)	Strength (grams)	Trans- lation (%)
100-50 HT-1	15.5	459	10/0.5 mil/ 3.1 Z Chromel R	---	131(X2)	80 S 65 Z	7	13.3	605	84
200-100 HT-1	12.6	957	10/10/0.5 mil/3.1 S/ 3.1 Z Chromel R	3.9	1310(X2)	31 S 21 Z	14-15	12.9	2345	66



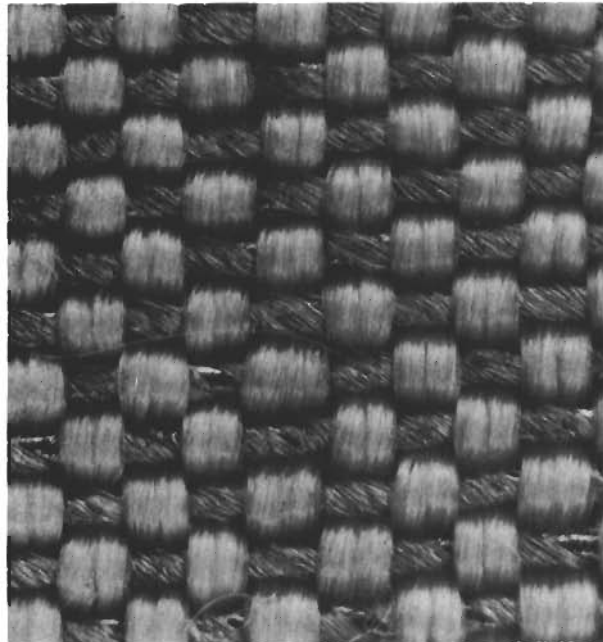


FIGURE 33      FABRIC, WIRE WRAPPED HT-1  
                         FILLING YARN (38 x 80)

VII. SILICA-CELLULOSE FIBER

A small sample of a four inch wide tape woven from a silica-cellulose fiber supplied by American Viscose Corporation was examined. It was a plain weave tape with approximately twenty picks and ends per inch. The yarn was a 2400 denier zero twist yarn composed of 1500 filaments.

American Viscose states the fiber composition is as follows<sup>(25)</sup>:

Cellulose	50%
Silica	35%
Moisture	7.5%
Finish and Size	7.5%
Ash (exclusive of SiO <sub>2</sub> )	0.17%

American Viscose indicates that when the fiber is fired at approximately 1700°F for three hours, single fiber tenacities of 0.75 gram per denier are obtained. The initial rate of combustion was usually retarded by blanketing with Argon for the initial 5-10 minutes of the firing schedule.

FRL<sup>®</sup> found that complete pyrolysis of the cellulose at 1000°F in air resulted in a very weak residue. Shrinkage amounted to only 15%. Exposure at 1800°F for three hours stiffened and strengthened the silica residue. However, the strength was still so low that fibers could not be removed from the fabric. Pyrolysis of the cellulose at 1800°F also resulted in a very weak residue. It appears that flaming of the cellulose must be prevented so as not to disrupt the silica residue. Slow pyrolysis at 600° to 800°F gave the best results.

Finishing the fabric with the reaction product of aluminum isopropoxide and 8-hydroxyquinoline, pyrolysis of the cellulose at 600°F for 48 hours, and firing at 1800°F for three hours gave the strongest silica residue. The fibers were not fused but still were not strong enough to withstand separation. The deposition of small amounts of alumina on the surface may aid in sintering the silica. It appears, however, that temperatures higher than 1800°F are required to achieve higher strengths.

VIII. GRAPHITE AND CARBON-BASED FIBROUS MATERIALS

The pick and end count, weight and weave of a series of graphite and carbon-based fabrics<sup>(8)</sup> are given in Table 18. The denier of the warp and filling yarns is also given. It appears that the warp and filling yarns in each fabric are identical. The average yarn cotton count is given for each fabric.

The yarn data given in Table 18 was determined by removing yarns from the fabrics and measuring their weight per unit length. The yarns exhibited crimp, therefore the yarn length was determined after stretching the yarn by hand. Although several specimens from each fabric were measured, the errors in the data presented may be considerable. The data should be considered as being only approximate.

TABLE 18

CONSTRUCTION OF GRAPHITE AND CARBON-BASED FABRICS

<u>Sample</u>	<u>Picks per Inch</u>	<u>Ends per Inch</u>	<u>Yarn Denier</u>		<u>Yarn Cotton Count (Average)</u>	<u>Weight (oz/yd<sup>2</sup>)</u>	<u>Weave</u>
			<u>Warp</u>	<u>Filling</u>			
101-A	62	64	311	321	16.8	5.3	7 by 1 twill
101-B	25	24	1202	1103	4.6	8.3	plain
101-C	25	22	2518	2703	2.0	12.9	plain
101A-A	86	80	141	130	39.3	3.0	5 by 1 twill
101A-B	32	30	681	545	8.8	6.6	plain
102D	23	26	1123	1069	4.8	7.8	plain
102E	25	26	1038	1059	5.1	7.2	2 by 2 basket
103-F1	48	53	678	695	7.7	9.0	4 by 1 twill
103-F2	48	53	667	692	7.8	8.4	7 by 1 left hand twill
103-F3	48	54	547	547	9.7	8.1	7 by 1 left hand twill

A. Tensile Properties

The graphite and carbon-based fabrics were tensile tested<sup>(8)</sup>. The rupture loads and elongations in the warp and filling directions were measured at several temperatures and the results are shown in Table 19.

**TABLE 19**  
**TENSILE PROPERTIES OF GRAPHITE AND CARBON-BASED FABRICS**

Sample	70°F						850°F					
	Warp			Filling			Warp			Filling		
	Elongation (%)	Load (lbs/in)		Elongation (%)	Load (lbs/in)		Elongation (%)	Load (lbs/in)		Elongation (%)	Load (lbs/in)	
101-A	3.0	28.3		5.5	22.0		1.6	1.4		3.5	2.5	
	3.0	26.8		5.4	12.2					5.3	7.2	
	2.5	23.2		6.5	21.7							
	3.1	27.2		4.6	18.7							
	2.6	24.2		5.4	15.2							
Average	2.8	25.9		5.5	18.0							
101-B	2.4	31.0		19.4	7.2		3.0	1.5		21.3	1.9	
	2.2	30.0		21.0	8.3		3.0	1.1		21.2	2.4	
	2.1	27.2		20.7	8.2		3.0	1.4		18.5	2.2	
	2.6	38.7		17.0	7.6		3.4	1.7		18.0	3.1	
	2.7	37.7		21.4	8.4					12.3	1.6	
Average	2.4	32.9		19.9	7.9		3.1	1.4		18.3	2.2	
101-C	17.2	44.5		11.8	43.2		3.8	0.3		12.3	0.2	
	18.7	45.1		14.4	58.5		4.9	0.6		13.2	0.4	
	17.3	37.7		19.2	40.7		5.8	0.4				
	12.6	39.1		16.5	52.5		6.6	0.6				
	16.2	41.4		14.6	60.0							
Average	16.4	41.6		15.3	51.0		5.3	0.5				
102-D	7.9	28.0		5.8	18.2		9.6	20.5		4.3	13.6	
	7.8	31.7		5.7	32.8		8.9	20.2		4.8	19.6	
	8.6	35.7		4.8	21.5		8.9	20.4		4.2	15.5	
	8.1	24.8		4.1	25.0		8.1	19.4		4.2	12.2	
	7.6	26.0		5.0	26.4		7.3	25.6		4.0	7.7	
Average	8.0	29.2		5.1	24.8		8.6	21.2		4.3	13.7	
102-E	2.5	6.5		3.4	13.2		3.3	6.6		3.7	8.8	
	2.1	7.1		3.6	13.0		3.1	6.6		3.6	13.2	
	2.2	6.1		3.1	10.4		3.3	5.5		3.2	10.7	
	2.0	8.0		3.0	10.7		3.2	5.5		3.7	11.2	
	1.9	5.9		3.0	9.1		3.1	7.8		3.3	10.1	
Average	2.1	6.7		3.2	11.3		3.2	6.4		3.5	10.8	

TABLE 19 (continued)

TENSILE PROPERTIES OF GRAPHITE AND CARBON-BASED FABRICS

Sample	70°F						350°F					
	Warp			Filling			Warp			Filling		
	Elongation (%)	Load (lbs/in)		Elongation (%)	Load (lbs/in)		Elongation (%)	Load (lbs/in)		Elongation (%)	Load (lbs/in)	
103-F1	2.1	39.7		7.2	81.8		2.5	53.0		9.8	64.8	
	1.8	33.7		6.0	97.5		4.3	45.4		8.3	52.0	
	2.1	39.8		6.8	85.3		9.4	59.0		9.9	80.0	
	2.2	43.1		7.7	106.5		3.6	47.8		7.8	57.0	
	1.8	35.7		7.0	96.5		5.0	40.0		7.0	71.8	
	Average	2.0	38.4		6.9	93.5		5.0	49.0		8.6	65.1
103-F2	0.9	7.4		6.7	6.2		2.5	7.8		6.3	4.2	
	1.0	5.4		6.3	7.1		2.3	5.5		6.3	3.7	
	0.9	6.7		6.0	6.6		2.7	8.3		7.0	4.9	
	0.9	6.5		6.0	6.2		2.2	7.1		7.5	5.5	
	1.0	6.2		6.9	6.6		1.9	6.8		8.4	4.5	
	Average	0.9	6.4		6.4	6.5		2.3	7.1		7.1	4.6
103-F3	2.0	97.8		4.3	70.0		4.0	61.0		7.3	35.3	
	2.0	100.5		4.5	88.0		3.8	68.8		10.5	33.5	
	2.1	116.5		4.9	64.0		4.1	56.5		8.4	40.8	
	1.8	84.0		5.4	95.5		3.9	51.0		10.9	62.0	
	2.1	102.0		5.5	71.0		4.2	47.0		10.3	61.5	
	Average	2.0	100.2		4.9	77.7		4.0	56.9		8.6	36.9

**TABLE 19 (continued)**  
**TENSILE PROPERTIES OF GRAPHITE AND CARBON-BASED FABRICS**

Sample	600°F						850°F					
	Warp			Filling			Warp			Filling		
	Elongation (%)	Load (lbs/in)	Load (lbs/in)	Elongation (%)	Load (lbs/in)	Load (lbs/in)	Elongation (%)	Load (lbs/in)	Load (lbs/in)	Elongation (%)	Load (lbs/in)	
103-F1	3.0	53.7	84.7	6.6	84.7	52.5	3.4	52.5	5.2	48.0	48.0	
	2.9	54.0	72.0	6.4	72.0	60.5	2.6	60.5	4.6	33.0	33.0	
	2.7	46.7	87.5	7.0	87.5	63.5	2.9	63.5	5.8	62.0	62.0	
	2.4	69.6	61.4	8.1	61.4	44.0	2.6	44.0	8.1	54.8	54.8	
	2.7	70.5	79.0	8.5	79.0	78.5	4.5	78.5	6.4	36.5	36.5	
			6.1	54.5	66.8	3.4	66.8					
			6.3	53.5								
	Average	2.7	58.9	7.0	70.4	61.0	3.2	61.0	6.0	46.9	46.9	
103-F2	2.6	4.8	5.2	5.0	5.2	7.9	1.1	7.9	8.2	6.8	6.8	
	3.7	9.0	6.0	7.4	6.0	8.4	1.9	8.4	8.7	6.9	6.9	
	2.7	6.4	4.5	7.0	4.5	9.4	2.0	9.4	6.5	5.4	5.4	
	2.8	4.0	7.5	8.4	7.5	8.6	1.7	8.6	7.6	6.0	6.0	
	2.6	5.0	6.0	7.6	6.0	5.5	1.5	5.5	6.6	6.2	6.2	
	Average	2.9	5.8	7.1	5.8	8.0	1.6	8.0	7.5	6.3	6.3	
103-F3	3.5	65.3	46.0	5.3	46.0	99.0	3.8	99.0	6.1	48.0	48.0	
	3.8	51.5	59.0	7.2	59.0	92.5	4.2	92.5	6.6	65.0	65.0	
	5.5	66.3	31.5	7.3	31.5	92.8	3.2	92.8	7.2	67.0	67.0	
	4.1	58.2	45.2	7.3	45.2	64.0	2.6	64.0	7.0	68.0	68.0	
	4.3	60.0	47.3	7.0	47.3	86.0	2.6	86.0	6.8	63.5	63.5	
	Average	4.2	60.3	6.8	45.8	86.9	3.3	86.9	6.8	62.3	62.3	

# Contrails

In most instances, five fabric specimens in both the warp and filling directions were tensile tested at each of the specified temperatures. All specimens were conditioned for a minimum of 24 hours at standard textile laboratory conditions of  $70 \pm 2^\circ\text{F}$  and  $65 \pm 2$  percent relative humidity prior to testing.

Fabric strips seven inches long and 1.5 inches wide were cut. These strips were then raveled to a one inch width by removing approximately the same number of yarns from each side of the strip. All specimens were taken at over one tenth the width of the cloth away from the selvage.

The tensile tests were performed on an Instron tensile tester using flat jaws, a gage length of five inches and a jaw speed of five inches per minute. The jaws were lined with masking tape for the  $70^\circ\text{F}$  tests and with graphite fabric for the elevated temperature tests.

The elevated temperature tensile tests were performed in a hot air chamber mounted in the Instron, Figure 34. The air in this chamber is normally heated by six glow coil heaters and continuously circulated by a blower.

Fabric specimens that did not exhibit excessive contraction when placed in high temperature air were clamped in the upper jaw, allowed to hang freely for approximately ten minutes, and then clamped in the lower jaw. The chamber was brought back to temperature (approximately five minutes), and then the specimen tensile tested.

Fabric specimens that were found to exhibit considerable contraction when placed in hot air were placed in the heated chamber and allowed to contract freely for ten minutes. The specimens were then removed from the chamber, clamped in the upper jaw, the upper jaw was mounted in the hot box, the specimens clamped in the lower jaw, the chamber brought back to temperature, and then the specimens tensile tested.

The tensile testing at elevated temperatures of the series of graphite and carbon-based fabrics was delayed by numerous failures of the environmental chamber. The glow-coil heaters and their sockets burned out frequently at the  $850^\circ\text{F}$  temperatures.

The glow-coils have recently been replaced with Calrod heaters and the modified box successfully tested at temperatures up to  $1000^\circ\text{F}$ . The surface area of the Calrod heaters is the same as that of the glow coils; the rise time is therefore the same as that obtained with glow-coil heaters. The details of the design modifications are given in Figure 35.

As a close examination of the data in Table 19 shows, there is considerable variation in the test results on some of the fabrics, particularly at elevated temperatures. This appears to be due to variability in the fabric itself.

One of the series of graphite and carbon-based fabrics, fabric sample 103-F3, was tensile tested at  $70^\circ\text{F}$  after exposures for various lengths of time in hot air. The strengths and elongations in the warp and filling directions after exposure in the hot air are given in Table 20.



FIGURE 34 FRL<sup>®</sup> ENVIRONMENTAL CHAMBER



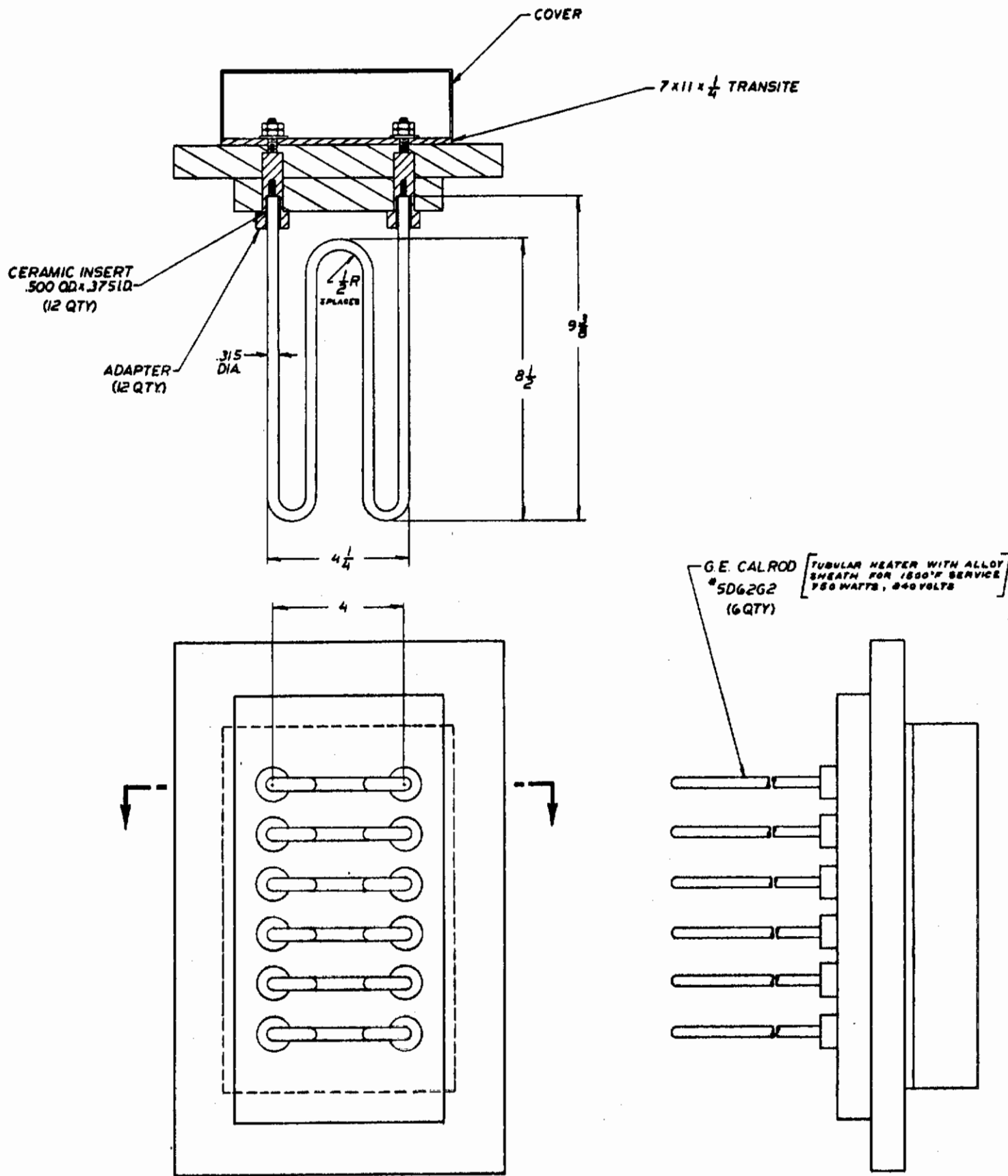


FIGURE 35 ENVIRONMENTAL CHAMBER DESIGN MODIFICATIONS

TABLE 20

TENSILE PROPERTIES OF GRAPHITE AND CARBON-BASED FABRICS  
AT 70°F AFTER EXPOSURE IN HOT AIR

Sample	Air Temperature (°F)	Time in Air (min)	Warp		Filling	
			Elongation (%)	Load (lbs/in)	Elongation (%)	Load (lbs/in)
103-F3	1000	20	1.9	92.0	4.2	46.0
			1.8	64.0	3.9	72.5
			1.7	77.0	4.0	75.5
			Ave. 1.8	77.7	4.0	64.5
103-F3	1000	60	1.9	89.0	3.8	53.0*
			1.7	68.0	3.7	46.0*
			1.5	63.0*	4.0	54.0*
			2.2	94.5	3.9	59.5
			1.6	90.0	3.3	20.0
			1.7	72.0	3.7	25.0*
Ave. 1.8	79.4	3.7	42.9			
103-F3	1500	20	Samples burned leaving a fossil-like residue			

\* jaw breaks

Fabric strips seven inches long and 1.5 inches wide were cut. These strips were then raveled to a one inch width by removing approximately the same number of yarns from each side of the strip. All specimens were taken at over one-tenth the width of the cloth away from the selvage.

The tensile tests were performed on an Instron tensile tester using flat jaws, a gage length of five inches and a jaw speed of five inches per minute. The jaws were lined with masking tape.

Due to the scatter of the data obtained it is difficult to draw conclusions. However, a comparison of the data in Tables 19 and 20 for fabric sample 103-F3 appears to indicate that the fabric elongation and strength are moderately decreased by exposure to 1000°F air. Note that the fabric burned when placed in 1500°F air leaving a fossil-like residue that could not be tested at 70°F.

The tensile properties at 70°F of fabric sample 103-F3 are also to be measured in the near future after a twenty minute exposure in 1000°F, 1500°F and 2000°F nitrogen. The fabric weight loss after a twenty-minute exposure in 1500°F nitrogen is also to be measured. It is anticipated that the absence of oxygen will prevent burning of the fabric and, therefore, will increase the fabric strength.

## B. Fold Endurance

The fold endurances in the warp and filling directions of the series of graphite and carbon-based fabrics are given in Table 21. The values were obtained with the MIT Folding Endurance Tester, ASTM D643-43 Method B. In this test both ends of the fabric specimen are clamped in jaws. The lower jaw is subjected to a rotary oscillating movement such that the specimen is folded through an angle of  $135 \pm 5$  degrees to both the right and left of the center-line position. The edge of the jaw has a radius of approximately 0.015 inch. A tension of from zero to 1.5 kg can be applied to the test specimen at the upper jaw.

Test specimens 0.59 inch wide and 4.5 inches long were used. At least one yarn was ravelled from each side of the fabric strips to attain the width dimension of 0.59 inch.

Because of the strong dependence of the fold endurance of graphite and carbon-based fabrics on tension, each fabric was evaluated at several tensions. Not enough fabric was available to run replicate tests on all the samples. However, as shown, in the cases where several tests were run at the same load considerable variability was observed.

The graphite and carbon-based fabrics tested do not have tensile strengths as high as those of multifilament yarn metal fabrics. However, some of them exhibit a larger strength-to-weight ratio and a larger fold endurance than is characteristic of the metal fabrics. Several of the graphite and carbon-based fabrics also exhibit a modest strength increase with increasing temperature (to 850°F).

As the quality of graphite and carbon-based fabrics is improved they should find numerous high temperature applications.

TABLE 21

FOLDING ENDURANCE OF GRAPHITE AND CARBON-BASED FABRICS

Sample	Warp			Filling				
	Jaw Opening Width (inch)	Tension (kgm) (lbs/in)		Endurance (cycles)	Jaw Opening Width (inch)	Tension (kgm) (lbs/in)		Endurance (cycles)
101-A	0.02	0.4	1.5	12,052	0.02	0.5	1.8	972
		0.7	2.6	8,993		0.7	2.6	403
		1.0	3.7	3,320		1.0	3.7	164
		1.5	5.5	168		1.5	5.5	17
101-B	0.03	0.4	1.5	1,948	0.03	0.4	1.5	186
				2,198				253
		0.5	1.8	986				284
		1.0	3.7	204		0.5	1.8	76
	0.05	1.5	5.5	32				192
		0.4	1.5	3,496				115
				3,498	1.0	3.7		22
		0.5	1.8	1,391				30
		1,638				21		

# Contrails

TABLE 21 (continued)

FOLDING ENDURANCE OF GRAPHITE AND CARBON-BASED FABRICS

Sample	Warp			Filling							
	Jaw Opening Width (inch)	Tension (kgm) (lbs/in)		Endurance (cycles)	Jaw Opening Width (inch)	Tension (kgm) (lbs/in)		Endurance (cycles)			
101-B	0.05	1.0	3.7	474	0.03	1.5	5.5	6			
				763				0			
		1.5	5.5	214		3					
				180							
101-C	0.05	1.0	3.7	1,105	0.05	0.5	1.8	4,478			
				875				5,021			
				1,388				2,981			
				1,960				10,954			
								2,404			
		1.1	4.0	1,052				0.55	2.0	2,404	
		1.3	4.8	657				0.6	2.2	707	
		1.5	5.5	510				0.7	2.6	517	
				250				1.0	3.7	59	
				195						1,630	
				349						882	
					567						
102-D	0.02	0.4	1.5	54	0.02	0.4	1.5	65			
				55				43			
				28				19			
				22				9			
		0.03	0.4	1.5		135	0.03	0.4	1.5	58	
						59				65	
						67				71	
		0.9	3.3			49		0.9	3.3		15
						7					29
						53					17
102-E	0.03	0.4	1.5	79	0.03	0.4		1.5	282		
				32					145		
				15					77		
				2					35		
				0			24				
	0.05	0.4	1.5	297	0.05	0.4	1.5	2,404			
				534				343			
				2,634				937			
				283				293			
				466				126			
				176				213			
1.0	3.7		8	1.0	3.7		53				
			3				50				
			5				23				
			0				5				
			1				2				
1.5	5.5		0	1.5	5.5		5				
			1				2				
			1				18				

TABLE 21 (continued)

FOLDING ENDURANCE OF GRAPHITE AND CARBON-BASED FABRICS

Sample	Warp				Filling					
	Jaw Opening Width (inch)	Tension		Endurance (cycles)	Jaw Opening Width (inch)	Tension		Endurance (cycles)		
		(kgm)	(lbs/in)			(kgm)	(lbs/in)			
103-F1	0.03	0.4	1.5	3,778	0.03	0.5	1.8	10,630		
				12,229				1.0	3.7	1,426
				2,135				1.2	4.4	664
		0.5	1.8	15,075		1.5	5.5	431		
				7,057						
				2,231						
		0.6	2.2	7,651						
				1.0		3.7	914			
				288						
				1,723						
				257						
			1.2	4.4		1,071				
			1.5	5.5		641				
		103-F2	0.03	0.3		1.1	95	0.03	0.4	1.5
29	104									
				10						
				2						
0.5	1.8			10	0.5	1.8	2			
				23			2			
				3			5			
				14						
				55						
				3						
				7						
1.0	3.7			1	0.6	2.2	21			
				2			0.7		2.6	4
				1			1.0		3.7	2
				1						
				1						
				0						
103-F3	0.03			0.5	1.8	>10,000	0.03		0.5	1.8
		>10,000	0.7			2.6		1,672		
		>10,000	1.0			3.7		553		
		1.0	3.7	4,321	1.5	5.5		185		
				2,428						
				2,092						
				1,129						
				1,129						
				2,140						
			1.2	4.4						
	1.3	4.8	1,702							

# Contrails

TABLE 21 (continued)

FOLDING ENDURANCE OF GRAPHITE AND CARBON-BASED FABRICS

Sample	Warp			Filling						
	Jaw Opening Width (inch)	Tension (kgm) (lbs/in)		Endurance (cycles)	Jaw Opening Width (inch)	Tension (kgm) (lbs/in)		Endurance (cycles)		
103-F3	0.03	1.5	5.5	1,151						
				859						
				364						
				686						
101A-A	0.02	1.2	4.4	9,480	0.02	0.45	1.7	1,962		
				1,523				0.5	1.8	1,852
				1,867				1.0	3.7	360
								1.5	5.5	110
101A-B	0.02	0.4	1.5	134	0.02	0.4	1.5	300		
				18				0.5	1.8	243
								0.7	2.6	60
								1.0	3.7	34

IX. SPECIAL TEST FIXTURES

The fine wire multifilament yarn fabrics woven to date have been evaluated at 70°F only. The proposed applications of these fabrics contemplate temperatures from cryogenic to 2000°F. It is intended that during the course of this continuing program wire fabrics, and fabrics woven from other materials, will be evaluated over this wide temperature range.

A. High Temperature Test Equipment

Special test fixtures have been designed for the evaluation of fibers, yarns and fabrics at elevated temperatures. This equipment will enable determination of fiber, yarn and fabric stress-strain response (i.e., tensile strength, rupture elongation, tensile modulus, repeated stress response, energy absorption and creep strength), yarn abrasion resistance, and fabric folding endurance, crease recovery, flexibility and permeability.

Discussions with the Huntington Alloy Products Division of the International Nickel Company, Inc., indicated that Inconel\* "702" should be the most satisfactory alloy that is readily available for the high temperature fixtures. It is a high-aluminum, low-titanium modification of Inconel, a nickel chromium alloy which has excellent oxidation resistance at high temperatures. This alloy can be readily forged, machined and welded, and can be annealed to facilitate fabrication. It is available as cold rolled, annealed sheet and round, and cold drawn wire and tubing.

The jaw assemblies that will be used in measuring the high temperature stress-strain response of fibers, yarns and fabrics are shown in Figure 36. The jaws will be connected to a standard Instron tensile tester through the walls of a clam-shell oven, Figures 37 and 38, capable of temperatures to 2200°F. Placing the jaws inside the heat chamber will result in all of the test specimen being at the same temperature, thereby enabling material elongations to be recorded directly on the Instron chart. The Instron will be thermally insulated from the jaws by couplings with ceramic inserts, Figure 36.

The clam-shell oven is resistance heated. A thermocouple, inserted through the wall of the clam-shell, will be used to measure the temperature of the air contained in the oven. Since some of the materials which will be tensile tested may be transparent to infrared radiation, the thermocouple junction must be shielded from the thermal radiation coming from the oven walls, which glow red at temperatures above 1200°F, i.e., the thermocouple must measure the temperature of the air in the oven and not the temperature of the oven walls.

A thermocouple is being made with a can, open at both ends, over the thermocouple junction. The outside surface of the can must have a low emissivity and the inside surface a low reflectivity. A limited survey of the literature on the properties of various materials indicates that a tantalum coated ( $\epsilon = 0.05$  at 0-2500°R) silicon carbide ( $r = 0.15$  at 0-2500°R) tube over the thermocouple junction should be satisfactory.

---

\* Trademark of the International Nickel Company, Inc.

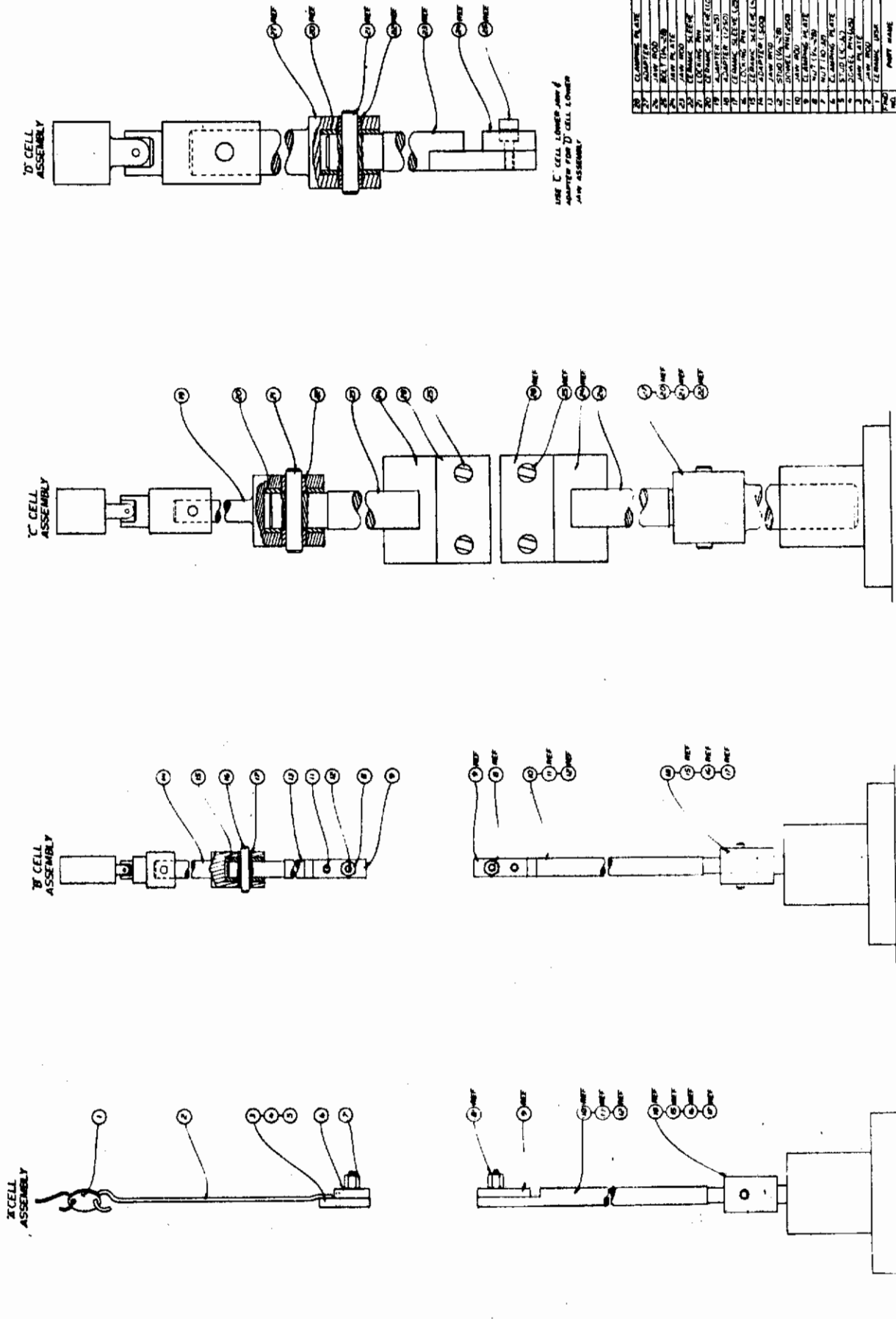


FIGURE 36 HIGH TEMPERATURE TENSILE TEST JAWS



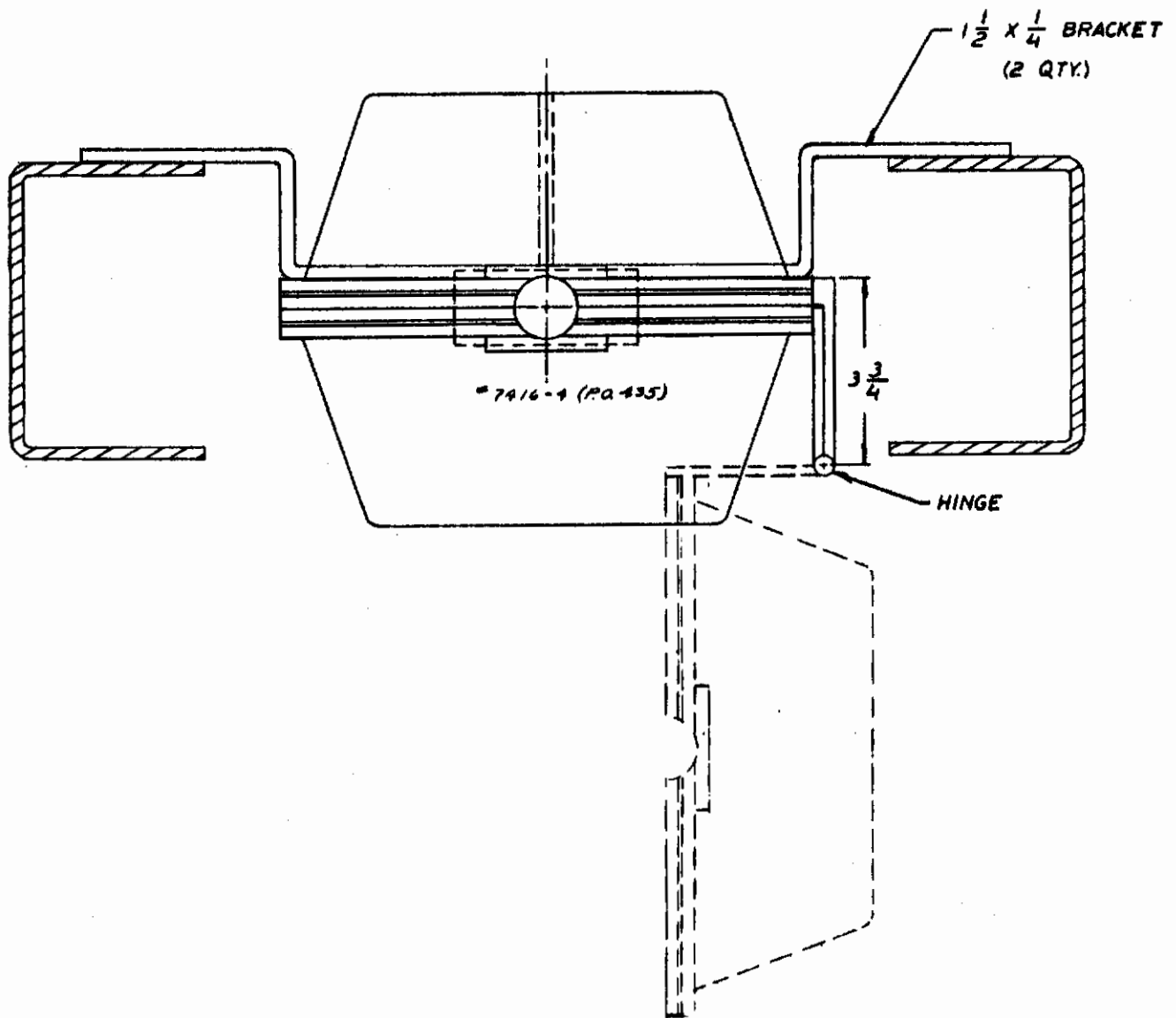
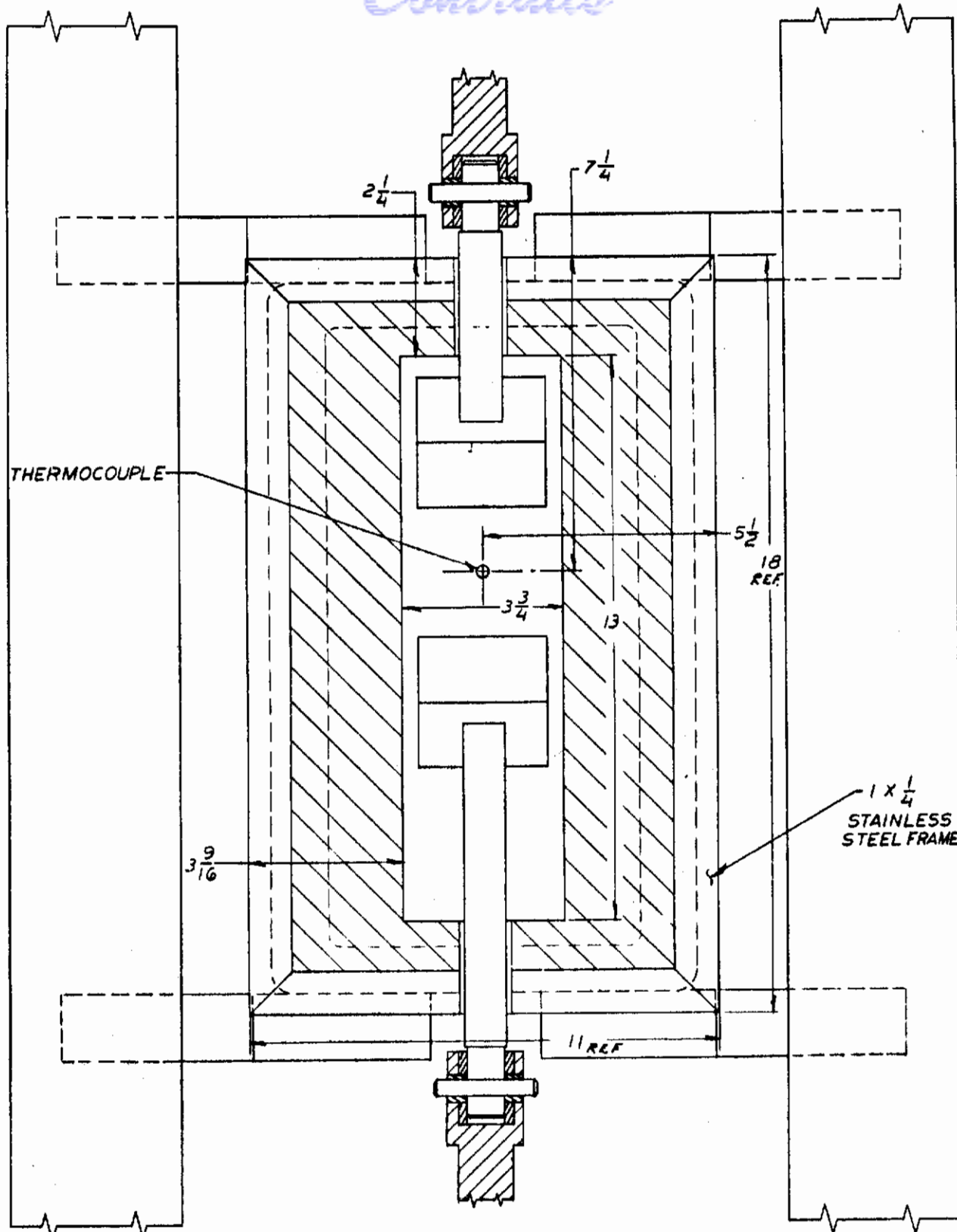


FIGURE 37(a) CLAM-SHELL OVEN DESIGN



(VIEW SHOWN WITH DOOR & HINGE REMOVED)

FIGURE 37 (b) CLAM-SHELL OVEN DESIGN



FIGURE 38 CLAM - SHELL OVEN

# Contrails

If meaningful tensile test results are to be obtained, jaw breaks and jaw slippage must be prevented. In the case of metal fabrics tested at 1000°F, the combination of serrated jaws with one layer of 181 quartz fabric between each jaw face and the fabric was found to give excellent results. This combination will be tried at the higher temperatures also.

If the quartz fabric is not completely satisfactory at the high temperatures, a thin sheet of Feltmetal\*, a sintered felt of fine metal fibers, will be tried. It is available in Inconel X and other high temperature alloys.

Fabric folding endurance, yarn abrasion resistance, fabric crease recovery, fabric permeability and fabric flexibility will be measured in a kiln capable of temperatures to 2200°F. A second door has been attached to the kiln and the test set-ups fastened to the inside face of the door as shown in Figures 39 through 43. This results in no work being required to be done in the kiln and the kiln can be kept closed. One door is hinged on the right side of the kiln and the other on the left. The procedure will be for the kiln to be brought up to temperature with the conventional door closed. The test specimen will be mounted in the appropriate fixtures on the inside face of the other door. When the kiln is up to temperature the conventional door is opened and swung out of the way and the kiln is closed with the other door, thereby placing the test set-up in the kiln. A thermocouple will be mounted near the test specimen. When it indicates the desired temperature, the test will be performed, after which the kiln will be opened, the door swung out of the way and the kiln closed again with the conventional door. Of course the inside face of the kiln doors will be hot and will radiate heat; however this quantity of heat will be considerably less than that radiated by the inside of the kiln.

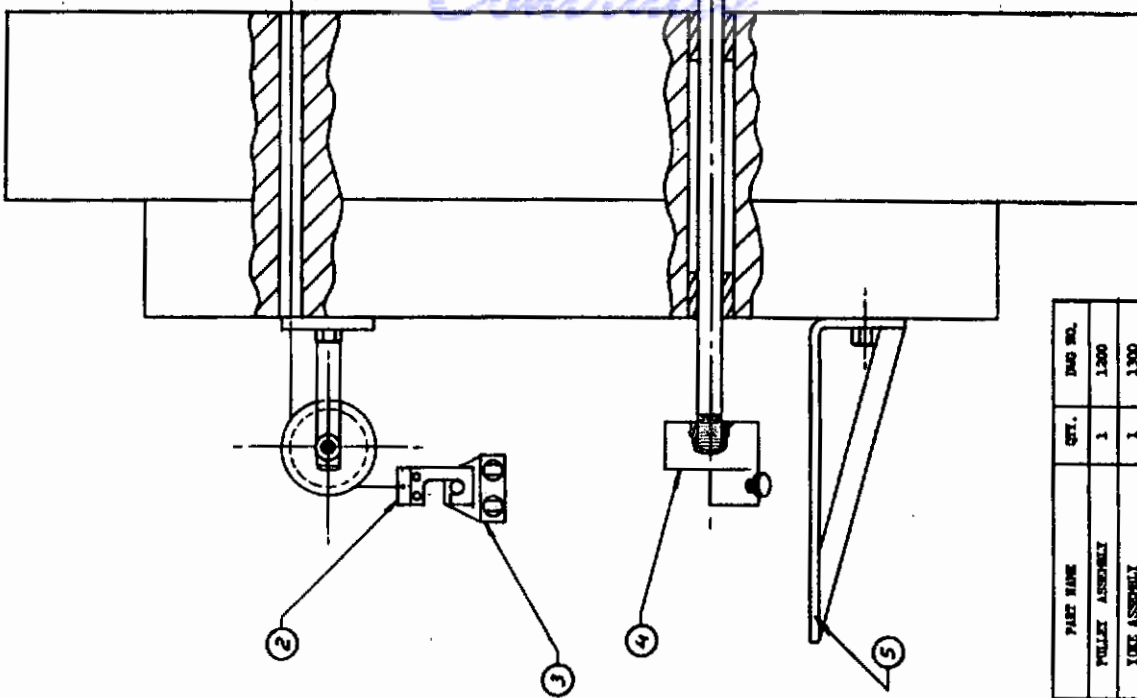
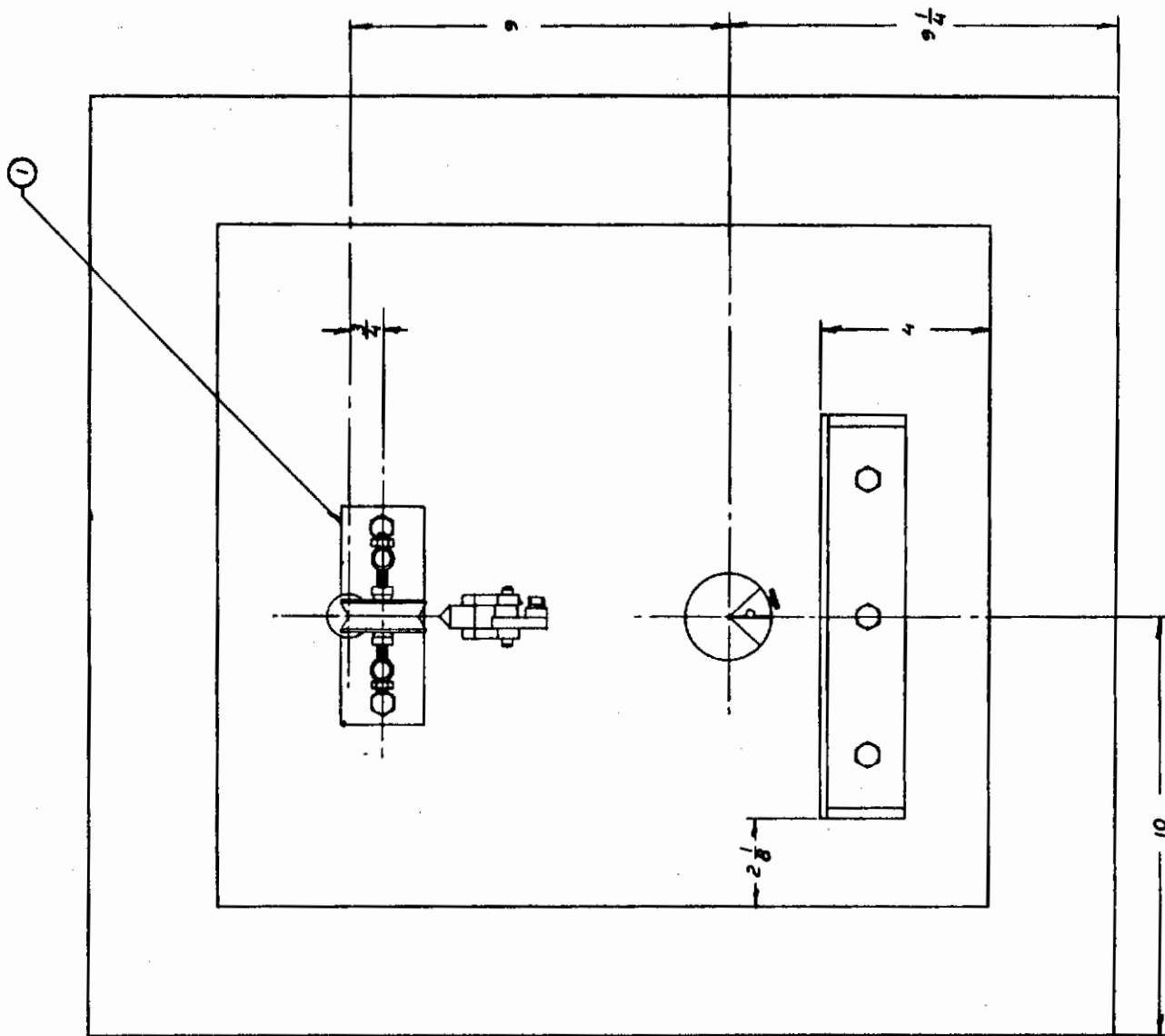
Each test set-up is designed so that it can be simply removed from the back of the door while it is hot and two of each of the assemblies will eventually be fabricated. Thus, there will not be a period of time spent waiting for fixtures to cool down before performing another test. The hot set-up will be replaced by a cold one, the specimen mounted, and the test performed. The hot set-up will be cooling off while the second test is being run.

The test set-up for determination of fabric bending endurance is shown in Figures 39(a) through 39(c). It is essentially the MIT Fold Endurance Tester, ASTM D643-43, Method B with the jaws placed inside a kiln. The jaws are fabricated from Inconel "702". The lower jaw is connected by a rod through the kiln door to a drive system similar to a conventional MIT tester and mounted on a platform on the back of the door. This subjects the lower jaw to the standard rotary oscillating movement where the fabric is folded through an angle of  $135 \pm 5$  degrees to both the right and left of the center-line position. The folding surfaces of the jaw have the required radius of curvature of approximately 0.015 inch. A tension is applied to the upper jaw by attaching a weight to a cable stranded from 5 mil Inconel wire and attached to the upper jaw through a hole at the top of the kiln door.

---

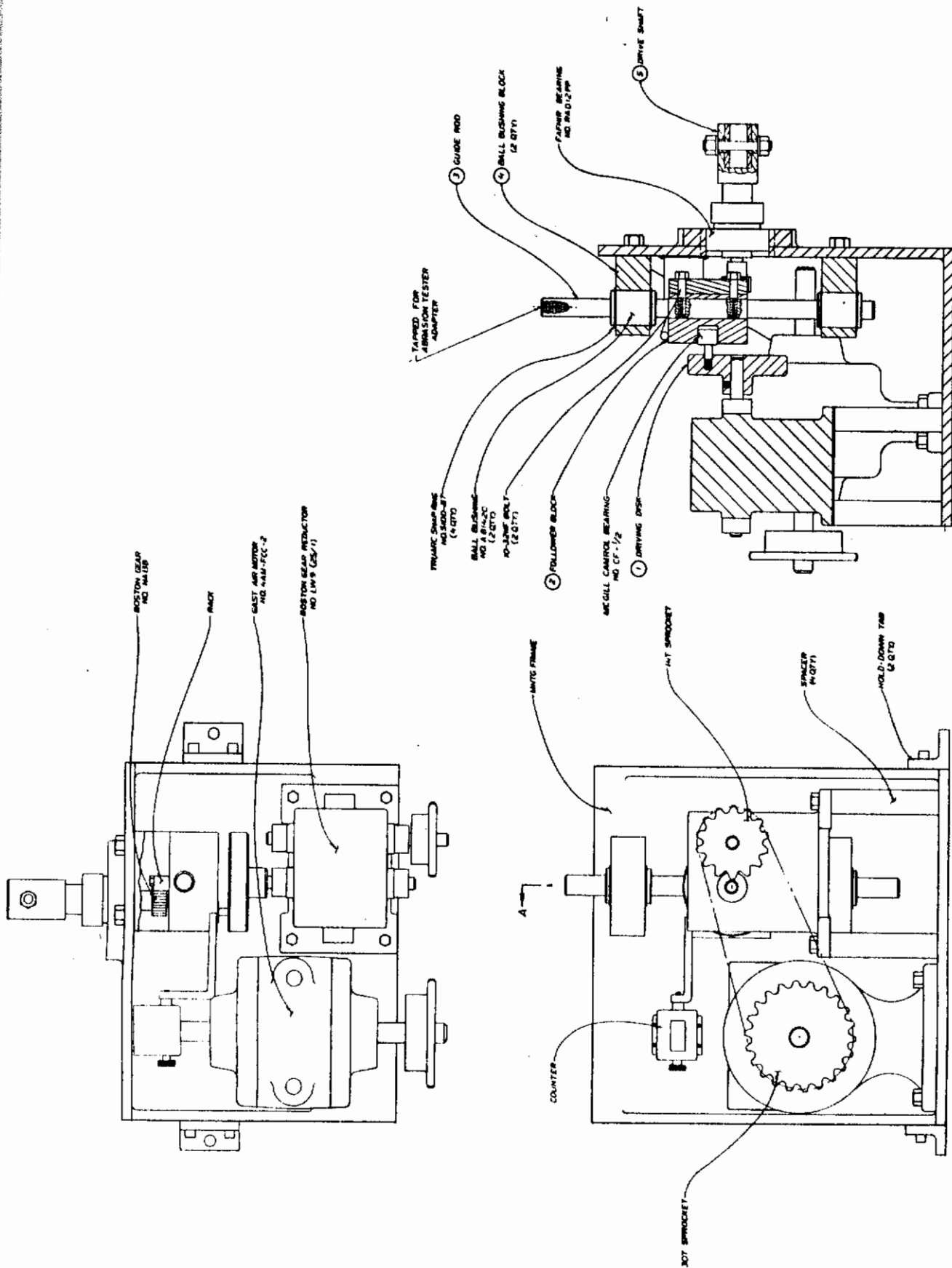
\* Trademark of The Huyck Corp.

Continental



PART NO.	PART NAME	QTY.	DWG NO.
1	PULLEY ASSEMBLY	1	1200
2	YOE ASSEMBLY	1	1300
3	TOP JAW ASSEMBLY	1	1400
4	BOTTOM JAW ASSEMBLY	1	1500
5	PLYWOOD	1	1600

FIGURE 39 (a) FABRIC FOLD ENDURANCE TESTER



SECTION A-A  
 (VIEW SHOWN WITH FOLLOWER  
 BLOCK IN MAX. POSITION)

FIGURE 39 (b) FABRIC FOLD ENDURANCE TESTER



FIGURE 39 (c) FABRIC FOLD ENDURANCE TESTER

# Contrails

A sketch of the drive assembly of the fold endurance tester is shown in Figure 39(b). It is powered by an air motor and it duplicates the motion of the standard MIT Fold Endurance Tester. The shaft is thermally insulated from the drive assembly by ceramic bushings.

As shown in Figure 39(a), the upper jaw can be easily removed while it is hot. The rod and lower jaw assembly can be disconnected at the outside of the kiln door and pulled through. Thus, a new set of jaws and the test specimen can be mounted without waiting for the door to cool down.

The test set-up for determination of yarn abrasion resistance is shown in Figures 40(a) and 40(b). It consists of pulling a yarn, one end attached to a weight and the other to a jaw, back-and-forth over a knife edge. The reciprocating motion is imparted to the jaw by the drive assembly used to power the fold endurance tester, rotated 90 degrees.

By means of a counter connected to the mechanical linkage, the number of yarn strokes until rupture will be noted for different fiber materials and finishes as a function of temperature, yarn tension and knife edge radius of curvature. Yarns can be mounted while the set-up is hot. The knife edge is made of Inconel 702.

No elaborate procedure for determining yarn rupture has been designed in the hope that the change in air motor load at yarn rupture or the sound of the weight falling to the support platform will be audible. If these events can not be easily detected a second wire will be attached to the yarn tension weight and led through the hole at the top of the kiln door and to a pointer indicator. Enough slack will be left in the wire so that the normal up-and-down motion of the tension weight will not move the pointer. However, when the yarn breaks the falling weight will move the pointer.

The test set-up for determination of fabric crease recovery is shown in Figures 41(a) and 41(b). The fabric specimen is folded and placed under the top plate assembly. The weight of the assembly is sufficient to hold the crease in the fabric. The top plate assembly is connected to a pointer on a vertical scale mounted outside the kiln by a cable running over a pulley and through a hole at the top of the door, Figure 41(a). The vertical motion of the top plate is guided by two vertical ceramic rods and is indicated by the pointer and scale.

The fabric recovers as the top plate is raised, the angular recovery being related to the vertical position of the pointer on the scale. At its position of maximum recovery the fabric is no longer in contact with the top plate. This can be detected, in the case of a metal fabric, by putting an electrical potential across the cable connected to the top plate and a wire attached to the clamping plate, and placing an indicator light in the circuit in series. The top plate assembly and the clamping plate are electrically insulated from each other by the ceramic guide rods and the ceramic brick in the oven door. The maximum fabric recovery will be given by the position of the pointer when the electrical circuit is opened (indicator light goes out).

In the case of nonconducting fabric materials a small diameter wire will be placed in the upper fabric edge and connected to the clamping plate in order to indicate when the fabric has reached its point of maximum recovery.



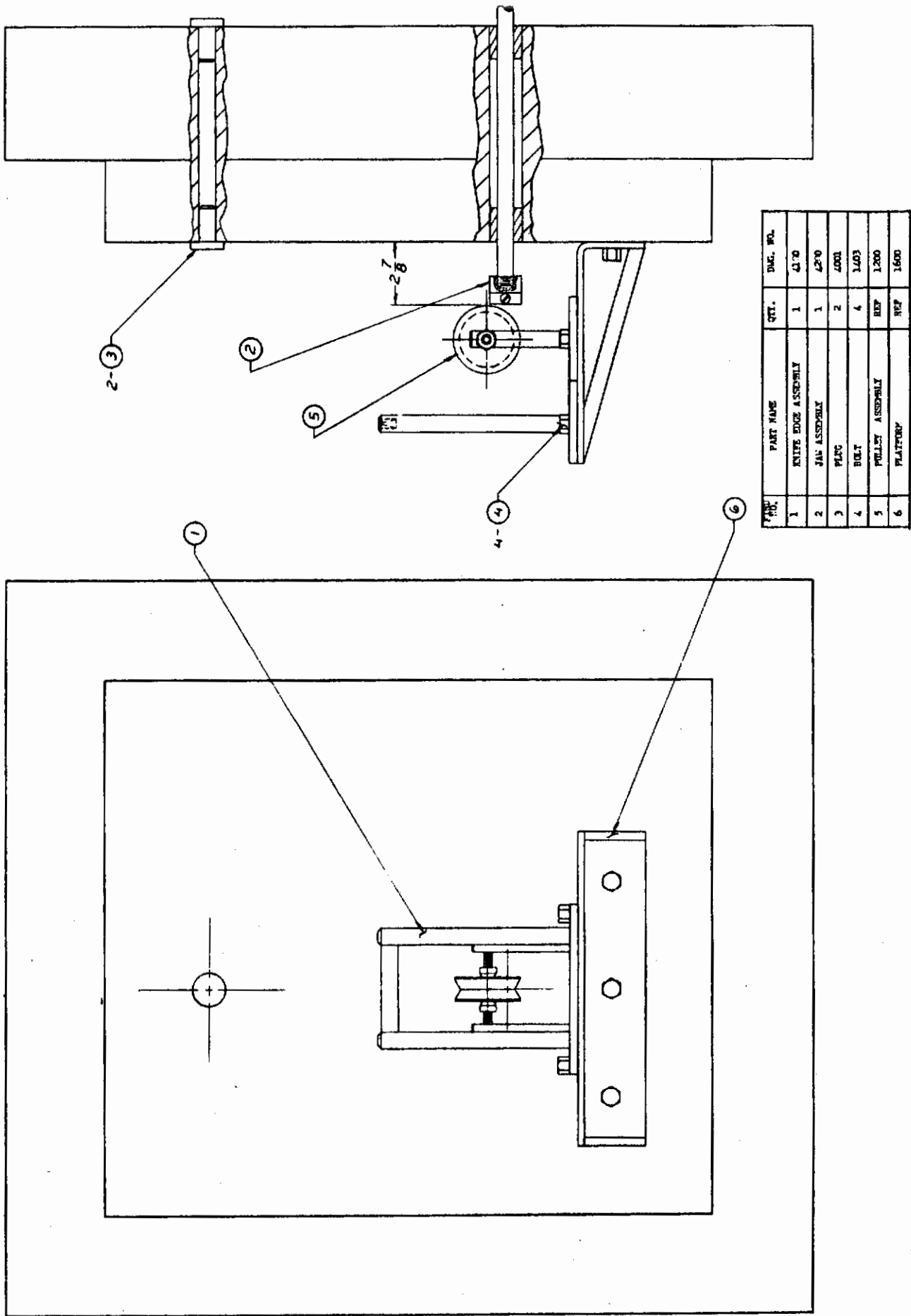


FIGURE 40 (a) YARN ABRASION RESISTANCE TESTER

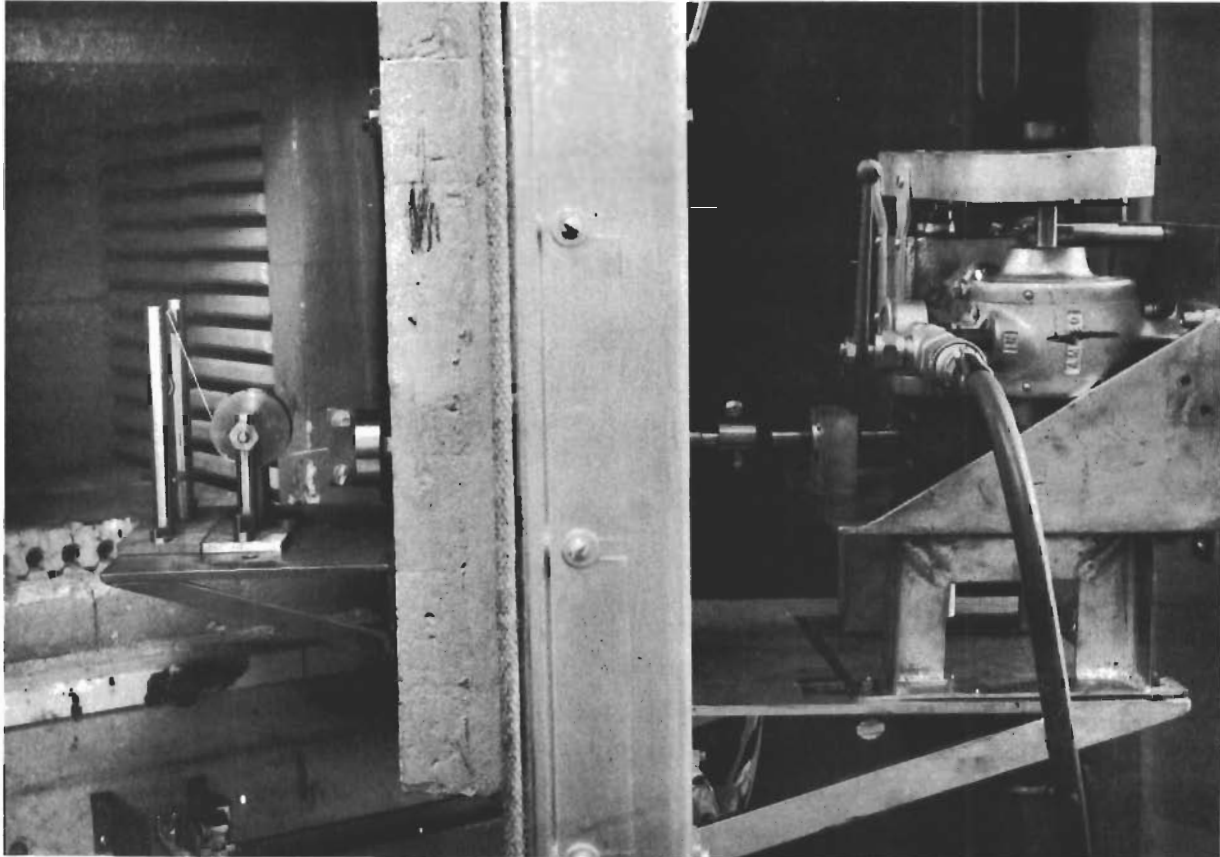


FIGURE 40 (b) YARN ABRASION RESISTANCE TESTER

*Contrails*

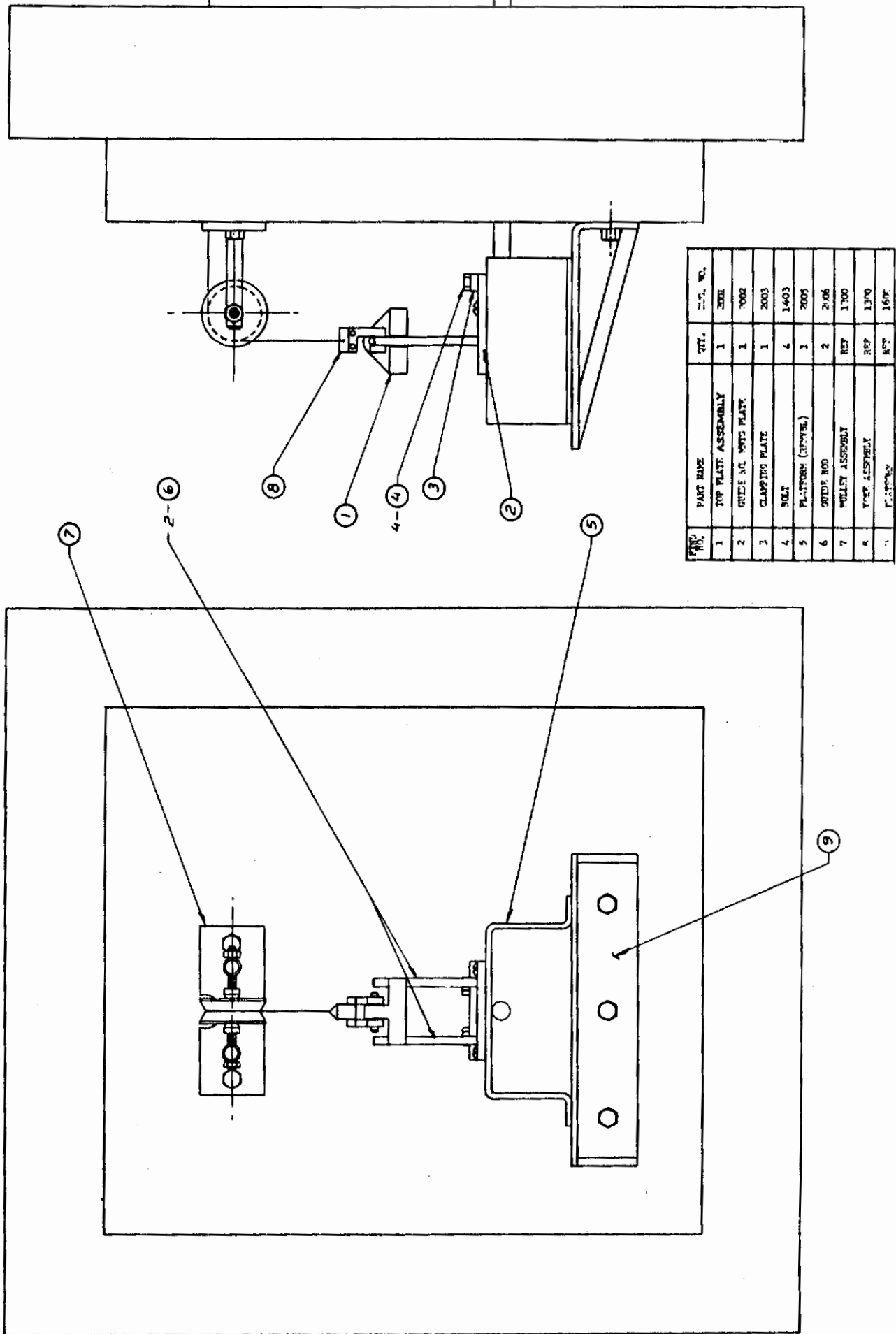


FIGURE 41(a) FABRIC CREASE RECOVERY TESTER

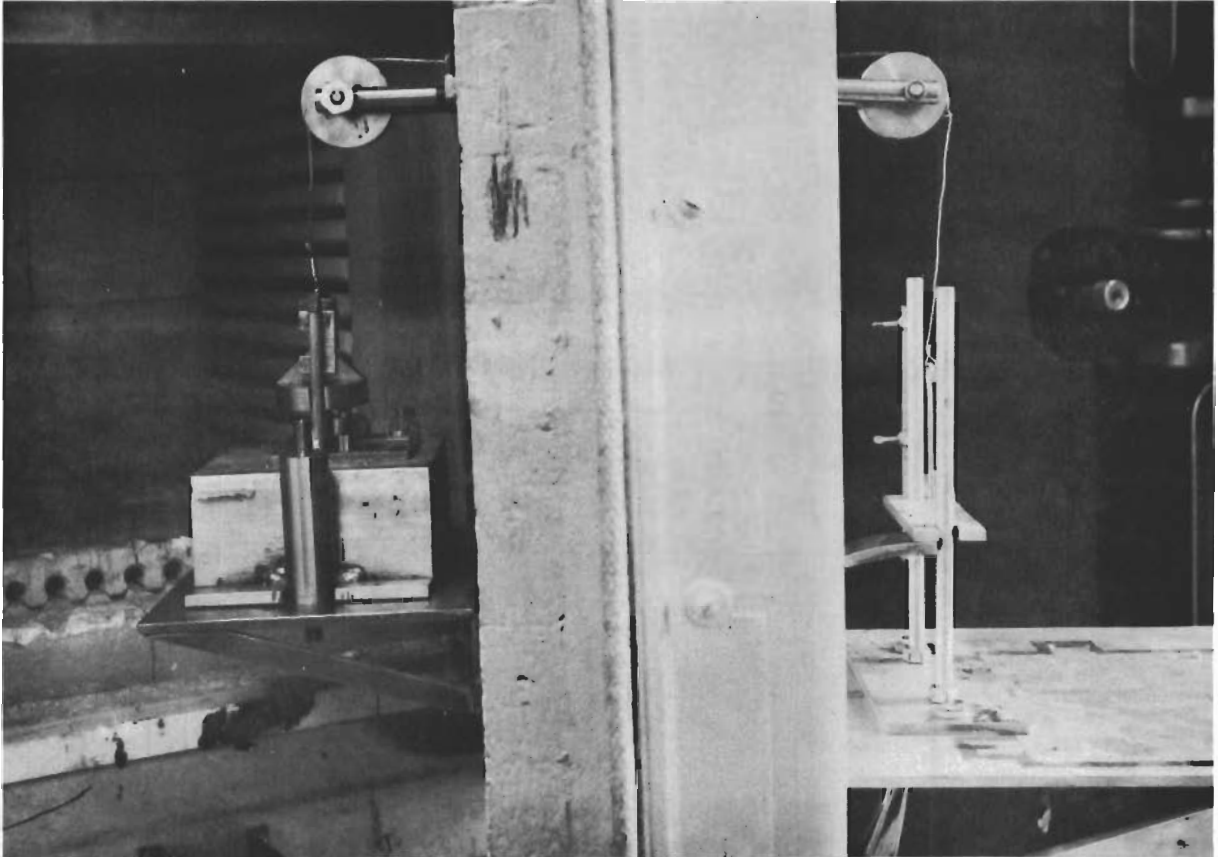


FIGURE 41(b) FABRIC CREASE RECOVERY TESTER

The test set-up for determination of fabric air permeability is shown in Figures 42(a) and 42(b). Air will be taken from an air cylinder attached to a pressure regulator valve. The air will successively flow through a gas flow meter, the kiln door, a coil mounted in the kiln, and the fabric specimen. The temperature and pressure of the air will be measured at the gas flow meter, as will be the temperature of the air flowing into the funnel. For small to moderate volume flow rates the temperature of the air will reach that of the inside of the kiln while flowing through the coil and the static pressure of the air at the flow meter and at the fabric will be approximately equal.

The fabric specimen to be tested will be clamped between two plates and this assembly clamped over the funnel as shown in Figure 42(a). Quartz fabric will probably be used for gasketing material. Two funnels have been fabricated, one 2-3/4 inches in diameter and the other 1.0 inch in diameter.

The gas flow meter gives the volume flow rate of air. Knowing the temperature of the air at the meter and at the fabric, the permeability of the known area of fabric sample to hot air at the known pressure differential can be determined.

The test set-up for measuring fabric flexibility at elevated temperatures is shown in Figures 43(a) and 43(b). In this test a length of fabric is passed through the opening in the plate shown at the top of Figure 43(a) and formed into a circle, the ends being overlapped and clamped together by the rod in the assembly shown at the bottom of Figure 43(a). The plate is connected to a pointer on a vertical scale mounted outside the kiln by a cable running over a pulley and through a hole at the top of the kiln door, Figure 43(b). There is provision for placing various loads on the end of this cable, thereby enabling the deflection of the loop of fabric to be measured at various loads. Having this data the fabric rigidity  $G$  will be given by<sup>(14)</sup>

$$G = k WL^2 \cos \theta / \tan \theta$$

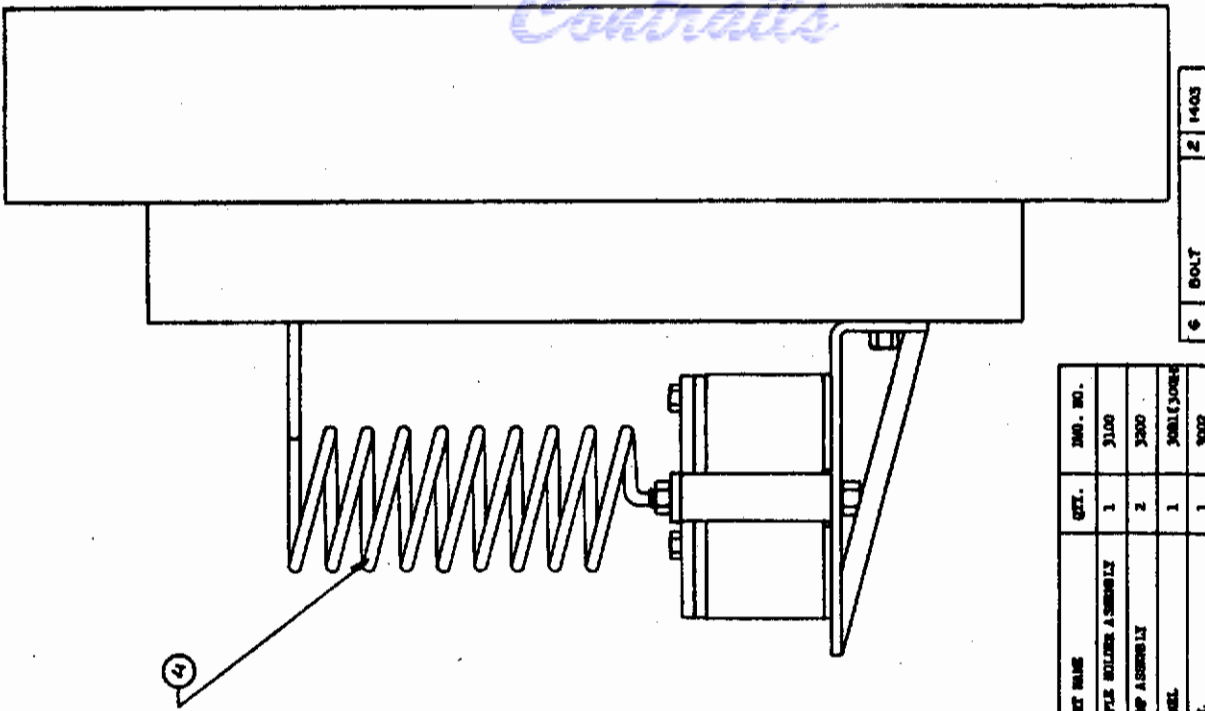
where

- $k = 0.0047$
- $W =$  applied load per unit width of the fabric
- $\theta = 493 e/L$
- $L =$  circumferential length of the undistorted ring of fabric
- $e =$  deflection of the upper end of the fabric loop under the applied load  $W$

## B. Low Temperature Test Equipment

The design of a test fixture for use in conjunction with the Instron tensile tester for measuring fiber, yarn and fabric tensile properties under liquid nitrogen ( $-320^\circ\text{F}$ ) is shown in Figures 44 and 45. The dewar is connected to the Instron cross-head. The upper jaws connect to the Instron universal. The lower jaws are connected to the tensile plug in the bottom of the dewar by a locking disk. This disk is slid up the lower jaw stem and a snap ring placed in the groove on the stem. The jaw is then inserted in the tensile plug and the locking disk screwed down securely. The thrust load strength of the snap ring far exceeds any load that will be encountered under this program.

*Contracts*



QTY	PART NAME	QTY	ING. NO.
1	SAMPLE HOLDERS ASSEMBLY	1	3100
2	CLAMP ASSEMBLY	2	3300
3	FRIBEL	1	3001 (3004)
4	CHILL	1	3002
5	PLATFORM	1	2005 (2005-3)

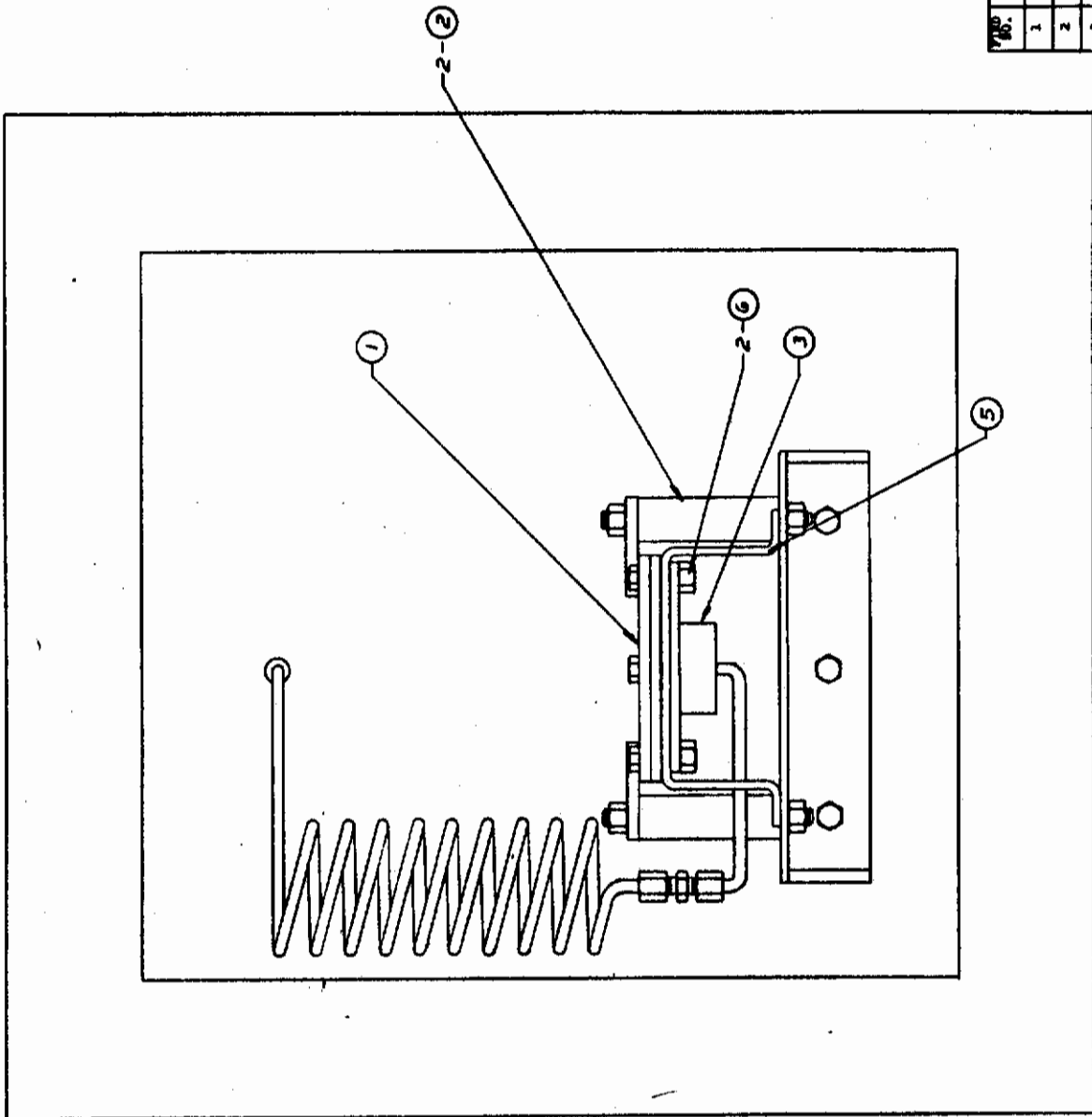


FIGURE 42 (a) FABRIC PERMEABILITY TESTER

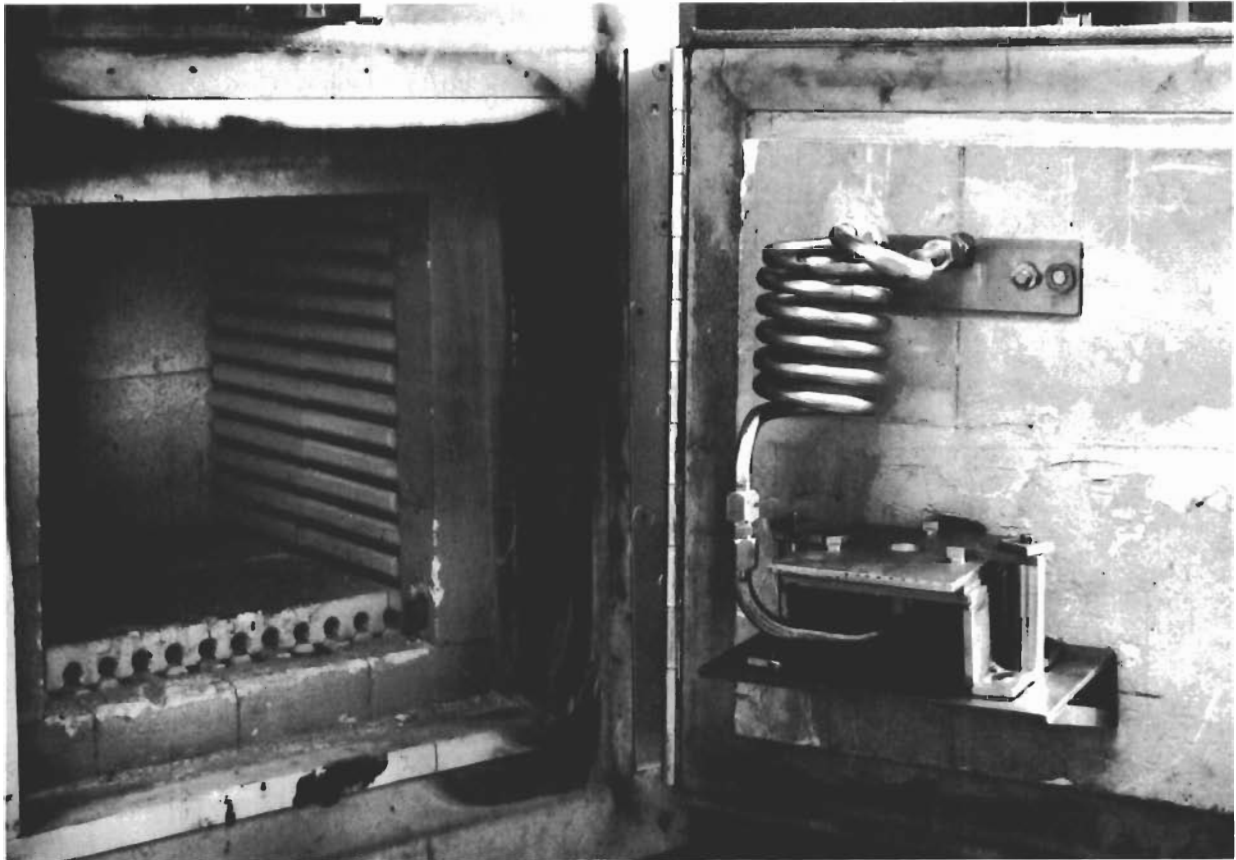
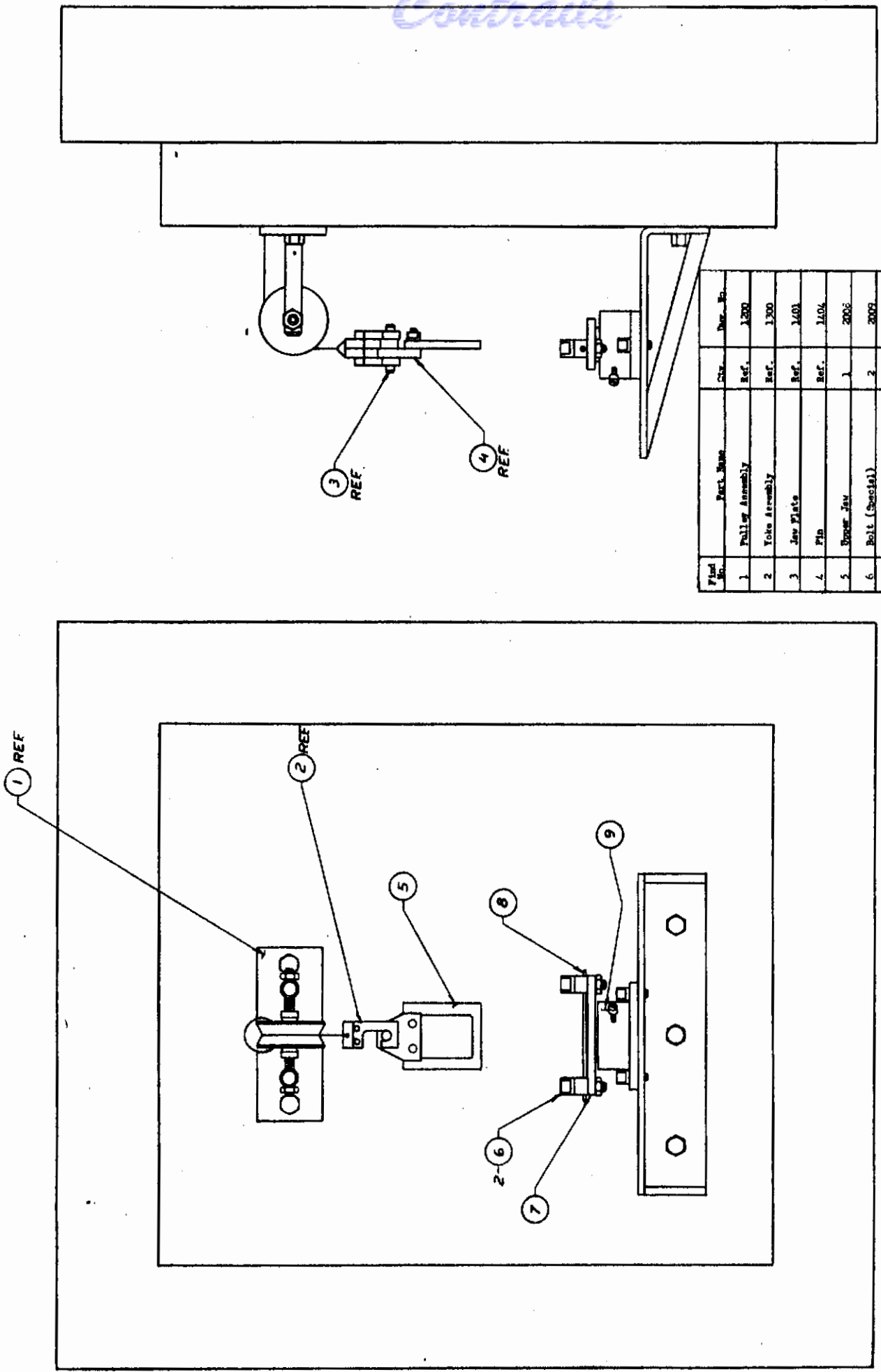


FIGURE 42 (b) FABRIC PERMEABILITY TESTER

*Contracts*



Part No.	Part Name	Qty	Rev. No.
1	Fuller Assembly	Ref.	1200
2	Yoke Assembly	Ref.	1300
3	Jaw Plate	Ref.	1401
4	Pin	Ref.	1404
5	Upper Jaw	1	2006
6	Bolt (Special)	2	2009
7	Lower Jaw	1	2010
8	Clamping Rod	1	2011
9	Platform Meas. Adaptor	1	2012

FIGURE 43 (a) FABRIC FLEXIBILITY TESTER



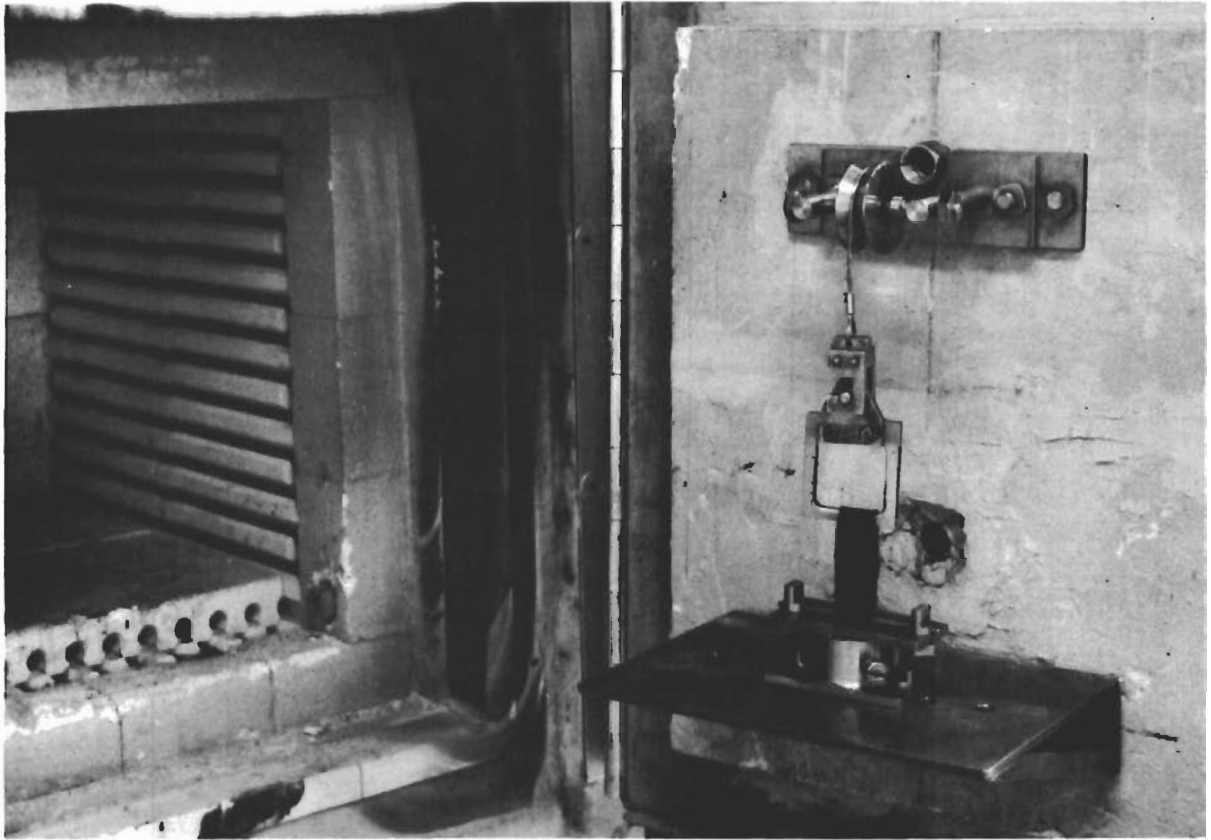


FIGURE 43 (b) FABRIC FLEXIBILITY TESTER

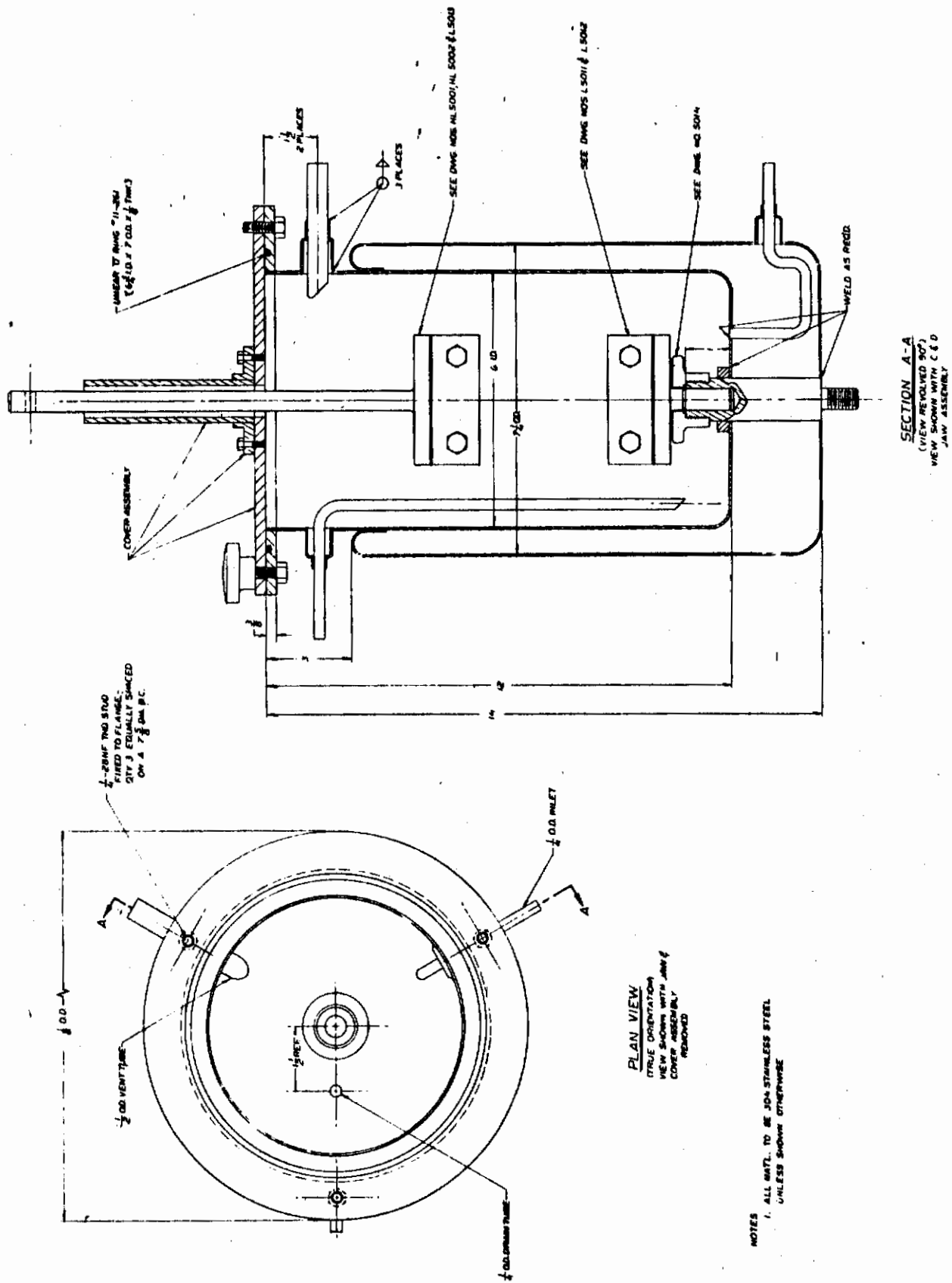


FIGURE 44 CRYOGENIC TENSILE TEST DEWAR

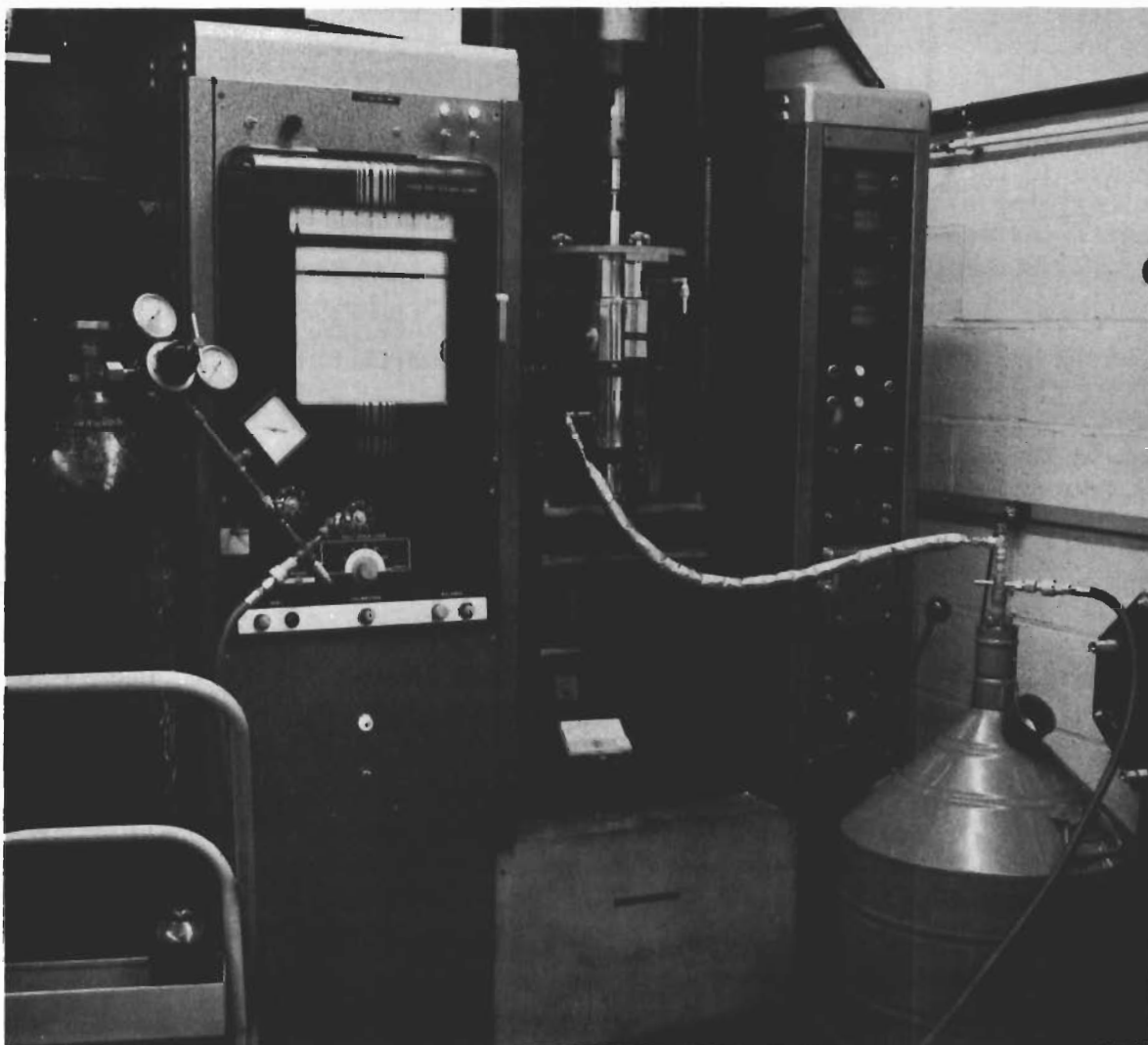


FIGURE 45 CRYOGENIC TENSILE TEST SET - UP

# Contrails

The piping diagram for the cryogenic test set-up is shown in Figure 46. The liquid nitrogen is stored in the 50 liter storage dewar. After the sample to be tested has been inserted in the jaws and the jaws in the dewar, the tensile dewar is filled by closing valve 2 and opening valve 1. Nitrogen gas, at a couple pounds pressure, forces the liquid nitrogen into the dewar. When the dewar is full and the boiling off due to cooling the jaws has ceased, valve 1 is closed and valve 2 opened.

After the test, the dewar is drained by opening valves 2 and 3, and closing the vent. Nitrogen gas, at a couple pounds pressure, forces the liquid back into the storage dewar. The jaws can then be removed and another sample inserted. Insulated flexible tubing is used to connect the tensile test dewar and the storage dewar.

The design of a test fixture to be inserted in the cryogenic tensile test dewar for measuring fabric fold endurance under liquid nitrogen is shown in Figure 47. This fixture is being fabricated at the present time.

An instrument that enables the permeability of a fabric to be measured on the Frazier Permeometer with the fabric at various levels of loads has been built, Figures 48(a) and 48(b). It uses a cruciform-shaped fabric sample and can subject the sample to various loads up to 240 pounds/inch of fabric width. The sample can be put under uniaxial or any ratio of biaxial loads.

One of each of the test fixtures discussed above has either been fabricated or is being fabricated. Some of the equipment has been checked out at 70°F. However, none of the equipment has been run at the extreme temperatures for which it was designed. This will be done in the near future using a monofilament stainless steel wire screen. During this evaluation of the equipment, the necessary test procedures will be developed and any design modifications which seem appropriate will be made. When this phase of the program has been completed, the fine wire multifilament yarn fabric and other fibrous materials will be evaluated at temperatures from cryogenic to 2000°F.

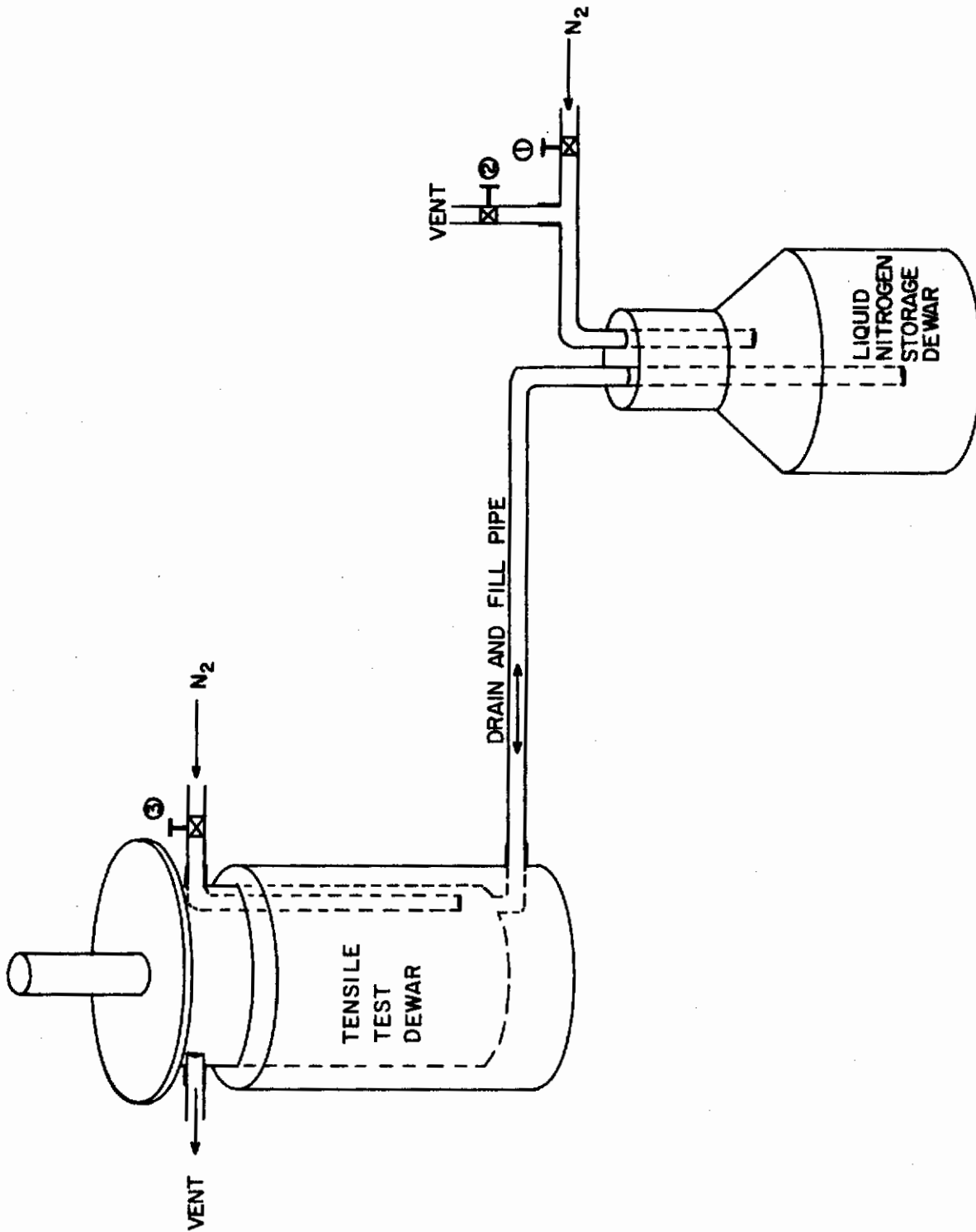


FIGURE 46 CRYOGENIC TEST SET - UP

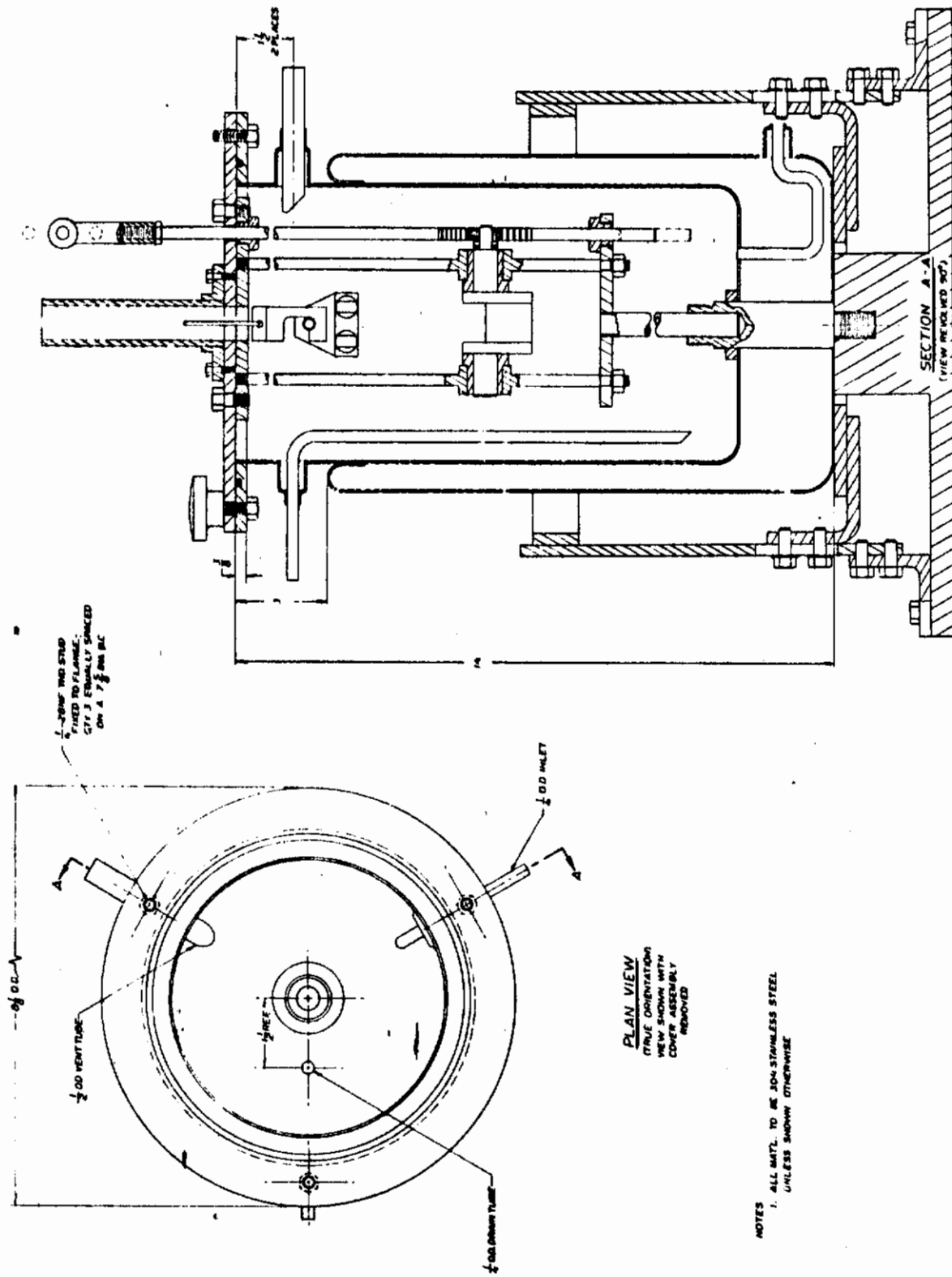


FIGURE 47 CRYOGENIC FABRIC FOLD ENDURANCE TESTER

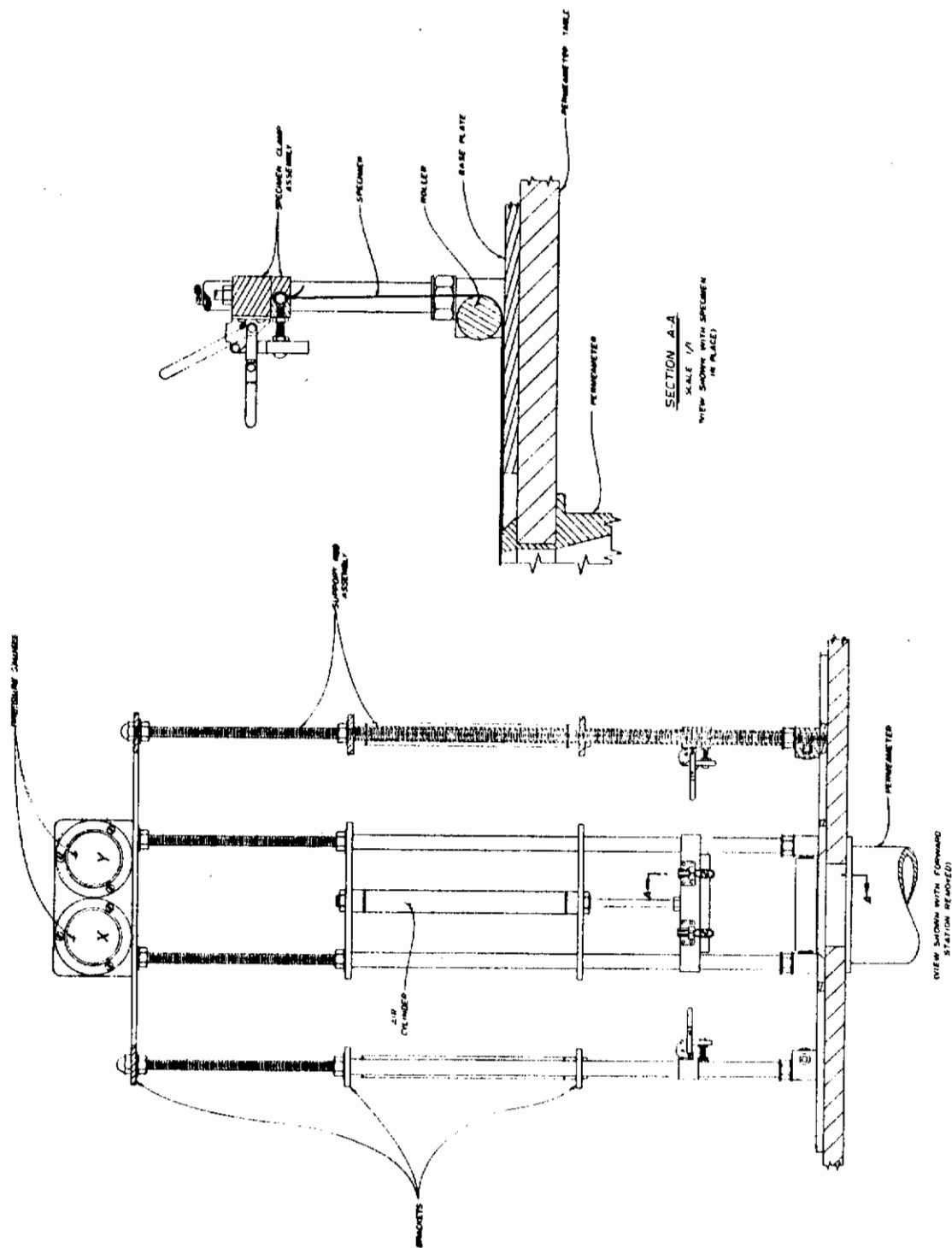


FIGURE 48 (a) FABRIC PERMEABILITY (under biaxial stress) TESTER

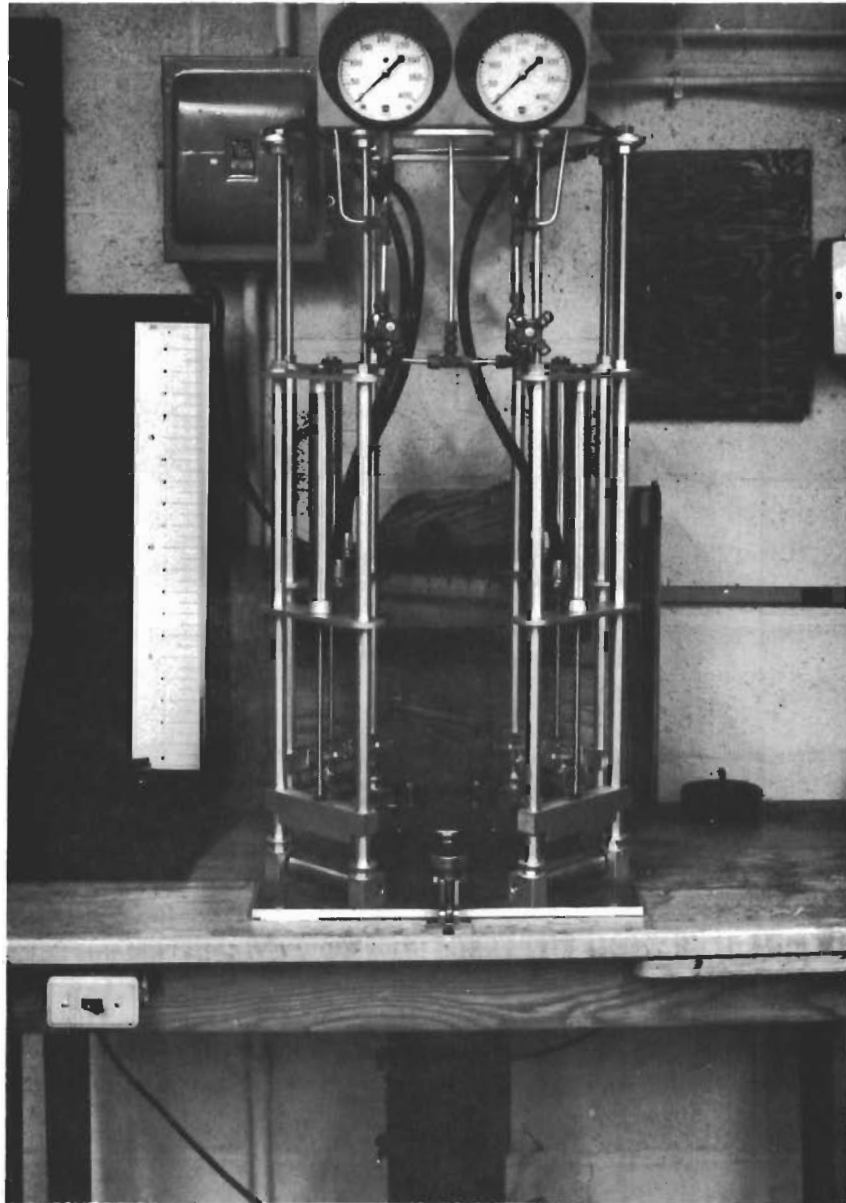


FIGURE 48 (b) FABRIC PERMEABILITY (under biaxial stress) TESTER



## X. BENDING RIGIDITY OF NONWOVEN FABRICS

One of the major differences between woven and nonwoven fabrics of today is the characteristically greater bending rigidity of nonwovens<sup>(1)</sup>. (The term nonwoven refers herein to a weblike assemblage of fibers bonded to each other at their cross-overs.) This is attributed to the different mechanisms governing deformations in the two structures.

The properties of both woven and nonwoven fabrics are determined by a complex interaction between fiber properties, structural geometry, and, in the case of nonwovens, bond properties. Although these interactions are not completely understood, the low bending rigidity of the woven fabric can be attributed, for the most part, to the high degree of freedom of individual fiber motion during fabric bending, and the high rigidity of the nonwoven, to the bonding together of the individual fibers by the binder used in the manufacture of nonwoven fabrics.

Most apparel applications of textiles require fabric with low bending rigidity -- fabric that can bend and drape under its own weight. However, adequate strength is achieved in current nonwovens by using a considerable quantity of binder. Therefore, these fabrics are not suitable for most apparel applications.

The analytical and experimental study reported in this section is aimed at achieving a better understanding of the mechanisms determining the bending rigidity of a nonwoven. Procedures for predicting quantitatively the bending rigidity in the two extreme cases of complete freedom of individual fiber motion during fabric bending and no freedom of fiber motion -- complete bonding -- are given. The effects of fiber orientation, fiber bending and fiber torsion are included. The results of these analyses indicate a possible avenue of approach whereby the bending rigidity of a nonwoven may be decreased to a level more closely approximating that of a woven fabric.

To simplify the determination of the strains in the fibers during the bending of a nonwoven fabric, the fabric is assumed to be composed of a large number of individual, square, planar, unit cells, Figure 49, whose boundaries are parallel and perpendicular to the direction of stress, and remain straight, the opposite boundaries remaining parallel, during displacement<sup>(15)</sup>. Taking the boundaries perpendicular and parallel to the direction of stress eliminates rotation of the cell boundaries for the type of fabric distortions being considered.

To describe the behavior of the fabric in terms of the behavior of one of the cells, the common cell boundaries must remain common and their projection on the original neutral plane straight. This condition can be fulfilled by considering the fabric as a matrix of bond points whose fibers radiate outward to other bond points, Figure 49. If a unit cell of sufficient size is selected, the number of fibers contained within the cell will be large enough for small changes in the number or orientation of the fibers from point to point in the cell to be negligible. Also, if a unit cell size is chosen so that sufficient bonds along each fiber are included between the cell boundaries, the influence of fibers ending within the cell boundaries will be negligible.

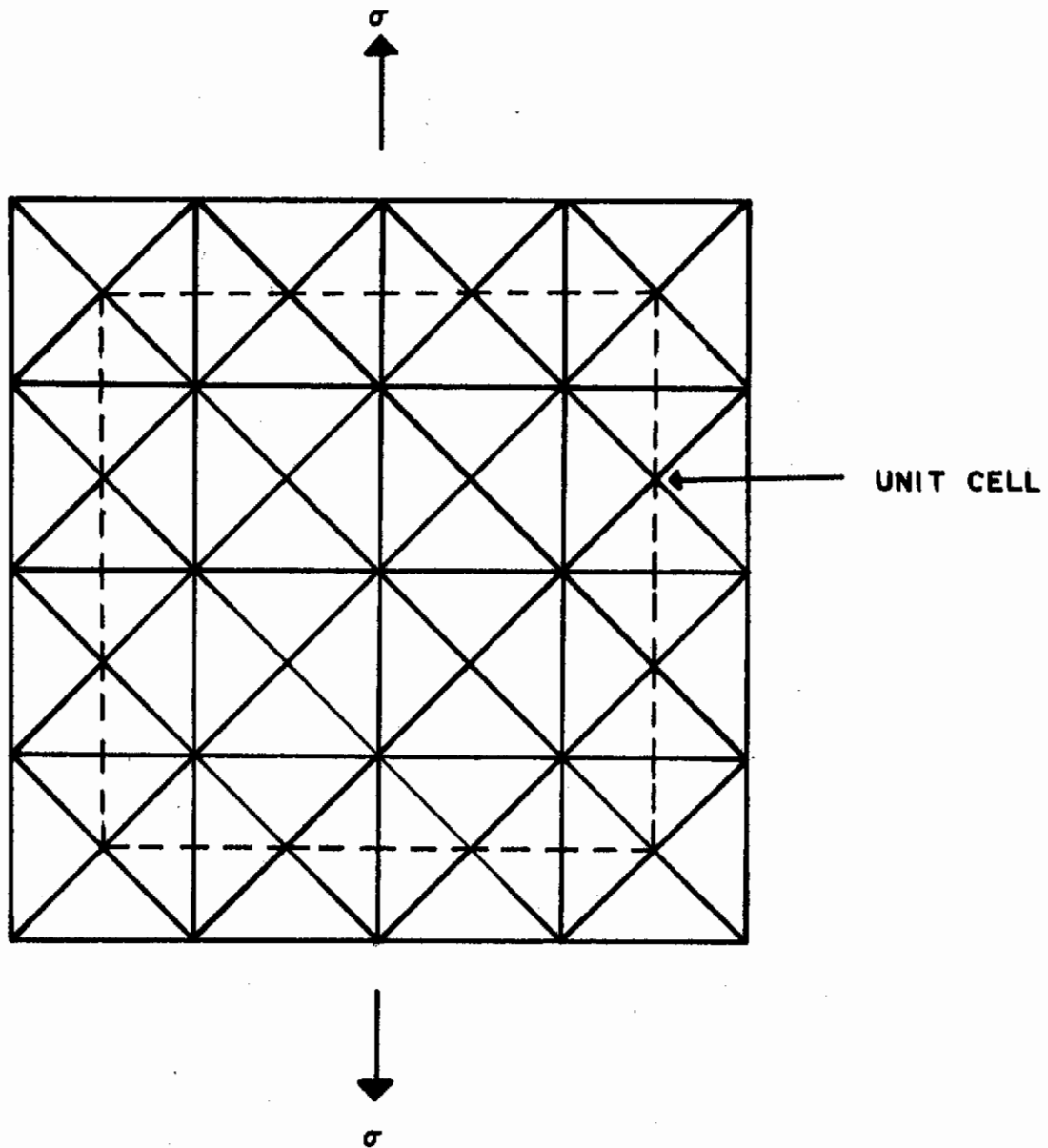


**FIGURE 49 NONWOVEN FABRIC**

# Contrails

Two cases are considered, complete freedom of relative fiber motion and no freedom of relative fiber motion.

## Complete Freedom of Relative Fiber Motion

Complete freedom of relative fiber motion can be visualized by imagining fiber ends to be bonded to each other and no bonding taking place at any other locations along the fibers, e.g. at fiber cross-overs. The average fiber strain in a unit cell whose geometry satisfies the above requirements will be approximated by that strain determined by considering the fibers to be bonded at the boundaries of the planar unit cell.

The degree to which the mechanical response of this unit cell approximates that of an actual nonwoven will depend on the method of fabrication of the nonwoven. In most instances this approximation would be crude at best. However, analysis of the tensile response of nonwovens has shown that this approach gives some insight into the mechanisms governing the deformation of a nonwoven fabric<sup>(1,7,15,16)</sup>.

In the case of bending of an homogeneous isotropically elastic element, the bending moment required for elastic equilibrium is given by

$$\vec{M}_B = \vec{T} \times EI\vec{K} \quad (1)$$

where  $\vec{T}$  is the unit vector tangent to the bent curve of the element,  $\vec{K}$  is the resultant curvature vector, and  $EI$ , assumed to be a scalar quantity, is the cross-sectional bending rigidity of the bent element.

The bending moment of a randomly oriented fiber about, for instance, the  $\vec{k}$  axis, Figure 50, is given by the  $\vec{k}$  component of  $\vec{M}_B$ , i.e.,

$$(\vec{M}_B)_{\vec{k}} = EI (\vec{T} \times \vec{K})_{\vec{k}} \quad (2)$$

Letting

$$\vec{T} = T_1 \vec{i} + T_2 \vec{j} + T_3 \vec{k} \quad (3)$$

and

$$\vec{K} = K_1 \vec{i} + K_2 \vec{j} + K_3 \vec{k} \quad (4)$$

$$\vec{T} \times \vec{K} = \vec{i} \left| \begin{matrix} T_2 T_3 \\ K_2 K_3 \end{matrix} \right| + \vec{j} \left| \begin{matrix} T_3 T_1 \\ K_3 K_1 \end{matrix} \right| + \vec{k} \left| \begin{matrix} T_1 T_2 \\ K_1 K_2 \end{matrix} \right| \quad (5)$$

and therefore

$$(\vec{T} \times \vec{K})_{\vec{k}} = T_1 K_2 - T_2 K_1 \quad (6)$$

The position vector  $\vec{R}$  of any point on any fiber at an angle to the  $\vec{i}$  axis is given by

$$\vec{R} = \vec{i} (\rho \cos \theta) + \vec{j} (\rho \sin \theta) + \vec{k} (\rho \tan \zeta \cos \theta) \quad (7)$$

The angles  $\theta$  and  $\zeta$  are as shown in Figure 50 with each fiber being defined by an angle  $\zeta$ . The magnitude of the position vector is

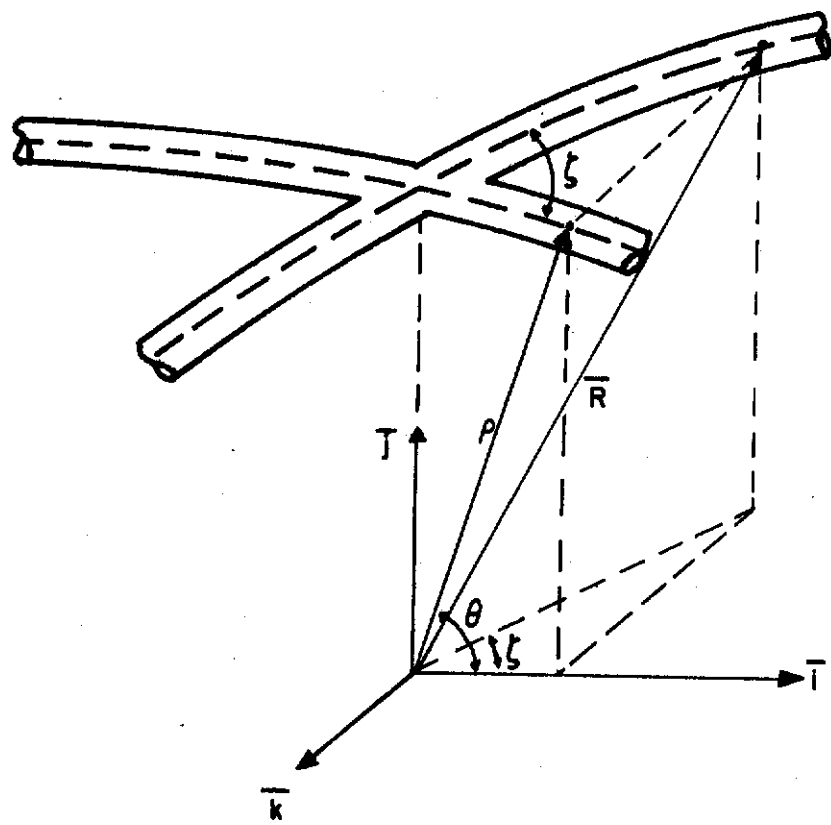


FIGURE 50 BENDING OF THE UNIT CELL

# Contrails

$$|\vec{R}| = \rho [1 + \tan^2 \zeta \cos^2 \theta]^{1/2} . \quad (8)$$

The unit tangent vector  $\vec{T}$  is given by

$$\vec{T} = \frac{d\vec{R}}{ds} \quad (9)$$

where

$$ds = \rho [1 + \tan^2 \zeta \sin^2 \theta]^{1/2} d\theta . \quad (10)$$

Therefore,

$$\vec{T} = \vec{i} \left( \frac{-\sin \theta}{[1 + \tan^2 \zeta \sin^2 \theta]^{1/2}} \right) + \vec{j} \left( \frac{\cos \theta}{[1 + \tan^2 \zeta \sin^2 \theta]^{1/2}} \right) + \vec{k} \left( \frac{-\tan \zeta \sin \theta}{[1 + \tan^2 \zeta \sin^2 \theta]^{1/2}} \right) \quad (11)$$

The curvature vector  $\vec{K}$  is given by

$$\begin{aligned} \vec{K} &= \frac{d\vec{T}}{ds} = \frac{d\vec{T}}{\rho [1 + \tan^2 \zeta \sin^2 \theta]^{1/2} d\theta} \\ &= - \frac{\vec{i}}{\rho [1 + \tan^2 \zeta \sin^2 \theta]^{1/2}} \left[ \frac{\beta^{1/2} \cos \theta - \sin \theta \frac{d}{d\theta} \beta^{1/2}}{\beta} \right] \\ &\quad - \frac{\vec{j}}{\rho [1 + \tan^2 \zeta \sin^2 \theta]^{1/2}} \left[ \frac{\beta^{1/2} \sin \theta + \cos \theta \frac{d}{d\theta} \beta^{1/2}}{\beta} \right] \\ &\quad - \frac{\vec{k}}{\rho [1 + \tan^2 \zeta \sin^2 \theta]^{1/2}} \left[ \frac{\beta^{1/2} \tan \zeta \cos \theta - \tan \zeta \sin \theta \frac{d}{d\theta} \beta^{1/2}}{\beta} \right] \end{aligned} \quad (12)$$

where

$$\beta = 1 + \tan^2 \zeta \sin^2 \theta . \quad (13)$$

Substituting Equations (11) through (13) into Equation (6)

$$(\vec{T} \times \vec{K})_{\vec{k}} = \frac{1}{\rho [1 + \tan^2 \zeta \sin^2 \theta]^{3/2}} \quad (14)$$

Taking  $\theta = 90^\circ$ , the bending moment,  $M_{r\zeta}$ , in the fiber at the angle  $\zeta$  about the  $\vec{k}$  axis is given by

$$M_{r\zeta} = \frac{E_f I_f}{\rho [1 + \tan^2 \zeta]^{3/2}} \quad (15)$$

where  $E_f I_f$  is the bending rigidity of the fiber about a diameter.

The bending rigidity of the fiber at the angle  $\zeta$  about the  $\vec{k}$  axis is given by the bending moment about the  $\vec{k}$  axis required to produce unit change in curvature in the  $i, j$  plane. Equation (15) gives a rigidity of  $E_f I_f$  for the fiber at  $\zeta = 0$  and a rigidity of zero for the fiber at  $\zeta = 90^\circ$ , as it should.

# Contrails

The angular distribution of fibers in the unit cell, i.e., the fraction of the total number of fibers in the cell which lie at any prescribed angle  $\zeta$  to the  $\bar{i}$  axis, is denoted herein by the function  $\phi(\zeta)$ , where

$$\int_{-\pi/2}^{\pi/2} \phi(\zeta) d\zeta = 1 \quad (16a)$$

and

$$\phi(\zeta) = \frac{N(\zeta)}{\sum_{\zeta=-\pi/2}^{+\pi/2} N(\zeta)} \quad (16b)$$

$N(\zeta)$  is the total number of fibers in the unit cell which lie at any prescribed angle  $\zeta$  to the  $\bar{i}$  axis per unit width perpendicular to the direction of the fibers. It is the number of fibers which intersect the diameter A-B of the circle inscribed in the unit cell (Figure 51) at  $90^\circ$ .  $\sum N(\zeta)$  is the sum of all such total numbers of fibers; it represents the total number of fibers in the circle inscribed in the unit cell. The relative frequency of fibers per unit width perpendicular to the  $\bar{i}$  axis is  $\phi(\zeta) \cos \zeta$ .

Assuming equal angular and numerical fiber distribution throughout the thickness of the unit cell approximating the nonwoven fabric and also assuming complete freedom of relative fiber motion and neglecting lateral contraction, the  $\bar{k}$  component of the bending moment in the unit cell,  $M_c$ , is given by the sum of the  $\bar{k}$  components of the bending moments in all the fibers in the cell, i.e.,

$$M_c = \frac{N_f E_f I_f}{\rho} \int_{-\pi/2}^{\pi/2} \phi(\zeta) \cos^4 \zeta d\zeta \quad (17)$$

where  $N_f$  is the total number of fibers in the circle inscribed in the square unit cell.

The bending rigidity,  $(EI)'$ , of the unit cell is given by the bending moment required to produce unit change in curvature. Therefore,

$$(EI)' = N_f E_f I_f \int_{-\pi/2}^{\pi/2} \phi(\zeta) \cos^4 \zeta d\zeta \quad (18)$$

Equation (18) assumes that the number of fibers in a unit cell is large enough for the cell to be approximated by a continuum.

The foregoing analysis assumes that the fibers are free to untwist during bending of the unit cell so that no fiber torques are set up. In a real fabric the fibers are not free to untwist. Taking the fibers to be securely fastened at the cell boundaries is probably a more realistic assumption.

# Contrails

The state of torsion of the fibers in a bent nonwoven can be found in the same manner as the state of torsion of the fibers in a single yarn of twist  $T_y$ . The helix angle of the fibers,  $\theta_y$  ( $\theta_y = \zeta$ ), is given by

$$\tan \theta_y = 2\pi T_y \rho \quad (19)$$

where  $\rho$  is the radius of curvature of the bent nonwoven. The equivalent fiber twist per unit length,  $T_f$ , which would be required to produce the same strain were the fiber axis straight, is given by<sup>(15)</sup>

$$T_f = T_y \cos^2 \theta_y \quad (20)$$

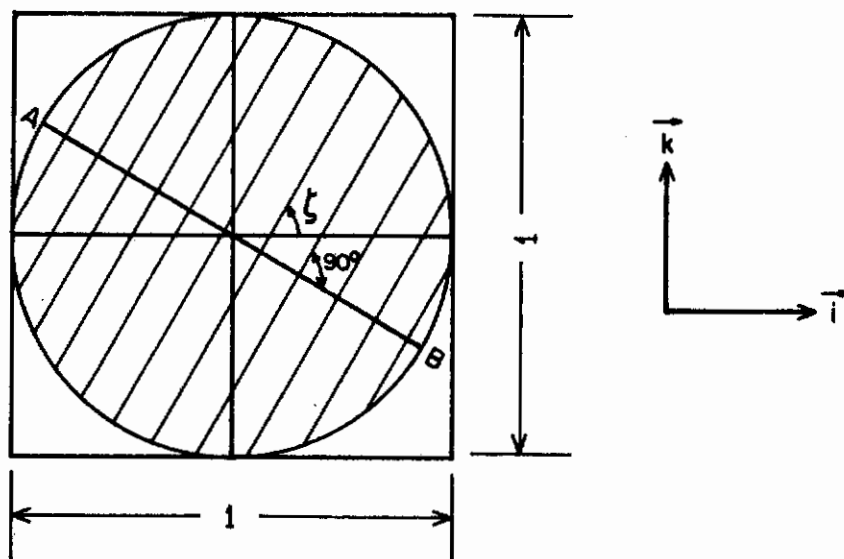


FIGURE 51 A UNIT CELL

# Contrails

Thus the fiber torque  $M_{Tf}$ , assuming linear elasticity, is given by

$$M_{Tf} = GI_p 2\pi T_f \quad (21)$$

where  $I_p$  is the polar moment of inertia of the fiber cross-section and  $G$  is the shear modulus of the fiber.

Substituting Equations (19) and (20) into Equation (21), it can be shown that

$$M_{Tf} = GI_p \frac{\sin \zeta \cos \zeta}{\rho} \quad (22)$$

The component  $M_{Tk}$  of this torque in the direction of the bending moment vector, the  $\bar{k}$  axis, is given by

$$M_{Tk} = M_{Tf} \sin \theta_y = GI_p \frac{\sin^2 \zeta \cos \zeta}{\rho} \quad (23)$$

The additional increment of unit cell bending rigidity,  $(EI)''$ , due to fiber torsion is obtained by summing the projections on the  $k$  axis of the torques in all the fibers in the cell required to produce a unit change in curvature. Therefore,

$$(EI)'' = N_f GI_p \int_{-\pi/2}^{\pi/2} \phi(\zeta) \sin^2 \zeta \cos^2 \zeta d\zeta \quad (24)$$

The bending rigidity of the unit cell due to fiber bending and fiber torsion is given by the sum of Equations (18) and (24).

$$(EI)_{\text{cell}} = N_f \int_{-\pi/2}^{\pi/2} \phi(\zeta) [E_f I_f \cos^4 \zeta + GI_p \sin^2 \zeta \cos^2 \zeta] d\zeta \quad (25)$$

The bending rigidity of an actual fabric is obtained by multiplying Equation (25) by the number of unit cells per unit width of fabric.

If the filaments in a unit cell are distributed in a manner such that the same number lie at each angle  $\zeta$ , that is, the fiber angular frequency distribution is constant,  $\phi(\zeta) = 1/\pi$ . From Equation (18), the bending rigidity of the unit cell due to fiber bending only is

$$(EI)' = \frac{3}{8} N_f E_f I_f \quad (26)$$

and from Equation (24) the corresponding increment to the bending rigidity of the unit cell due to fiber torsion is

$$(EI)'' = \frac{1}{8} N_f GI_p \quad (27)$$



# Contrails

The total bending rigidity of the unit cell with a constant fiber frequency distribution, therefore, is

$$(EI)_{\text{cell}} = \frac{1}{8} N_f (3 E_f I_f + G I_p) \quad (28)$$

For circular fibers the polar moment of inertia  $I_p = 2I_f$  and, from strength of materials,  $G = E/2(1 + \mu)$  where  $\mu$  is Poisson's Ratio. Equation (28) can, therefore, be reduced to the following expression

$$(EI)_{\text{cell}} = \frac{1}{8} N_f E_f I_f \left( 3 + \frac{1}{(1 + \mu)} \right) \quad (29)$$

From Equation (29) it can be seen that the contribution of fiber torsion to the total bending rigidity of the unit cell in the case of a cell with constant fiber frequency distribution decreases with increasing Poisson Ratio. This contribution is 25% for  $\mu = 0$  and 18% for  $\mu = 1/2$ .

## No Freedom of Relative Fiber Motion

The above analysis assumes complete freedom of individual fiber motion, i.e., it assumes that the fibers are able to move with respect to each other without any restriction. However, as binder is added to a nonwoven, this motion is prohibited to increasing degrees. Any restriction of fiber motion results in increased fabric bending rigidity. It is therefore appropriate to investigate the extreme case opposite to that of complete freedom, namely, no freedom of relative fiber motion.

By definition, during the bending of a completely bonded nonwoven, any plane perpendicular to the surface of the fabric and parallel to the axis of bending will remain plane. Therefore the strain  $\epsilon_f$  in any fiber in the fabric is given by

$$\epsilon_f = y |\vec{K}| \quad (30)$$

where  $\vec{K}$  is given by Equations (4) and (12) and  $y$  is the distance of any point in the fiber from the mid plane (neutral plane of bending) of the fabric.

$$|\vec{K}| = \sqrt{K_1^2 + K_2^2 + K_3^2} \quad (31)$$

Substituting Equation (12) into Equation (31) and taking  $\theta = 90^\circ$

$$|\vec{K}| = \frac{\cos^2 \zeta}{\rho} \quad (32)$$

Therefore

$$\epsilon_f = \frac{y \cos^2 \zeta}{\rho} \quad (33)$$

Assuming linear elasticity, the stress  $\sigma_f$  in the fiber is

$$\sigma_f = \frac{E_f y \cos^2 \zeta}{\rho} \quad (34)$$

# Contrails

and the total axial force  $F_f$  on the fiber is

$$F_f = \sigma_f A_f = \frac{E_f A_f y \cos^2 \zeta}{\rho} \quad (35)$$

The moment  $M_f$  of this force about the axis of bending is

$$M_f = F_f y \cos \zeta = \frac{E_f A_f y^2 \cos^3 \zeta}{\rho} \quad (36)$$

As previously noted, assuming equal angular and numerical fiber distribution throughout the thickness of the fabric, the relative frequency of fibers in a unit cell per unit width parallel to the axis of bending can be given by  $\phi(\zeta) \cos \zeta$ . Also, the number of fibers in a cross-sectional area of the unit cell,  $P$ , is given by

$$P = \frac{N_f}{bt} \quad (37)$$

where again  $N_f$  is the number of fibers in the circle inscribed in the unit cell,  $b$  is the cell width (square cells are assumed) and  $t$  is the fabric thickness.

The sum of the moments of all the fibers about the axis of bending is given by

$$M = P \int_{-\pi/2}^{\pi/2} \phi(\zeta) \cos \zeta \left\{ \int_{-t/2}^{t/2} \int_{-b/2}^{b/2} M_f dx dy \right\} d\zeta \quad (38)$$

Substituting Equations (36) and (37) into Equation (38) and carrying out the indicated integration

$$M = \frac{N_f E_f A_f t^2}{12 \rho} \int_{-\pi/2}^{\pi/2} \phi(\zeta) \cos^4 \zeta d\zeta \quad (39)$$

The bending rigidity of the unit cell of the fabric about the axis of bending,  $(\overline{EI})_{\text{cell}}$ , is therefore given by

$$(\overline{EI})_{\text{cell}} = \frac{N_f E_f A_f t^2}{12} \int_{-\pi/2}^{\pi/2} \phi(\zeta) \cos^4 \zeta d\zeta \quad (40)$$

If the fiber angular frequency distribution is constant,  $\phi(\zeta) = 1/\pi$  and Equation (40) reduces to

$$(\overline{EI})_{\text{cell}} = \frac{1}{32} N_f E_f A_f t^2 \quad (41)$$

# Contrails

The ratio  $\gamma$  of the bending rigidity of a unit cell with constant angular fiber frequency distribution in a nonwoven fabric with no freedom of relative fiber motion to that of a similar cell in a fabric with complete freedom of relative fiber motion (neglecting fiber torsion) is given by the ratio of Equation (41) to Equation (26)

$$\gamma = \frac{4}{3} \left( \frac{t}{d} \right)^2 . \quad (42)$$

As shown by Equation (42), for fabrics only a few fiber diameters thick, the bending rigidity of the fabric will increase rapidly with increasing restriction of freedom of individual fiber motion.

## Comparison of Crossed-Rod Matrix and Nonwoven Rigidities

The bending rigidity of a cross-rod matrix, Figure 52, about the  $\vec{k}$  axis, is given by

$$(EI)_{\text{matrix}} = n_f' E_f I_f \quad (43)$$

where  $n_f'$  is the number of rods per unit width. Complete freedom of motion at rod cross-overs is assumed.

The tensile strength,  $S$ , per unit width in the  $\vec{i}$  direction of the crossed-rod matrix is given by

$$S = n_f' \sigma_{\text{ult}} A_f \quad (44)$$

where  $\sigma_{\text{ult}}$  is the ultimate tensile stress of the rods and  $A_f$  is the cross-sectional area of a rod.

The tensile strength in the  $\vec{i}$  direction of a unit cell of a nonwoven with constant angular fiber frequency distribution, assuming the cell is stressed between two parallel flat plates, is given by<sup>(17)</sup>

$$S = \int_{-\pi/2}^{\pi/2} \left( \frac{N_f}{\pi} \right) \sigma_{\text{ult}} A_f \cos^4 \zeta \, d\zeta = \frac{3}{8} N_f \sigma_{\text{ult}} A_f . \quad (45)$$

Assuming the crossed-rod matrix and the unit cell are composed of the same fibers and equating Equations (44) and (45)

$$n_f' = \frac{3}{8} N_f . \quad (46)$$

The rigidity of the crossed-rod matrix of the same tensile strength as the nonwoven is obtained by substituting Equation (46) into Equation (43)

$$(EI)_{\text{matrix}} = \frac{3}{8} N_f E_f I_f . \quad (47)$$

Noting Equation (26),

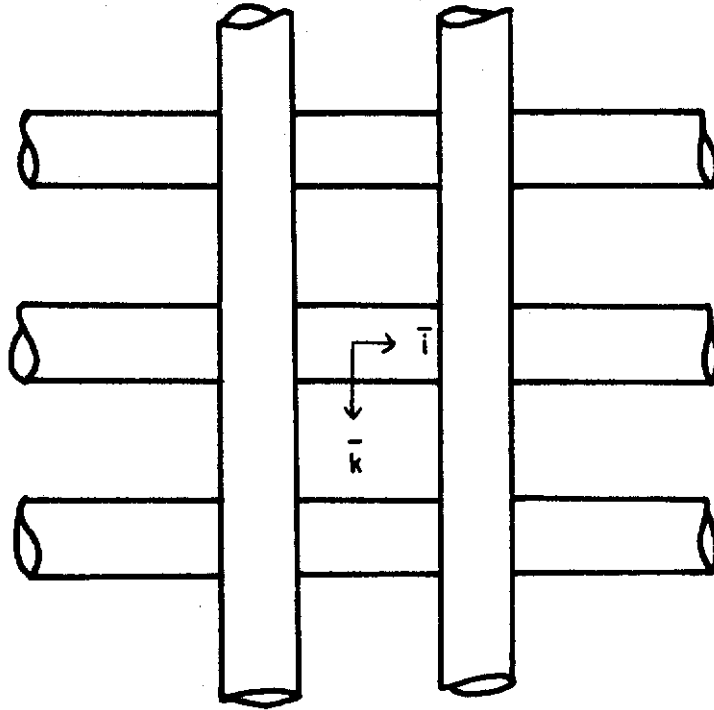


FIGURE 52    CROSSED-ROD MATRIX

$$(EI)_{\text{cell}} = (EI)_{\text{matrix}} \cdot \quad (48)$$

Therefore, a nonwoven fabric with constant fiber frequency distribution (assuming the fibers can untwist during bending of the unit cell) has the same bending rigidity as a crossed-rod matrix of the same fibers and having the same tensile strength. Also, the weight per unit area of the nonwoven fabric is 33-1/3% greater than that of the crossed-rod matrix.

The fact that commercial nonwovens are considerably less flexible than woven fabrics points out the rigidifying effect of the binders presently used to give nonwovens adequate strength.

## EXPERIMENTAL PROCEDURE AND RESULTS

The fiber distribution in textile nonwovens is a function of the process by which they are fabricated. It depends on the manner in which the fibers are laid down, and, also, on subsequent treatment. However, the spatial distribution of fibers in most nonwovens cannot be taken as constant. Therefore, in an effort to obtain some insight as to where an actual textile nonwoven fits between the two extremes, complete freedom of relative fiber motion and no freedom of relative fiber motion, analyzed herein, the predicted and experimentally observed bending rigidities of a waterlaid nonwoven fabric<sup>(15)</sup> composed of short (1/4 to 3/8 inch), straight, 1.5 denier viscose rayon fibers are compared. The fibers were bonded together with a regenerated viscose solution adding 1 to 2 percent onto the weight of fibers. The fabric was quite uniform, exhibited few clumps, and weighed approximately 16 gms/yd<sup>2</sup>. The fiber distribution in the fabric was such that the ratio of the number of fibers in the machine direction to the number in the cross-machine direction was approximately 5:1<sup>(15,16)</sup>.

The bending rigidity of the fabric was measured by the cantilever beam test (ASTM D-1388-55T). In this test one end of a fabric sample one inch wide is clamped in a horizontal position and the free length  $l$  of the sample is measured when the angle of the cord of the bent sample with the horizontal is 41.5°. The rigidity  $(EI)_{\text{exp}}$  is then given by

$$(EI)_{\text{exp}} = w \left( \frac{l}{2} \right)^3 \quad (49)$$

where  $w$  is the fabric weight per unit area.

The actual fabric weight was  $12.56 \times 10^{-3}$  gm/in<sup>2</sup>. The bending rigidity of the fabric in the machine direction ( $\zeta = 0^\circ$ ) was found to be

$$(EI)_{\text{exp}} \Big|_{\zeta=0^\circ} = 2.39 \times 10^{-4} \text{ lb in}^2/\text{in} \quad (50)$$

and in the cross machine direction ( $\zeta = 90^\circ$ )

$$(EI)_{\text{exp}} \Big|_{\zeta=90^\circ} = 0.62 \times 10^{-4} \text{ lb in}^2/\text{in} \quad (51)$$

# Contrails

These results are the average of ten measurements.

The diameter of the fibers in the fabric was measured with a fiber projection microscope. The average of two hundred measurements was 11.8 microns (0.000472 inch). This agrees closely with the calculated value obtained using a fiber diameter of 1.5 denier and a specific gravity of 1.52<sup>(12)</sup>. The calculated diameter,  $d = 0.000466$  inch, is used in the calculations that follow.

Using a Shirley thickness gauge with a 100 gram load on 10 square centimeters of fabric area, the fabric thickness was found to be 0.0047 inch.

The tensile modulus  $E$ , modulus of elasticity, of the fibers which constitute the fabric, was determined before and after processing. Fibers were removed from the tow from which the fabric was made and tensile tested<sup>(15)</sup>, and fibers were removed from the fabric and tested. Both procedures gave approximately the same modulus,  $E = 1.4 \times 10^8$  psi.

The shear modulus  $G$  of fibers removed from the fabric was measured with a galvanometer torsion tester. The average modulus was found to be  $G = 1.8 \times 10^5$  psi.

The fiber orientation distribution function used for the fabric is that determined by Petterson<sup>(15)</sup>. A brief description of the procedure used is as follows: Photomicrographs of the fabric were taken at a magnification of 100 times. A square unit cell of edge length 0.0225 inch was selected. The number of fibers at each angular interval of  $10^\circ$  from minus  $90^\circ$  ( $\zeta = -90^\circ$ ) to the machine direction to plus  $90^\circ$  ( $\zeta = 90^\circ$ ) in the circle of diameter 0.0225 inch inscribed in each cell was counted. The results for ten unit cells were averaged. The average number of fibers per unit cell,  $N_f$ , was 50.

The average fiber frequency, i.e., the number of fibers in each  $10^\circ$  interval over the total number of fibers in a unit cell, was plotted as a function of angle. The curve was symmetrical about  $\zeta = 0^\circ$ . This fiber frequency curve was approximated by a cosine power series of the following form<sup>(15)</sup>

$$\phi(\zeta) = K(a + b \cos \zeta + c \cos^3 \zeta + d \cos^5 \zeta + e \cos^7 \zeta) \quad (52)$$

The selection of the powers of cosine was arbitrary but designed to keep the number of terms to as few as possible, to simplify the calculations, and still closely approximate the frequency curve.

The values of the five constants in Equation (52) were determined from the equations:

$$\int_{-\pi/2}^{\pi/2} \phi(\zeta) d\zeta = 1 \quad (16a)$$

$$\zeta = 0^\circ, \quad \phi(\zeta) = \text{measured frequency distribution} \quad (53)$$

$$\zeta = 20^\circ, \quad \phi(\zeta) = \text{measured frequency distribution} \quad (54)$$

$$\zeta = 40^\circ, \quad \phi(\zeta) = \text{measured frequency distribution} \quad (55)$$

$$\zeta = 90^\circ, \quad \phi(\zeta) = \text{measured frequency distribution} \quad (56)$$

# Contrails

The selection of 20° and 40° rather than some other two angles is arbitrary.

By solving Equations (53) through (56) and Equation (16a) simultaneously Petterson found the following expression for the fiber frequency distribution function of the fabric

$$\phi(\zeta) = 0.10 + 0.036 \cos \zeta + 0.31 \cos^3 \zeta - 0.72 \cos^5 \zeta + 1.31 \cos^{16} \zeta \quad (57)$$

## ANALYTICAL RESULTS

Using the fiber and unit cell data given above and noting that

$$\cos (90 - \zeta) = \sin \zeta$$

$$\begin{aligned} \int_0^{\pi/2} \sin^n \zeta \, d\zeta &= \int_0^{\pi/2} \cos^n \zeta \, d\zeta \\ &= \frac{1 \cdot 3 \cdot 5 \dots (n-1)}{2 \cdot 4 \cdot 6 \dots n} \cdot \frac{\pi}{2} \quad (\text{n even}) \\ &= \frac{2 \cdot 4 \cdot 6 \dots (n-1)}{1 \cdot 3 \cdot 5 \dots n} \quad (\text{n odd}) \end{aligned}$$

$$\int_0^{\pi/2} \sin^2 \zeta \cos^n \zeta \, d\zeta = \frac{1}{n+2} \int_0^{\pi/2} \cos^n \zeta \, d\zeta$$

$$\int_0^{\pi/2} \cos^4 \zeta \sin^n \zeta \, d\zeta = \left(\frac{3}{n+4}\right) \left(\frac{1}{n+2}\right) \int_0^{\pi/2} \sin^n \zeta \, d\zeta$$

$$\int_0^{\pi/2} \cos^2 \zeta \sin^n \zeta \, d\zeta = \int_0^{\pi/2} \sin^2 \zeta \cos^n \zeta \, d\zeta$$

the bending rigidity of the viscose rayon fiber waterlaid nonwoven fabric was calculated in both the machine and cross machine directions for the cases of complete freedom of relative fiber motion (Equation (25)) and no freedom of relative fiber motion (Equation (40)). The results of the computations are given in Table 22.

TABLE 22  
BENDING RIGIDITY OF NONWOVEN FABRIC  
(lb in<sup>2</sup>/in)

<u>Direction of Bending</u>	<u>Complete Freedom of Relative Fiber Motion</u>	<u>No Freedom of Relative Fiber Motion</u>	<u>Experimental</u>
Machine Direction ( $\zeta = 0^\circ$ )	$4.9 \times 10^{-8}$	$6.4 \times 10^{-4}$	$2.4 \times 10^{-4}$
Cross Machine Direction ( $\zeta = 90^\circ$ )	$1.3 \times 10^{-8}$	$1.6 \times 10^{-4}$	$0.62 \times 10^{-4}$

The calculated ratio of the bending rigidity of the fabric in machine direction to that in the cross machine direction is 3.7 for the case of complete freedom of relative fiber motion, and 4.1 for the case of no freedom of relative fiber motion. The experimentally measured ratio is 3.9.

The ratio of the bending rigidity of the fabric in the machine direction for the case of no freedom of relative fiber motion to that for the case of complete freedom of relative fiber motion is 132, and in the cross machine direction 119.

Note that the measured bending rigidity of the fabric is more closely approximated by a unit cell model that assumes no freedom of relative fiber motion.



## XI. CONCLUSION

The feasibility of bunching and twisting 0.0005 inch diameter nickel chromium alloy wire into yarn and weaving the yarn into fabric has again been demonstrated<sup>(9)</sup>. The weight, permeability, flexural rigidity, wrinkle recovery, tensile properties, tear strength, and fold endurance of the fabric at 70°F were obtained. The fabric will be evaluated under liquid nitrogen and at elevated temperatures up to 2000°F during the next year's activity under the program.

The critical velocities of the multifilament wire yarn from which the fabric was woven were measured under longitudinal ( $\beta = 0^\circ$ ), 45°, and transverse ( $\beta = 90^\circ$ ) impact. The metal yarn exhibited critical velocities of one-half to one-third those of HT-1 and nylon yarn (Table 7).

The critical velocities of an HT-1 yarn wrapped with metal yarn were also measured. Under longitudinal impact the critical velocity was twice that of the metal yarn by itself; however, the transverse impact critical velocity remained essentially unchanged. This appears to indicate that it may be possible to enhance the high speed impact performance of metal yarns by blending them with other fibers by procedures that build in metal filament geometric elongation.

The impact test results were correlated with an analysis of impact stresses and strains. The impact rupture strains, determined by combining the analysis and test results, were found to be approximately the same for the three different impact angles for each of the three yarns tested. The impact rupture strains of the nylon and HT-1 yarns are considerably greater than that of the metal yarn (Table 8).

The results of a preliminary investigation of the joining of panels of metal fabric by sewing with metal sewing thread were disappointing. However the investigation will be continued during the next year and it is anticipated that by pursuing some of the ideas that have come from the preliminary investigation, a tolerably high seam efficiency will eventually be obtained.

The feasibility of braiding fine wire into coreless cord was demonstrated, and measurements were made of the tensile properties of a variety of cords. It was found that 0.5 mil wire does not have to be used in such structures. Cord braided from 1.0 mil wire exhibits adequate flexibility.

The feasibility of texturing metal yarns was demonstrated. However, in fabric form the yarns did not exhibit much bulk. The forces to which the yarns were subjected in weaving removed most of the crimp.

Fabrics woven from yarns composed of metal filaments and fibers that do not volatilize but decompose at elevated temperatures look promising. It appears that this type of a structure may give a fabric with high flexibility, low permeability, and moderate weight and tensile strength over a broad temperature range. Blended yarns and fabrics will be given further consideration.

The investigation of a typical nonwoven shows that the bending rigidity of nonwovens is more closely approximated by a unit cell model that assumes no freedom of relative fiber motion than by the same unit cell model with complete freedom of relative fiber motion. This points out the reason why the nonwovens produced by current methods, as a class, are too stiff for many textile applications. The binder gives them tensile strength but prevents relative fiber motion during bending.

## XII. FUTURE PLANS

During the next year under this continuing program Fabric Research Laboratories, Inc., will perform studies to determine the mechanical properties of polymeric, metallic, carbonaceous and oxide materials in fiber form (if they are available as continuous filaments) and in yarn and woven fabric form after various environment-time cycles. Exposure times will be varied in increments from a practical minimum of a couple of minutes to one hundred hours, and the temperature varied in increments over the range 70°F to 2000°F. The evaluation of properties following the end of the time-temperature cycle will be made both at the elevated temperatures and at ambient temperature, 70°F. Materials will be pre-conditioned at 70°F and 65% relative humidity, and under a semi-hard vacuum ( $10^{-5}$  mm Hg) prior to the time-temperature cycles. The materials will also be conditioned in an inert atmosphere (nitrogen) at temperatures from 70°F to 2000°F for varying lengths of time prior to evaluation at 70°F.

Fiber (where possible), yarn and fabric tensile strength, rupture elongation, yield strength, yield elongation, tensile modulus, energy absorption and repeated tensile stress response, and also fabric tear strength, folding endurance, crease recovery, flexibility and permeability will be measured at temperatures from 70°F to 2000°F. The tensile properties of the fibers, yarns and fabrics, and the bending endurance of the fabrics will also be measured under liquid nitrogen (-320°F).

As discussed in Section IX the special fixtures required for the above testing program have been designed and, in most instances, fabricated. The fixtures will be checked out at the extreme temperatures for which they are designed in the near future. The necessary test procedures will be developed during this evaluation of the equipment.

As soon as this special test equipment is ready for use, the fine wire multifilament yarn fabric discussed in Section II will be evaluated at the cryogenic and elevated temperatures up to 2000°F.

The investigation of blended yarn fabrics will be continued during the next year. Several yards of fabric will be woven from each of a couple of composite yarns. The fabrics will be evaluated at temperatures from cryogenic to 2000°F.

The metal fabric seaming investigation will be continued. It is anticipated that by pursuing some of the ideas that came out of the preliminary investigation discussed in Section III, a high seam efficiency will be obtained.

## XIII. RECOMMENDATIONS

Although the fibrous material evaluation program outlined in Section XII is quite extensive, it is not complete enough to give all the data on fibrous materials that most certainly will be required if such structures are to be successfully utilized in the various space applications presently being contemplated. The additional areas of investigation that Fabric Research Laboratories recommends be included in this fibrous material evaluation program are outlined briefly below.

1. Evaluation of fibrous materials at elevated temperatures in a vacuum and in inert atmospheres -- Numerous contemplated applications of fibrous materials dictate that a capability be established for determining the tensile properties of fibrous materials at temperatures up to 3000°F in a hard vacuum ( $10^{-7}$  mm Hg) and in inert atmospheres.

2. High speed - high temperature impact properties of fibrous materials -- Some deceleration systems, for instance the Hyperflo canopy parachute, incorporating fibrous materials anticipate the rapid application of load with the fabric at elevated temperatures. Therefore, a test facility with the capability of simulating this type of loading and environment should be established.

The importance of this type of an evaluation of fibrous materials cannot be overemphasized. The critical longitudinal velocity of metal wire at 70°F is low, approximately 200 ft/sec, which indicates that such material has a low rupture elongation at high rates of straining. It is also known that at low rates of straining (0.5 - 2.0 inches/minute) the yield elongation of some superalloy metals increases with increasing temperature (to 2000°F) and the yield elongation of others decreases. One would therefore anticipate a difference in the impact behavior among the various alloys.

3. Vibration -- All applications of fibrous materials anticipate vibration. The amplitude and frequency of vibration will, however, vary from one system to another. The flutter of the leading edge of a Hyperflo canopy parachute or the trailing edge of a paraglider wing are probably extreme cases.

A test instrument capable of subjecting fabrics to a range of amplitudes and frequencies of vibration should be developed. The various candidate fibrous materials should then be evaluated subsequent to vibration.

4. Joints -- As a result of work now in progress under this program, FRL® believes that greater emphasis should be placed on the joining of panels of woven metal fabric. The bending endurance, crease recovery, and tensile strength efficiency of sewn seams over a range of temperatures should be investigated in detail. The potential of high temperature adhesives for the joining of panels of fabric should be considered.

5. Pressure packing -- Since most systems utilizing woven fabrics will be packaged into a small container prior to use, the effect of such packaging in air and in a vacuum on the tensile properties of the fabric over a range of temperatures should be investigated.

6. Investigation of fabrics woven from hard wire -- The tensile strength of hard (unannealed) superalloy wire is considerably greater than that of fully annealed wire in the 70°F to 1800°F range. (At temperatures above 1800°F

annealing occurs resulting in both having approximately the same tensile strength.) Therefore, the strength to weight ratio of fabrics woven from hard wire would be considerably greater than that of fabrics woven from fully annealed wire over a wide temperature range.

To date only fabrics woven from fully annealed superalloy wire have been evaluated. This is because it was anticipated that fully annealed wire would be easier to twist and weave. However, it would probably now be appropriate to investigate the processing of hard wire and the properties of fabric woven from this wire.

7. Coated fabrics -- An investigation to determine the optimum substrate structure in a coated fabric should be carried out. The effect of fiber diameter, yarn diameter, yarn structure (blended, textured, etc.), fabric weave, pick and end count, and fabric permeability on the mechanical properties of coated fabrics should be noted. Preliminary investigations have shown that good coating adhesion is not obtained with a metal fabric tightly woven from low twist yarns.

8. Research on organic and inorganic coatings and lubricants -- Investigation of coatings to improve the abrasion resistance and oxidation resistance of various fibrous materials should receive greater emphasis and research on lubricants for enhancing the freedom of motion of filaments and yarns in fabrics should be initiated.

Preliminary investigations indicate that lubrication will be an extremely important consideration. The folding endurance of a metal fabric at 70°F lubricated with oil is twice that of the same fabrics washed in perchlorethylene. Most commercial lubricants would be burned off at elevated temperatures, possibly resulting in a fabric with low folding endurance and high flexural rigidity.

## XIV. LIST OF REFERENCES

1. Backer, S. and Petterson, D. R., Textile Research Journal 30, 704-711 (1960).
2. Chu, C. C., Coskren, R. J., and Morgan, H. M., WADD-TR-60-511, Part I (1960).
3. Coplan, M. J. and Block, M. G., WADC-TR-56-313, Part I (1956).
4. Coplan, M. J., Freeston, W. D., Jr., and Platt, M. M., ASD-TDR-62-851 (1962).
5. Coskren, R. J. and Chu, C. C., ASD-TR-60-511, Part II (1962).
6. Coskren, R. J. and Chu, C. C., ASD-TR-60-511, Part III (1963).
7. Cox, H. L., British Journal of Applied Physics 3, 72-79 (1952).
8. Dawn, F. S. and Ross, J. H., ASD-TDR-62-782 (1962).
9. Freeston, W. D., Jr., and Gardella, J. W., ASD-TDR-63-542, Part II (1963).
10. Hamburger, W. J., Platt, M. M., and Morgan, H. M., Textile Research Journal 22, No. 11 (1952).
11. Harris, M., "Handbook of Textile Fibers" (1954).
12. Kaswell, E. R., "Wellington Sears Handbook of Industrial Textiles," Wellington Sears Company, Inc., New York, N. Y., 1963.
13. Military Specification, Cord, Nylon, Coreless, MIL-C-7515B (USAF), Amendment 1 (29 July 1960).
14. Pierce, F. T., The Journal of the Textile Institute 21, T377 (1930).
15. Petterson, D. R., "On the Mechanics of Nonwoven Fabrics," Sc.D. Thesis, M.I.T. (1959).
16. Petterson, D. R. and Backer, S., Textile Research Journal 33, 809-816 (1963).
17. Platt, M. M., Textile Research Journal 24, 132-134 (1954).
18. Platt, M. M., Klein, W. G., and Hamburger, W. J., Textile Research Journal 28, (1958).
19. Platt, M. M., Klein, W. G., and Hamburger, W. J., Textile Research Journal 31, (1959).
20. Platt, M. M., Klein, W. G., and Hamburger, W. J., Textile Research Journal 22, (1952).

# Contrails

21. Ringleb, F. O., "Cable Dynamics", Report NAEF-ENG-6169 (1956).
22. Textured Yarns, Technical Information on Processing Chemstrand Nylon (March 1963).
23. Walton, R. R., U. S. Patent 2,765,514.
24. Walton, R. R., U. S. Patent 2,765,513.
25. Wison, I., American Viscose Corporation, private correspondence (1963).

## APPENDIX

### ANALYSIS OF IMPACT STRESSES AND STRAINS

#### LONGITUDINAL IMPACT

The velocity of propagation  $c$  of a longitudinal stress wave (a wave traveling along a filament axis) differs from the longitudinal velocity given to the cross-sections by the stresses. The velocity of the filament cross-sections  $v$  can be obtained by noting that the strained portion of the filament shortens in the case of compressive stresses or lengthens in the case of tensile stresses by the amount

$$\epsilon c t$$

where  $\epsilon$  denotes strain and  $t$  denotes time. Therefore, the velocity of the cross-sections is given by

$$v = \epsilon c . \quad (1)$$

The velocity  $c$  of the propagation of a longitudinal wave can be obtained from impulse and momentum considerations. The contribution of the lateral contraction to the momentum is neglected. The momentum of the strained segment of the filament is given by

$$\rho A c t v$$

where  $\rho$  is the filament density and  $A$  is the filament cross-sectional area, and the impulse of the compressive stress by

$$A \sigma t .$$

Equating the impulse to the change in momentum

$$A \sigma t = \rho A c t v .$$

Therefore

$$c = \frac{\sigma}{\rho v} . \quad (2)$$

Substituting Equation (1) into Equation (2)

$$c = \sqrt{\frac{\sigma}{\rho \epsilon}} \quad (3)$$

and substituting Equation (3) into Equation (1)

$$v = \sqrt{\frac{\sigma \epsilon}{\rho}} . \quad (4)$$

If the relationship between stress and strain is linear at impact speeds,  $\sigma = E\epsilon$ , Equation (3) reduces to

$$c = \sqrt{\frac{E}{\rho}}$$

which results in the longitudinal wave velocity  $c$  being independent of the stress level.

OBLIQUE IMPACT

In Figure 53 ABFDG is the initial configuration of a filament at the instant impact by a body moving with a velocity  $V_0$  at an angle  $\beta$  to the filament occurs at F. At a later time  $t$  the configuration is ABCDG, assuming the structure to be infinitely flexible. This configuration spreads out uniformly (parallel) with time. C moves with the velocity  $V_0$  at angle  $\beta$  with the x-axis. G is the wave front of a longitudinal tensile stress wave propagated with the velocity  $c$  (see Equation (3)). As will be shown later, a longitudinal wave propagates with a greater velocity than a transverse wave.

D is the wave front of the lateral motion which is propagated with the velocity  $V$ . The longitudinal stress wave produces a tension  $T$  in the filament with the corresponding strain  $\epsilon$ , and gives the filament in the region DG a velocity  $u$  towards F. This feeds mass into the lateral wave front D. Assuming no length transfer at C, i.e., assuming the filament is rigidly clamped by the impacting body, the lateral wave is not associated with any further longitudinal strain.

Equating the y component of the impulse at D to the y component of the change in momentum for the portion CDG of the filament gives the following expression.

$$T(\sin \theta)t = \left[ m \sqrt{(V_0 \sin \beta)^2 + (V + V_0 \cos \beta)^2} t \right] V_0 \sin \beta \quad (5)$$

where  $m$  is the filament mass per unit length when stressed to the tension  $T$  and

$$\sin \theta = \frac{V_0 \sin \beta}{\sqrt{(V_0 \sin \beta)^2 + (V + V_0 \cos \beta)^2}} \quad (6)$$

Substituting Equation (6) into Equation (5)

$$T = m [V^2 + 2V V_0 \cos \beta + V_0^2] \quad (7)$$

Equating the x component of the impulse at D to the x component of the change in momentum for the portion CDG of the filament gives the following expression.

$$T(1 - \cos \theta)t = \left[ m \sqrt{(V_0 \sin \beta)^2 + (V + V_0 \cos \beta)^2} t \right] (u - V_0 \cos \beta) \quad (8)$$

where

$$\cos \theta = \frac{V + V_0 \cos \beta}{\sqrt{(V_0 \sin \beta)^2 + (V + V_0 \cos \beta)^2}} \quad (9)$$



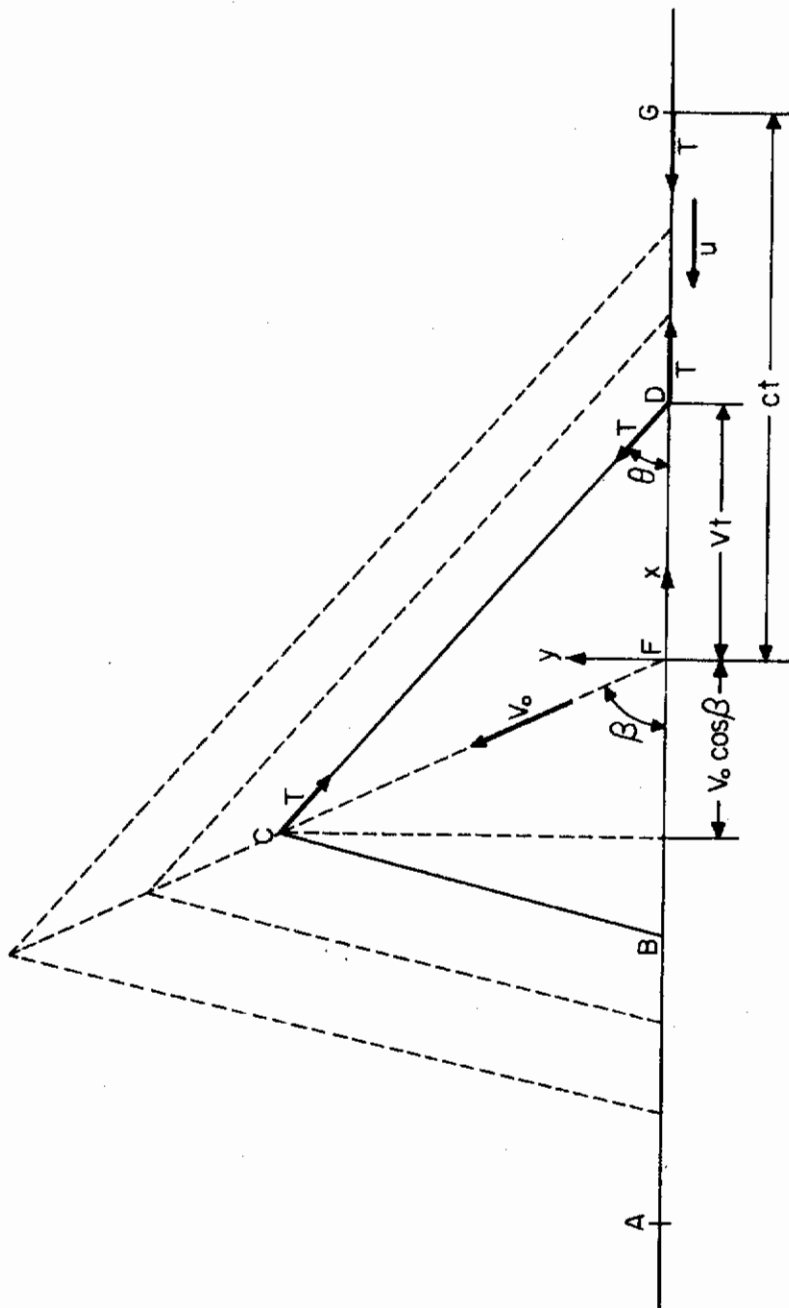


FIGURE 53 OBLIQUE IMPACT

# Contrails

Conservation of mass at the wave front D gives

$$u = \left[ \sqrt{(V_0 \sin \beta)^2 + (V + V_0 \cos \beta)^2} - V \right] . \quad (10)$$

Substitution of Equations (9) and (10) into Equation (8) reduces Equation (8) to Equation (7).

Equating the impulse to the change in momentum at the wave front G

$$T t = \rho A c u t .$$

Therefore

$$u = \frac{T}{\rho A c} . \quad (11)$$

The stress  $\sigma$  in the filament is given by

$$\sigma = \frac{T}{A} . \quad (12)$$

Noting Equations (1) and (2)

$$u = \epsilon c = v .$$

The mass per unit length of the stretched filament is given by

$$m = \frac{\rho A}{1 + \epsilon} \quad (13)$$

where  $A$  is the initial filament cross-sectional area,  $\rho$  the initial density and  $\epsilon$  the strain.

Substituting Equations (12) and (13) into Equation (7), and Equations (11) and (12) into Equation (10),

$$\sigma = \frac{\rho}{1 + \epsilon} [v^2 + 2v V_0 \cos \beta + V_0^2] \quad (14)$$

and

$$\frac{\sigma}{\rho c} = \left[ \sqrt{v^2 + 2v V_0 \cos \beta + V_0^2} - v \right] . \quad (15)$$

Substituting Equation (14) into Equation (15) and solving for  $v$

$$v = \sqrt{\frac{\sigma}{\rho} (1 + \epsilon)} - \frac{\sigma}{\rho c} . \quad (16)$$

Substituting Equations (16) and (3) into Equation (14) gives the following relationship between filament strain, impact velocity and angle<sup>(21)</sup>.

# Contrails

$$\left(\frac{V_0}{c}\right)^2 + 2\left(\frac{V_0}{c}\right) \left[ \sqrt{\epsilon} \sqrt{1+\epsilon} - \epsilon \right] \cos \beta = 2\epsilon \sqrt{\epsilon} \sqrt{1+\epsilon} - (\epsilon)^2 . \quad (17)$$

Using Equation (17) the oblique impact strain is plotted in Figure 54 as a function of the ratio of the impact velocity to the velocity  $c$  of propagation of a longitudinal wave for longitudinal impact ( $\beta = 0^\circ$ ),  $10^\circ$  impact,  $45^\circ$  impact, and transverse impact ( $\beta = 90^\circ$ ).

For  $\beta = 0^\circ$  Equation (17) reduces to the expression previously derived for longitudinal impact.

$$\left(\frac{V_0}{c} - \epsilon\right)^2 + 2\sqrt{\epsilon} \sqrt{1+\epsilon} \left(\frac{V_0}{c} - \epsilon\right) = 0 .$$

Thus, either

$$\epsilon = \frac{V_0}{c} \quad (18)$$

or

$$\epsilon - 2\sqrt{\epsilon} \sqrt{1+\epsilon} = \frac{V_0}{c} .$$

The first of these two expressions is identical with Equation (1). The second does not have a real solution for  $\sigma$  for a positive value of  $V_0$ .

For transverse impact,  $\beta = 90^\circ$ , Equation (17) gives the following expression.

$$\left(\frac{V_0}{c}\right)^2 = 2\epsilon \sqrt{\epsilon} \sqrt{1+\epsilon} - (\epsilon)^2 . \quad (19)$$

If  $\epsilon$  is negligibly small compared to unity, as is usually the case, particularly for metals, Equation (19) simplifies to the following expression.

$$\left(\frac{V_0}{c}\right)^2 + 2\frac{V_0}{c} (\sqrt{\epsilon} - \epsilon) \cos \beta = 2\epsilon \sqrt{\epsilon} - (\epsilon)^2 . \quad (20)$$

If the relationship between stress and strain is linear at impact speeds, elastic impact,  $\sigma = E\epsilon$ , Equation (20) takes the following form

$$\left(\frac{V_0}{c}\right)^2 + 2\frac{V_0}{c} \left(\sqrt{\frac{\sigma}{E}} - \frac{\sigma}{E}\right) \cos \beta = 2\frac{\sigma}{E} \sqrt{\frac{\sigma}{E}} - \left(\frac{\sigma}{E}\right)^2 .$$

For a given  $\frac{V_0}{c}$ ,  $\frac{\sigma}{E}$  increases with decreasing angle  $\beta$ ; transverse impact,  $\beta = 90^\circ$ , is the least severe case. Also, utilization of a material with a low longitudinal wave velocity  $c$ , i.e., a low modulus  $E$ , decreases the impact stress.

If  $\epsilon$  is negligibly small compared to  $\sqrt{\epsilon}$  (i.e.,  $\epsilon \ll 1$ ), Equation (20) reduces to

$$\left(\frac{V_0}{c}\right)^2 + 2\left(\frac{V_0}{c}\right) \sqrt{\epsilon} \cos \beta = 2\epsilon \sqrt{\epsilon} . \quad (21)$$

In the special case of transverse impact,  $\beta = 90^\circ$ , Equation (21) reduces to

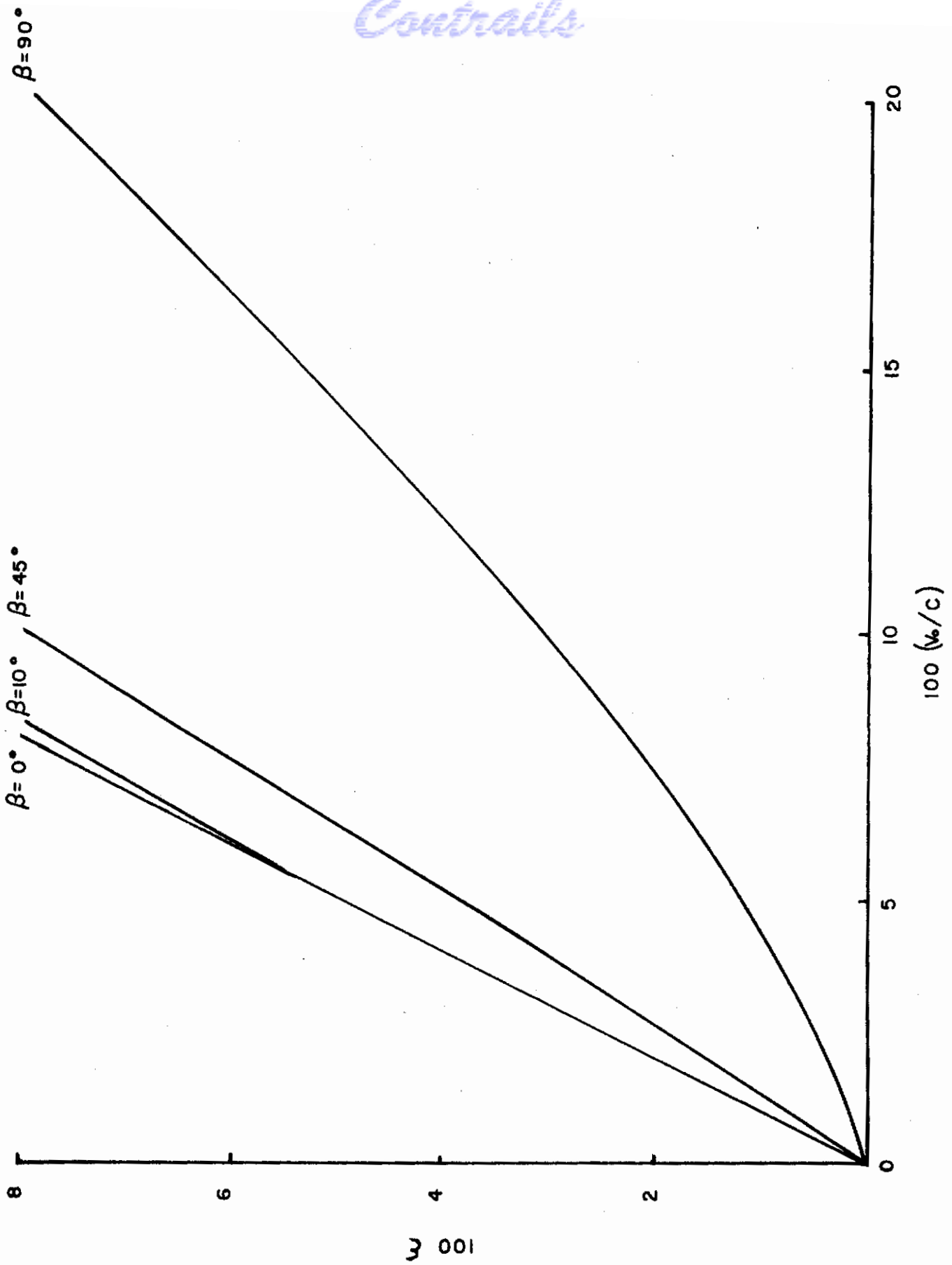


FIGURE 54 OBLIQUE IMPACT STRAIN

# Contrails

$$\epsilon = \sqrt[3]{0.25} \left( \frac{V_0}{c} \right)^{4/3} . \quad (22)$$

The velocity  $V$  of the lateral wave front (point D, Figure 53) is given by Equation (16).

$$V = \sqrt{\frac{\sigma}{\rho} (1 + \epsilon)} - \frac{\sigma}{\rho c} .$$

Assuming  $\epsilon$  is negligibly small compared to 1

$$V = \sqrt{\frac{\sigma}{\rho}} - \frac{\sigma}{\rho c} . \quad (23)$$

The transverse wave velocity  $\bar{c}$  is the velocity of the point which corresponds to D at  $t = 0$ . This point moves toward D at a velocity  $u$  and D moves toward it at a velocity  $V$ ; therefore

$$\bar{c} = V + u . \quad (24)$$

Substituting Equations (16), (11) and (12) into Equation (24)

$$\bar{c} = \sqrt{\frac{\sigma}{\rho} (1 + \epsilon)} . \quad (25)$$

Assuming  $\epsilon$  is negligibly small compared to 1, Equation (25) reduces to the following expression for the transverse wave velocity.

$$\bar{c} = \sqrt{\frac{\sigma}{\rho}} . \quad (26)$$

## ENERGY

The initial mass of the segment FG (Figure 53) of the filament is

$$\rho A c t .$$

The mass of the segment CD of the filament is

$$\frac{\rho A}{(1 + \epsilon)} \sqrt{(V_0 \sin \beta)^2 + (V + V_0 \cos \beta)^2} t .$$

Noting Equation (14), this reduces to

$$\frac{\rho A t}{(1 + \epsilon)} \sqrt{\frac{\sigma}{\rho} (1 + \epsilon)} .$$

The mass of the segment DG of the filament is

$$\rho A c t - \frac{\rho A t}{(1 + \epsilon)} \sqrt{\frac{\sigma}{\rho} (1 + \epsilon)} .$$

# Contrails

The kinetic energy of the segment DC of the filament is

$$(KE)_{CD} = \frac{\rho A t}{(1 + \epsilon)} \sqrt{\frac{\sigma}{\rho} (1 + \epsilon)} \frac{V_0^2}{2} . \quad (27)$$

The kinetic energy of the segment DG of the filament is

$$(KE)_{DG} = \rho A c t \left[ 1 - \frac{1}{c(1 + \epsilon)} \sqrt{\frac{\sigma}{\rho} (1 + \epsilon)} \right] \frac{U^2}{2} .$$

Noting Equation (11)

$$(KE)_{DG} = \rho A c t \left[ 1 - \frac{\sqrt{\frac{\sigma}{\rho} (1 + \epsilon)}}{c(1 + \epsilon)} \right] \frac{\sigma^2}{2 \rho^2 c^3} . \quad (28)$$

The strain-energy U in the filament is

$$U = \frac{1}{2} \sigma \epsilon A c t . \quad (29)$$

If  $\epsilon$  is negligibly small compared to unity, Equations (27) and (28) simplify to the following expressions.

$$(KE)_{CD} = \rho A t \sqrt{\frac{\sigma}{\rho}} \frac{V_0^2}{2} . \quad (30)$$

$$(KE)_{DG} = \rho A c t \left( 1 - \sqrt{\frac{\sigma}{\rho c^2}} \right) \frac{\sigma^2}{2 \rho^2 c^3} . \quad (31)$$

In the special case of transverse impact,  $\beta = 90^\circ$ , and assuming  $\frac{\sigma}{\rho c^2}$  is negligibly small compared to one and  $\sqrt{\frac{\sigma}{\rho c^2}}$ , Equation (30) can be rewritten in the following form, noting Equations (21) and (3)

$$(KE)_{CD} = \sigma \epsilon A c t \quad (32)$$

$$(KE)_{DG} = \frac{1}{2} \sigma \epsilon A c t \quad (33)$$

$$U = \frac{1}{2} \sigma \epsilon A c t . \quad (34)$$

Therefore, in the case of transverse impact, the kinetic energy of the transverse moving segment of the filament is approximately 50 percent of the total energy, the kinetic energy of the longitudinally moving segment 25 percent, and the strain energy 25 percent regardless of the shape of the material stress-strain diagram.

## BOUNDARY CONDITIONS

In a longitudinal compression wave, the velocity  $v$  (Equation (1)) of the particles is in the same direction as the velocity of wave propagation, and in a tension wave the velocity  $v$  is in the opposite direction from that of the wave. If a compression wave is moving along a filament in one direction and a tension wave with the same magnitude of stress in the opposite direction, the tension and compression annul each other when the waves come together. In the portion of the filament in which the two waves are superimposed, the stress is zero and the particle velocity is doubled. The region of zero stress can be thought of as a free end. Thus, in the case of a free end, a compression wave is reflected as a tension wave of the same stress magnitude and a tension wave is reflected as a compression wave of the same magnitude.

If two waves of the same stress magnitude and moving in the opposite direction come together, the stress will be doubled and the particle velocity will be zero in the portion of the filament in which the waves are superimposed. The region of zero velocity can be thought of as a fixed (clamped, built-in) end. Thus a wave is reflected from a fixed end entirely unchanged, i.e., a stress doubling takes place.

In practice, most boundary conditions are neither free nor fixed, but something in between. Thus there will be a partial stress reflection at the boundary. For instance, at a partially clamped end a tension stress wave will be reflected as a tension wave of a smaller magnitude. Therefore, in most cases of impact, there will be a stress increase in a filament after the longitudinal wave reaches the boundary.

The reflected wave will be reflected at the point of impact, and this wave will be partially reflected at the boundary, etc. Thus the stress in the filament will build up continuously due to successive stress wave reflections. This can cause the filament to rupture before the kinetic energy of the impacting body is absorbed.